Preparation and Functionalization of Macromolecule-Metal and Metal Oxide Nanocomplexes for Biomedical Applications

by

Michael L. Vadala

Dissertation submitted to the Faculty of the Virginia Polytechnic Institute and State University in partial fulfillment of the requirements for the degree of

Doctor of Philosophy

in

Macromolecular Science and Engineering

Approved By:
Judy S. Riffle
James E. McGrath
Timothy E. Long
Rick Davis
Alan Esker

April 18, 2006
Blacksburg, Virginia

key words: cobalt, polysiloxane, phthalonitrile, nanoparticle, poly(ethylene oxide)

Preparation and Functionalization of Macromolecule-Metal and Metal Oxide Nanocomplexes For Biomedical Applications

Michael L. Vadala

Abstract

Copolymer-cobalt complexes have been formed by thermolysis of dicobalt octacarbonyl in solutions of copolysiloxanes. The copolysiloxane-cobalt complexes formed from toluene solutions of PDMS-*b*-[PMVS-*co*-PMTMS] block copolymers were annealed at 600-700 °C under nitrogen to form protective siliceous shells around the nanoparticles. Magnetic measurements after aging for several months in both air and in water suggest that the ceramic coatings do protect the cobalt against oxidation. However, after mechanical grinding, oxidation occurs. The specific saturation magnetization of the siliceous-cobalt nanoparticles increased substantially as a function of annealing temperature, and they have high magnetic moments for particles of this size of 60 emu g^{-1} Co after heat-treatment at temperatures above 600 °C.

The siliceous-cobalt nanoparticles can be re-functionalized with aminopropyltrimethoxysilane by condensing the coupling agent onto the nanoparticle surfaces in anhydrous, refluxing toluene. The concentration of primary amine obtained on the surfaces is in reasonable agreement with the charged concentrations. The surface amine groups can initiate L-lactide and the biodegradable polymer, poly(L-lactide), can be polymerized directly from the surface. The protected cobalt surface can also be re-functionalized with poly(dimethylsiloxane) and poly(ethylene oxide-*co*-propylene oxide)

providing increased versatility for reacting polymers and functional groups onto the siliceous-cobalt nanoparticles.

Phthalonitrile containing graft copolysiloxanes were synthesized and investigated as enhanced oxygen impermeable shell precursors for cobalt nanoparticles. The siloxane provided a silica precursor whereas the phthalonitrile provided a graphitic precursor. After pyrolysis, the surfaces were silicon rich and the complexes exhibited a substantial increase in M_s. Early aging data suggests that these complexes are oxidatively stable in air after mechanical grinding.

Aqueous dispersions of macromolecule-magnetite complexes are desirable for biomedical applications. A series of vinylsilylpropanol initiators, where the vinyl groups vary from one to three, were prepared and utilized for the synthesis of heterobifunctional poly(ethylene oxide) oligomers with a free hydroxy group on one end and one to three vinylsilyl groups on the other end. The oligomers were further modified with carboxylic acids via ene-thiol addition reactions while preserving the hydroxyl functionality at the opposite terminus. The resulting carboxylic acid heterobifunctional PEO are currently being investigated as possible dispersion stabilizers for magnetite in aqueous media.

Acknowledgements

I would like to express my sincere gratitude and appreciation to my advisor Dr. Judy Riffle for her support, guidance, and encouragement throughout my education at Virginia Tech. She has given me the opportunity to grow as a scientist and a person through many years. I am grateful to the opportunity and path she put me on 8 years ago. I am honored to be advised by such a prominent and brilliant chemist. I also would like to thank my committee members, Dr. James E. McGrath, Timothy Long, Dr. Alan Esker, and Dr. Richey Davis.

I would like to extend my deepest gratitude to Angie Flynn for her unselfish help. She is always one step ahead of me and has saved me from catastrophe many times over. She is an invaluable resource and person. I would especially like to thank Mark Flynn for GPC and the Australian folks for magnetization analysis. I extend many thanks to my group members who helped me in my quest for the Ph.D. including Dr. Michael Zalich for countless advice on both the scientific and personal level, and for his amazing help with TEM, magnetization, and metal complex characterization. Thank you to my SURP students David Fulks and Maggie Ashworth. You are both are huge part of this dissertation. In addition, Shane Thompson for his invaluable help with poly(ethylene oxide) without whom chapter 6 would not be possible. I am indebted to Dr. Yinian Lin for his tremendous help in small molecule synthesis. Jonathan Goff deserves a huge thank you for his scientific advice, help, and support. Nikorn Pothayee is owed my sincerest gratitude for his amazing synthetic skills and help in phthalonitrile-cobalt complexes. My deepest thanks to the rest of Dr. Riffle's research group past, present, and future.

Dedication

To **Jonathan Goff**, for our countless nights that the Cellar, the laughs, the taquitos, and everything else in between especially the friendship. Salut, A Santé, Prost and a huge Cheers to you!

To **Nikorn Pothayee**, for the beat of the music, for the faith in things to come. I wish you the best of luck in your scientific pursuit.

To **Dr. Casey Gaunt**, we have finally reached our goal that we have pursued for so many years now. You have made the last four years the happiest of my life. I hope that you become that clinician you have always aspired to be. Without you, I don't think I would be receiving the Ph.D. You gave me strength I never thought I had. Thank you for being with me through this.

To **Chris Severance**, for the best friendship I've ever known. Who knew 8 years ago we'd be here. Thank you for the undying support, reality checks, and conversations. Thanks for the laughs, the tears, the dancing, the 2 am thoughts. You are the sole person that has truly helped me to become a better person. Thank you for 525, 600 minutes (x 8 years) and no day but today. The curtain rises now. It's showtime! How is the house?

To my sister **Nicole Vadala**, you are truly the strongest person I know. I have learned so much from you. You have survived so much and pushed yourself so hard. You have succeeded and that I admire. Always trust in yourself, Nic and believe in the future. Thank you for being such a great friend to me. I love you. Cheers to awesome A1C's!

To my sister **Lindsay Vadala**, thank you for our late night conversations, our nights on the couch, being my friend and roommate. You are an amazing person with such a heart and soul to offer the world. Don't let anyone take that from you. People like you are a diamond in the rough. I am so glad I got the opportunity to know you more. Our time at Virginia Tech is over but will be a great memory. I love you.

To my brother **Timothy Vadala**, thank you for the laughter. You have a way to make things so much easier. You can lighten my mood on any day. You are on your way to great things, bro whether in science or elsewhere. You can achieve anything if you keep believing in yourself. Thank you for letting me get to know you and being a great friend to me. I love you.

To **Mom**, it is all worth it now. I took me such a long time to realize everything you did for me. Thank you for pushing me when I wanted it least. Thanks for giving me the best foundation in life and academics I could have ever hoped for. Thanks for the lunch bags with notes in it. Thanks for the endless support. Thanks for the donuts by the runway. Of course, I mustn't forget thanks for you. This dissertation is a culmination of all the years you helped me, pushed me, and were there for me. Life begins now and I am so excited. Thank you for this chance. It is because of you. I love you!

To **Dad**, I'm here at the end. Life sure has taken its wild turns. I want you to know that you have given me (and the rest of us) the best life. We want for nothing. You made sure that we were educated in the best places and were independent. You supported all of us in everything you did whether here or abroad. And today, you still continue to do so. My motivation for this Ph.D. was you. My hat is off to you! Thank you for the inspiration. This dissertation is yours too, Dad (Drs. Vadala)!

In loving memory of my grandmother,
Anne Catherine Neil,
whose inspiration and love of life helped shape who I am today.

Table of Contents

Abbreviations

D_3	1,1,3,3,5,5-hexamethylcyclotrisiloxane
D_3^V	1,3,5-trivinyl-1,3,5-trimethylcyclotrisiloxane
D_4	octamethylcyclotetrasiloxane
D_4H	1,3,5,7-tetramethylcyclotetrasiloxane
DMSO	dimethylsulfoxide
HMPA	hexamethylphosphoramide
THF	tetrahydrofuran
T_g	glass transition temperature
T_m	crystalline melting point
DSC	differential scanning calorimetry
TGA	thermal gravimetric analysis
NMR	nuclear magnetic resonance spectroscopy
FT-IR	fourier transform infrared spectroscopy
GPC	gel permeation chromatography
PDI	polydispersity index
M_n	number average molecular weight
VSM	vibrating sample magnetometry
TEM	transmission electron microscopy
PEO	poly(ethylene oxide)
PDMS	polydimethylsiloxane
PHTH	poly(methyl-3-propylphenoxyphthalonitrile)
PMHS	poly(methylhydrosiloxane)

List of Figures

List of Tables

CHAPTER 1 Introduction

The design, synthesis and characterization of well-defined, macromolecular magnetic nanoparticle complexes has been the focus of our research for many years.[1-4] Methods to stabilize dispersions of the polymer-nanoparticle complexes in both aqueous and organic media have been investigated wherein cobalt nanoparticles were coated with polysiloxanes[1-3] or polystyrenes[5]. The iron oxide nanoparticles have been coated with biocompatible polymers such as polydimethysiloxane[4], poly(L-lactide), and poly(ethylene oxide)[6].

The utilization of cobalt nanoparticles in biotechnological applications has been limited due to the oxidative instability of the transition metal nanoparticle surfaces. Once oxidized, the cobalt complexes substantially lose the magnetic properties. Therefore, the first chapters of this dissertation discuss methods to protect the cobalt nanoparticles against surface oxidation.

Previous investigations into preventing oxidation of the cobalt have involved poly(dimethylsiloxane-*b*-[methylvinyl-*co*-methyl-2-ethyltrimethoxysilylsiloxane]) (PDMS-*b*-[PMVS-*co*-PMTMS) as a dispersion stabilizer.[3,7,8] It was found that annealing the copolysiloxane-cobalt complexes at high temperatures formed a siliceous shell around the complexes. In addition, the elevated heat treatments substantially increased the magnetic susceptibility of these materials. The siliceous surfaces provided a substrate that could be re-fucntionalized with a variety of macromolecules.[7] However, the surfaces were not sufficient for preventing oxidation after the nanoparticles were mechanically ground to minimize aggregates. Investigating the magnetic properties and surface properties were key to understanding the materials which is discussed in chapter 3.

Research by Baranauskas et al. suggested that forming cobalt nanoparticle shells from poly(styrene-*b*-4-vinylphenoxyphthalonitrile) (PS-*b*-PVPPHTH) dispersion stabilizers resulted in a graphitic surface that efficiently protected the cobalt surfaces from oxidation.[5,9] However, those graphitic surfaces could not be functionalized, and thus the complexes were not dispersible after formation of the graphite coatings at elevated temperatures. Therefore, a copolymer shell precursor was designed to combine the advantages of the PDMS-*b*-[PMVS-*co*-PMTMS] and the PS-*b*-PVPPHTH shell precursors. The family of copolymers discussed in this dissertation is comprised of poly(methyl-2-propyl-2-phenoxypthalonitrilesiloxane-*g*-styrene) (PHTH-PS) graft copolymers wherein the backbones are polysiloxanes with pendent phthalonitrile groups, and where each chain has an average of approximately one polystyrene graft (figure 1.1). The synthesis and characterization of these graft copolymers will be discussed in chapter 4. Chapter 5 will discuss the preparation of cobalt ferrofluids templated from the PHTH-*g*-PS graft copolymers in solution. In addition, a discussion of their surfaces and magnetic properties after elevated heat treatments is provided in chapter 5.

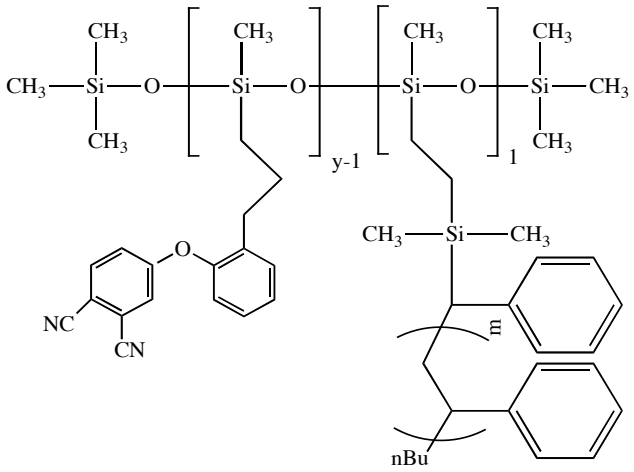

Figure 1.1 Chemical structure of a PHTH-*g*-PS graft copolymer utilized as a cobalt shell precursor

The ability to disperse magnetic iron oxide nanoparticles in aqueous media is desired for biomedical applications. Previous work in our laboratories focused on triblock copolymers compromised of poly(ethylene oxide) tail blocks and a center polyurethane block containing pendent carboxylic acid groups.[6] A method in which the concentrations of carboxylic acids could be precisely controlled is the focus of chapter 6. A series of vinylsilylpropyl alcohol initiators for the polymerization of ethylene oxide were prepared via several chemical modifications. These vinyl functional PEO oligomers were further modified to contain carboxylic acid functionality in precise amounts on one chain end (figure 1.2).

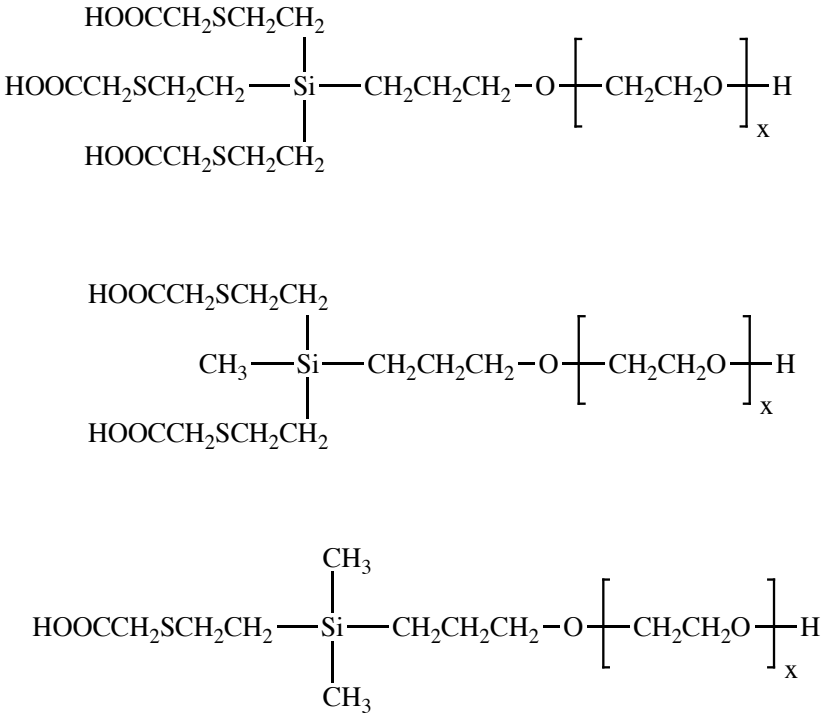

Figure 1.2 A series of carboxylic acid terminated poly(ethylene oxide)s as possible magnetite dispersion stabilizers.

CHAPTER 2 Literature review

2.1 Overview

This literature review will discuss areas directly related to the research topic and is divided into four sections. The first section presents an overview of the chemistry of silica surfaces. Surface functionalization reactions with aminoalkylalkoxysilane coupling agents will be discussed in the second section. Polysiloxane chemistry is presented in section three as it pertains to the synthesis, properties, and applications of polymethylhydrosiloxane and its copolymers. An overview of poly(ethylene oxide) is provided in the fourth section including a discussion of its functionalization and utilization as a dispersion stabilizer for magnetite.

2.2 Silica: Preparation and Surface Properties

Silica is defined as having the formula SiO_2 or $SiO_2 \bullet xH_2O$, where x is the degree of hydration on the silica surface. Silica has a structure in which each silicon atom is bonded to four oxygens, and each oxygen atom is bound to two silicons. Each silicon is at the center of a regular tetrahedron of oxygens. Silica is a solid at ambient temperature with a high melting point (~1700 °C), a density of 2-3 g cm^{-3}, and a refractive index in the range of 1.5-1.6. Naturally occurring silica is mostly crystalline whereas synthetic silica is mainly amorphous depending on temperature, pressure, and degree of hydration. Amorphous silica can be in the form of colloidal silica or silica sols, silica gels (hydrogels, xerogels, and aerogels), pyrogenic silicas (aerosols, arc silicas, and plasma silicas), and precipitates (formed by the precipitation of silicic acid solutions).[10] Only synthetic silica pertaining directly to this research will be discussed herein.

2.2.1 Synthesis of Colloidal Silica via Sol-Gel Methods

The most investigated synthetic method for the preparation of silica is via sol-gel routes. Brinker and Scherer defined sol-gel as the fabrication of ceramic materials by the preparation of a sol, gelation of the sol, and removal of the solvent.[11] They defined a sol as being a colloidal suspension of solid particles in a liquid, analogous to an aerosol which is a colloidal suspension of particles in a gas. The sol-gel process involves precursors for the preparation of colloids that consist of metal or metalloid elements surrounded by various types of ligands. Metal alkoxides belong to a family of organometallic compounds which contain an organic ligand attached to the metal or metalloid element. The most common example of silyl alkoxides is tetraethoxysilane (TEOS), $Si(OC_2H_5)_4$.[12] Ebelman first reported the implementation of TEOS in a sol-gel process in 1846.[13] He observed monolithic products resulting from the hydrolysis and condensation of TEOS over several months. In the 1930's, Geffcken recognized that oxide films could be prepared from silyl alkoxides.[14] Schroeder further supported this methodology in his reviews of Geffcken's work in the late 60's.[15] During the 1960's and 1970's, the ceramics industry focused on gels formed from the controlled hydrolysis and condensation of alkoxides. Multi-component glasses were independently developed by Levene and Thomas[16], and Dislich.[17]

Sol-gel reactions of organometallic precursors are usually conducted in an inert solvent or an alcohol (such as the parent alcohol, ethanol), as opposed to water due to incompatibility of TEOS with H_2O (figure 2.1). However, the products depend largely on the reaction medium.[18,19] The concentrations of catalyst, solvent, water, and TEOS also influence the product structure.[12]

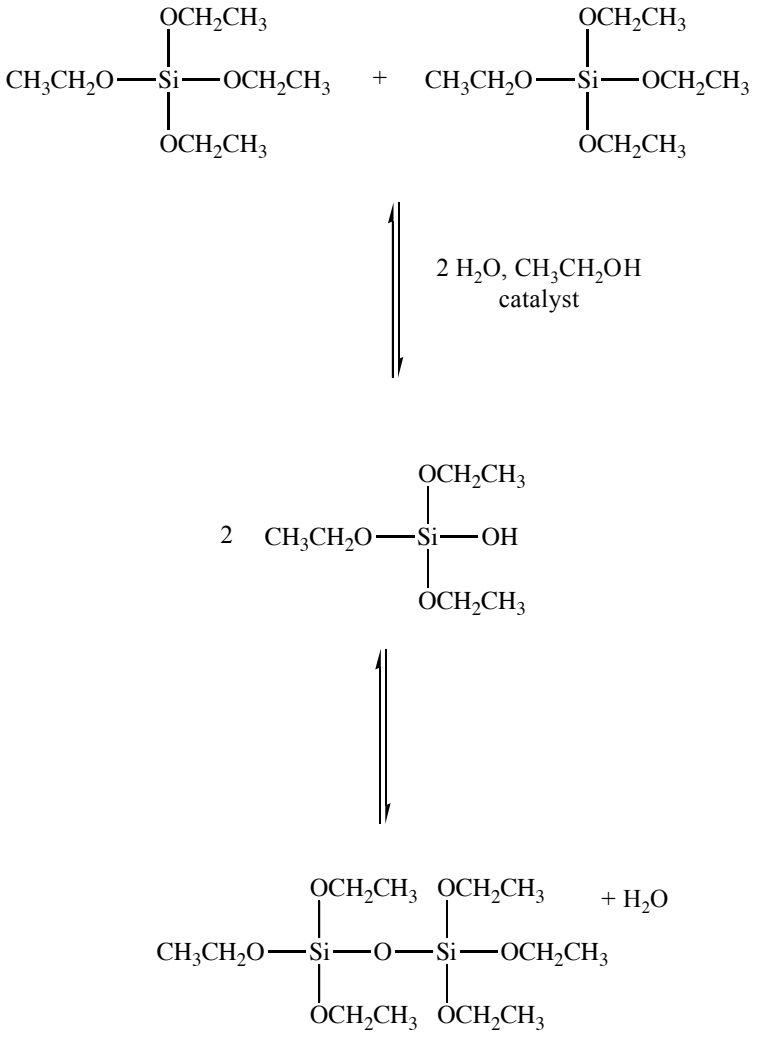

Figure 2.1 Hydrolysis and condensation reactions of TEOS performed in ethanol with stoichiometric concentrations of water. The catalyst may be either an acid or base.[20]

The tetravalent silicon monomer can have one to four hydrolyzable -OR groups. The process occurs via two main pathways, hydrolysis and condensation, to produce the desired silica network. The reactions of TEOS proceed by producing trialkoxysilanols, dialkoxysilanediols, and alkoxysilanetriols. Processing methods for such materials involve densification of the intermediate gels with elevated temperature treatments (200 – 400 °C) (figure 2.2).[21]

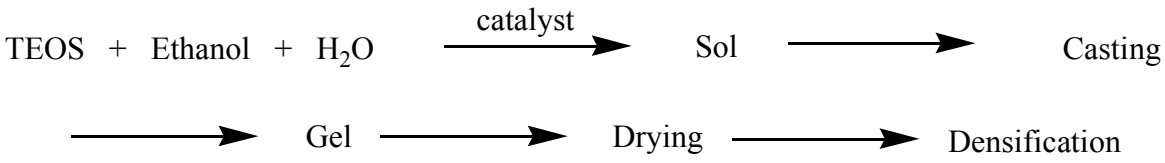

Figure 2.2 Processing of a TEOS-ethanol-water system.[21]

The sol-gel process for siloxane and silicate formation proceeds via hydrolytic condensation of an alkoxysilane, often conducted in the parent alcohol of the alkoxysilane (figure 2.1).[20] These hydrolytic condensations are catalyzed by metal salts, acids, or bases.[22] Acid- and base-catalyzed reactions are more common than those catalyzed by metal salts. However, when room-temperature, mild, neutral reaction conditions are needed, metal salts such as dibutyltin diacetate or dibutyltin dilaurate can be utilized. There have been several studies of attempts to understand hydrolysis and condensation reactions in aqueous media.[23,24] These investigations were not conclusive due to the difficulty in separating the hydrolysis from the condensation reactions. Therefore, Pohl and Osterholtz et al. utilized fundamental S_N1 and S_N2 mechanisms to explain the *hydrolysis*. Bimolecular nucleophilic substitution reactions were also utilized to explain

both acid-catalyzed and base-catalyzed *condensation* reactions. All of the reactions are assumed to be in dynamic equilibrium.

2.2.2 Synthesis of Pyrogenic Silica

High temperature processes are also useful in preparing silica in addition to their liquid, low-temperature counterparts. Three synthetic methodologies are typically utilized for high temperature silica formation: flame, arc, or plasma techniques. The most widely employed source of pure silicas involves pyrolysis of $SiCl_4$ with hydrogen and oxygen (figure 2.3).

$$2\,H_2 + O_2 \longrightarrow 2\,H_2O$$

$$SiCl_4 + 2\,H_2O \longrightarrow SiO_2 + 4\,HCl$$

$$2\,H_2 + O_2 + SiCl_4 \longrightarrow SiO_2 + 4\,HCl$$

Figure 2.3 Preparation of pyrogenic *fumed silicas* (Aerosil®,[25] Cab-O-Sil®)

Arc silicas are produced by the reduction of high-purity sand in a furnace. This class of silicas usually has a larger particle size distribution as compared to other pyrogenic silica products. Ultra-fine silica powders are synthesized by volatizing sand in a plasma jet (plasma silicas). The surface area and aggregate size (4-20 nm) of the agglomerates depend on the synthetic conditions. Silica formed at lower flame temperatures (e.g., 1200 °C) usually has a high surface area resulting from surface roughness.[26,27] Hurd et al. also investigated the pyrolysis of hexamethyldisiloxane and its products. Morphological differences were observed between aggregates and primary particle size in different regions of the flame.

2.2.2.1 Polymer Route to Silicon-Carbide Formation: High Temperature

The sol-gel or solution methods to prepare silica ceramics can lead to monolithic particles, fibers, or coatings. Oxide ceramics are primarily produced from the sol-gel method, whereas siliceous networks, in the form of either coatings or fibers, are often obtained from high temperature pyrolyses of polymers. These high temperature treatments (500 – 1000 °C) can yield non-oxide ceramics such as carbides and nitrides.[28,29]

Yajima et al. first reported the formation of silicon carbide via polymer pyrolysis.[30] Their work describes the formation of polycarbosilane derived from pyrolysis of polydimethylsilane. Silicon alkoxides with a source of carbon have been utilized to produce silicon carbide by carbothermal reduction of silica.[31] Babonneau et al. investigated dimethyldiethoxysilane as a precursor for Si-C-O networks. Silicon oxycarbides were obtained when gels, formed from silicon alkoxides, were heated above 900 °C. The presence of Si-C bonds was revealed by ^{29}Si MAS NMR. The pyrolysis products at these temperatures consisted of silicon carbide, silica, and carbon. The relative amount of each component depended on the conditions during the heat treatment. Cleavages of Si-C bonds occurred at 300 °C and were converted to Si-O bonds, forming a silica network. However, residual Si-C bonds remained until above 900 °C.[28] Pyrolyses of metal oxide ceramics from a combination of polydimethylsiloxane, tetraethoxysilane, and triethylborate have also been reported. Silicon-carbide glasses after high temperature treatments in inert atmosphere are obtained as pyrolysis products.[32]

Other investigations of pyrolysis effects on silicon oxide structures in the presence of a metal catalyst were conducted by Bourget et al.[33] Silicon loss was observed during pyrolysis. This loss was dependent on the nature of the metal catalyst and oxygen donor that were utilized during the sol-gel preparation of the material. $FeCl_3$ seemed to catalyze the most loss of silicon during pyrolysis whereas $TiCl_4$ in the system retained the most silicon.

2.2.3 Silica Surfaces and Adsorption

2.2.3.1 Silica Surface

Sol-gel reactions of alkoxysilanes produce silica gel dispersed throughout the whole solution in which it is prepared.[34] Amorphous silica gels are sometimes viewed as polymers formed by randomly oriented and coiled chains. The chains are comprised of SiO_4 tetrahedra where OH termini occur periodically.[35]

The siloxane bond is robust with a Si-O bond energy of approximately 127 kcal mol^{-1}.[36] Si-O bonds only cleave homolytically at elevated temperatures. The thermal stability results from the electronic configuration of the network. The oxygen has two unpaired *p* electrons in the $2p_y$ and $2p_z$ orbitals and the silicon possesses empty *d* orbitals. A pronounced π component is superpositioned over σ bonds resulting in an overall increase in the energy of the bonds, yielding high thermal resistance.[37] However, the siloxane bond in silica is susceptible to cleavage by acids, bases, and water. Water, in addition to other acids or bases, can cleave this bond (figure 2.4).

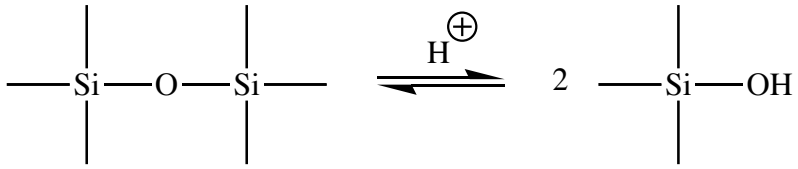

Figure 2.4 Siloxanes are cleaved under acidic and basic conditions.[34]

Silanol surface groups result from incomplete condensation during silica synthesis. The most suitable atom to complete surface oxygen bonding is the proton abstracted from surrounding water molecules in the preparation medium. Electronic effects from the high polarizability of the oxygen as compared to silicon allow for the oxygens to rest further from the surfaces than those of near-surface silicon atoms.[38] Brunauer et al. determined a surface energy value of 129 ± 8 ergs cm^{-2} which is only slightly higher than the surface energy of water, 118.5 ergs cm^{-2}.[39] Iler et al. suggested that the surface energy of SiO_2 and H_2O should be considerably similar if the hydroxyls rest above the silica matrix and the silicon atoms are held below the OH groups.[20,40]

The number of silanol groups present on the surface is highly dependent on preparation method and the degree of hydration of the surface. It ranges from 5 nm^{-2} for fully hydrated silica surfaces to 2 nm^{-2} for non-rehydrated Aerosils.[41] High temperature treatments above 450 °C yield approximately 1 silanol nm^{-2}.[42] In contrast, high concentrations of silanol groups (from 20-30 nm^{-2}) may be obtained on "precipitated silica".[43]

Several different types of silanols can exist at the surface of silica. They vary in the number of bonds between the silicon atom and the solid as well as in the coordination number of the silicon atom with hydroxyl groups. They may exist as pairs or isolated groups with singly, doubly, or triply linked Si tetrahedra (figure 2.5).

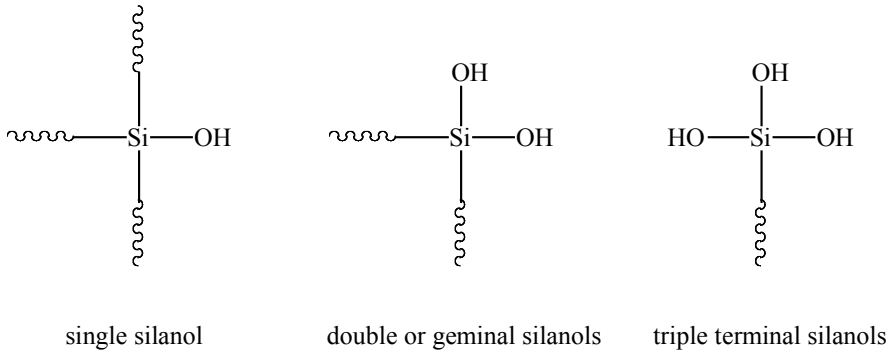

single silanol double or geminal silanols triple terminal silanols

Figure 2.5 Schematic of silica surface silanol groups.

The reactivity of the solid silica surface in wet media is largely determined by the pH. Below the isoelectric point (acidic solutions, < pH 2), protonation of the silanol occurs and the surface acquires a positive charge, acting as an ion exchange material.[44] Silica surfaces are mostly deprotonated above the isoelectric point (> pH 3) adopting a negative charge, and these surfaces can serve as cation adsorption sites.[45] The surface hydroxyls are characterized as weak acids and weak bases (figure 2.6).

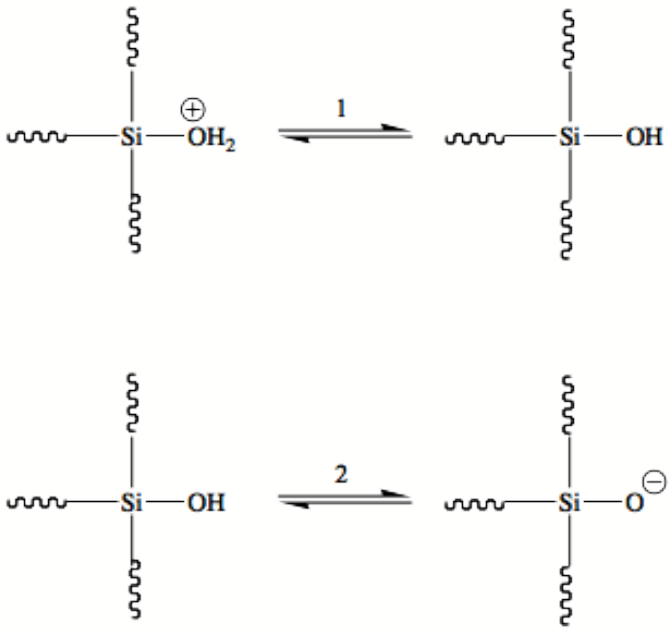

Figure 2.6 Dissociation reactions for silica: 1) $pK_a = 1.9$[44], 2) $pK_a = 7$[45]

2.2.3.2 Surface Reactivity

Surface hydroxyls may undergo several key physical or chemical reactions that ultimately yield a functionalized surface. The reactivity differences on the silica surface are dependent on the non-uniform distribution of hydroxyl functionality. Reactivity differences are attributed to the reactivity of an isolated OH versus that of a group of silanols perturbed by mutual hydrogen bonding.[38] The surface functionality demonstrates a strong dependence on the method by which the underlying matrix was formed.

One reaction involves displacement of hydrogen from the silanol groups by metal salts such as $AlCl_3$, $TiCl_4$, $FeCl_3$, and $SiR_{(4-x)}Cl_x$. Reactivities of alcohols (carbinols) with the silanol surface have also been investigated. The reaction can involve free or hydrogen bonded silanol groups, and the particular silanol species which react can depend on the carbinol size. For example, methanol was found to react with both types of silanol species[46] whereas *t*-butanol reacted only with isolated silanols.[47] The reaction

differences were attributed to steric effects due to the size of *t*-butanol versus methanol. It was concluded that primary alcohols react with a silanol surface to a somewhat greater extent than secondary alcohols.

2.3 Surface Functionalization with Silane Coupling Agents
2.3.1 Physisorption and Condensation of Aminoalkylsilanes on Silica Gel

Modifications of silica surfaces are industrially important due to the widespread use and applications of silica. Much research on silica surface functionalization has focused on the use of aminoorganosilanes. These functional silanes are special members of the alkoxysilane group.[48] They differ from general organosilanes in that they possess an amine group bound to a carbon on the organic chain. The three most widely studied aminosilanes are listed in figure 2.7.[22] The chemical behavior and reactivity of aminoalkylsilanes is attributed to the electron rich amine group. The nitrogen can hydrogen bond with proton donors such as hydroxyls or other amines and is moderately basic with the corresponding ammonium ions having a pK_a of ~10.8.[10,49] This is the pH where the quaternized aminoalkylsilyl group loses a proton to form a primary amine.

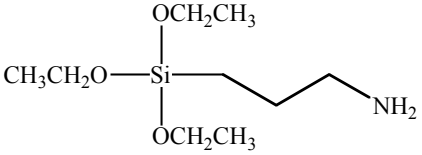

APTS, γ-aminopropyltriethoxysilane

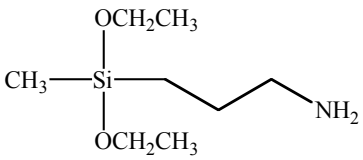

APDMS, γ-aminopropyldiethoxymethylsilane

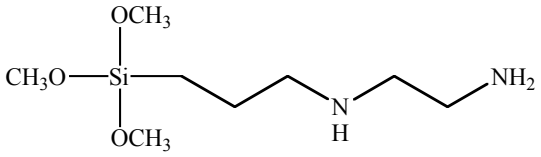

AEAPTS, N–*B*–aminoethyl-γ-aminopropyltrimethoxysilane

Figure 2.7 Aminoalkylsilane coupling agents[22]

Aminoalkylsilane coupling agents can be synthesized by various techniques. Silicon hydrides, such as triethoxysilane, can be reacted with allylaminotrimethylsilane in ethanol with the addition of chloroplatinic acid (Speier's catalyst) to promote the hydrosilation reactions. The primary product of the hydrosilation is 3-triethoxysilylpropylaminotrimethylsilane (figure 2.8). Other by-products can include hydrogen gas as well as the reverse-addition hydrosilation product. The Si-N bond of the intermediate reacts with ethanol to form the final product, 3-aminopropyltriethoxysilane.[50,51]

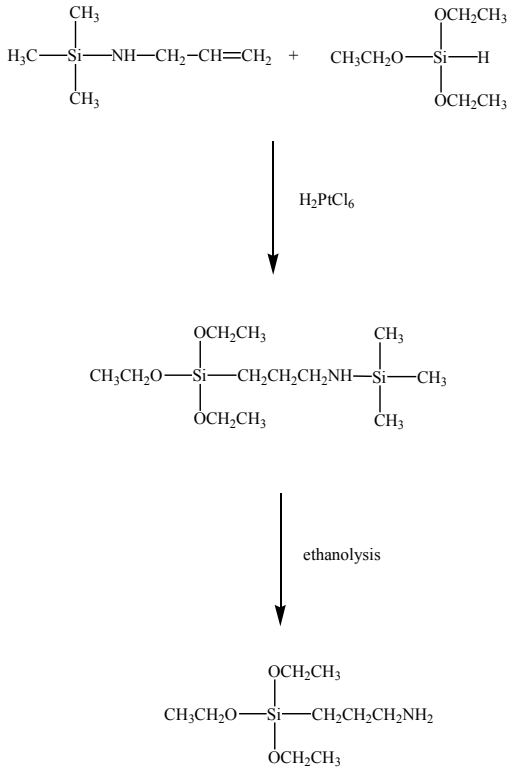

Figure 2.8 Synthetic scheme for the preparation of aminopropyltrialkoxysilanes

The mechanism for covalent coupling of aminoalkyltrialkoxysilanes to the surface of silica has been well-studied. The aminoalkylsilane undergoes fast adsorption onto silica gel by a hydrogen bonding mechanism of the amine to a surface silanol. The amine self-catalyzes the condensation reaction of the alkoxysilane with the silanol by a series of proton transfers (figure 2.9). At long reaction times and high aminosilane concentrations, non-hydroxyl adsorption has been observed with the first monolayer remaining chemisorbed after washing. Four types of interactions can exist on the surface: hydrogen bonded amines, ionic ammonium siloxanolates, chemically bonded amines or physically bonded amines.[48,49]

These self-catalyzed reactions allow for the formation of siloxane bonds in the absence of water.[52] If these reactions are performed in aqueous media, the hydrolyses are uncontrollable and this leads to polymerization of the aminoalkoxysilanes. Organic solvents are preferred for these chemical modifications in order to better control the reaction parameters. It has also been shown that high concentrations of surface hydration leads to condensation and polymerization of the aminoalkylalkoxysilane and is generally not preferred. In anhydrous organic media, the aminoalkoxysilane can also physically adsorb onto the substrate surface. Therefore, it is necessary to increase the reaction temperature substantially in order to drive the chemical reaction and the formation of chemical bonds between the substrate and aminoalkoxysilanes.[53,54]

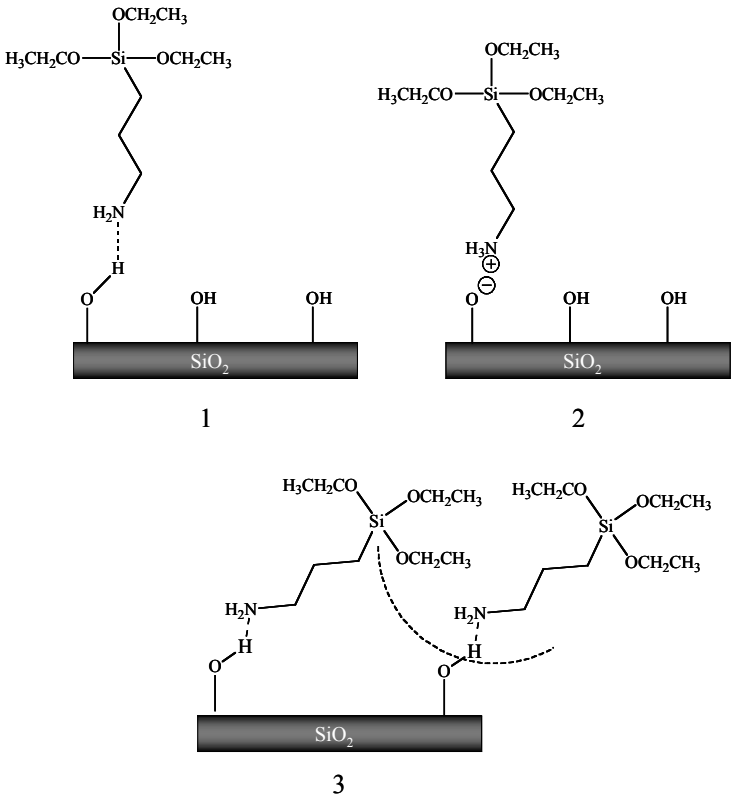

Figure 2.9 Surface-aminoalkylsilane interactions: 1) hydrogen bonding, 2) proton transfer, and 3) condensation to siloxane

2.3.2 Aminoorganosilanes as a Route to Formation of Biocompatible Microparticle Coatings

The ability to chemically modify surfaces using silane coupling chemistry provides a means for coating these surfaces with biocompatible polymers such as polypeptides, polylactides, and polysiloxanes. The primary focus is divided into three parts: 1) aminoalkyltrialkoxysilane coupling to afford reactive surfaces for biocompatible coatings, 2) core-shell particles developed from surface-bound amine initiation and polymerization of polylactides and polypeptides, and 3) polysiloxane or poly(ethylene oxide) grafts.

2.3.2.1 Aminoalkyltrialkoxysilane surface coupling for the formation of biocompatible coatings

As discussed in section 1.3.1, silica surfaces can be functionalized with amine groups through coupling reactions. However, the coupling of aminoalkyltrialkoxysilanes is not limited solely to silica-silanol surfaces. The surface functionalization of magnetite (Fe_3O_4) with aminopropyltriethoxysilane has also been explored.[55] Energy dispersive X-ray spectroscopy (SEM-ED) suggested a near-monolayer coating of aminosilane on the surface (calculated from atomic ratios). Further analysis by FT-IR supports successful functionalization of the magnetite surface. Stretches and bends corresponding to Si-O, C-N, and C-H bonds were evident in the IR spectrum. Ming et al. also described linking the enzyme horseradish peroxidase (HRP) to the surface of the aminoalkylsilyl-coated magnetite.

In addition, aminoalkyltrialkoxysilanes have been reacted with surface groups on magnetite nanoparticles to prepare precursors to water-soluble biocompatible polymer-magnetite complexes. Muhammed et al. modified the surface of magnetite with aminopropyltrimethoxysilane under anhydrous conditions where approximately two or three molecular layers of tightly cross-linked silica with a large surface density of amines resulted.[56,57] These amine functional magnetite nanoparticles were subsequently coupled with monomethoxy terminated poly(ethylene glycol) (PEG). The PEG coating was verified by X-ray diffraction patterns and thermal gravimetric analysis.

Amine functional-magnetite nanoparticles have also been coupled with *N*-hydroxysuccinimide-terminated-PEG.[58] Intracellular uptake of these PEG-modified magnetite nanoparticles for biomedical applications has been investigated. This work also focused on utilizing fluorescent labels (fluorscein-labeled-PEG) to track these

nanoparticles, and they studied their use for breast cancer treatments (figure 2.10). Fluorescence measurements showed that these PEG-modified nanoparticles were internalized by the breast cancer cells, but the nanoparticles did not disrupt normal bio-function, and this suggested their biocompatibility. Data also suggested that the magnetite modification with PEG increased intracellular uptake partially due to the PEG-mediated solubilization of the nanoparticles in the cell membrane lipid bilayer.

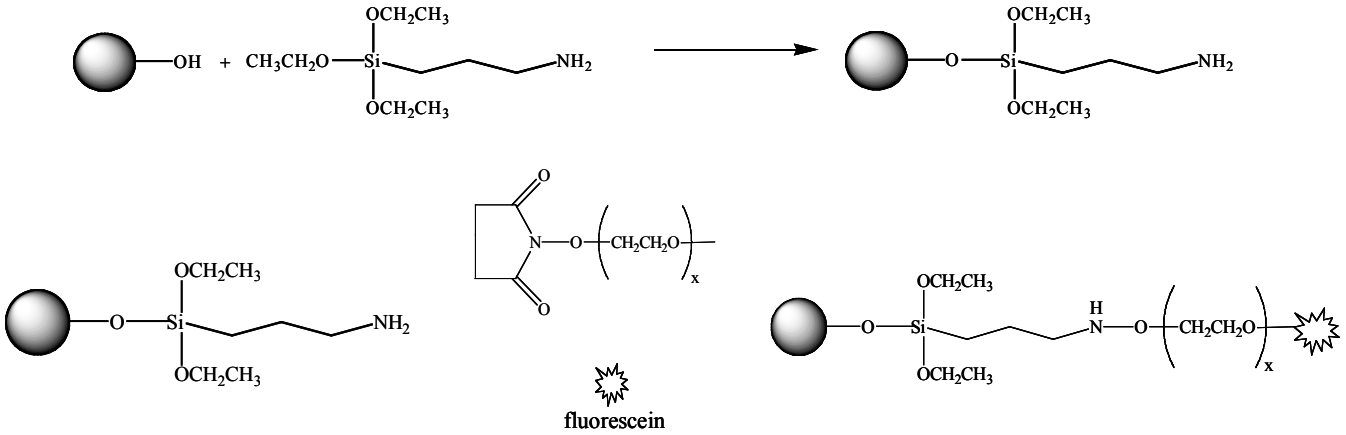

Figure 2.10 Functionalization of magnetite nanoparticles with aminopropyltriethoxysilane and fluorescent-labeled PEO.

Amine-functional silica nanoparticles have also been investigated as novel therapeutic delivery systems.[59] Utilizing acid/base chemistry, an overall positive zeta potential was achieved on the surface attributed to positive charges on the amine groups. DNA (with an overall negative charge) was bound with the positively charged particles. The cationic nanoparticles served as biocompatible carriers of DNA for gene delivery. In recent work by Healey et al., *N*-(2-aminoethyl)-3-aminopropyl-trimethoxysilane was utilized as the primary aminoalkylsilane coupling agent. Their work focused on forming a maleimide-activated surface amenable to tethering molecules with a free thiol (e.g.,

cysteine). This was created by coupling sulfosuccinimidyl 4-(N-maleimidomethyl)cyclohexane-1-carboxylate (sulfo-SMCC) to the terminal amine on *N*-(2-aminoethyl)-3-aminopropyltrimethoxysilane (figure 2.11). Moreover, polypeptides with terminal cysteine residues were immobilized on the surfaces of the silica particles.[60]

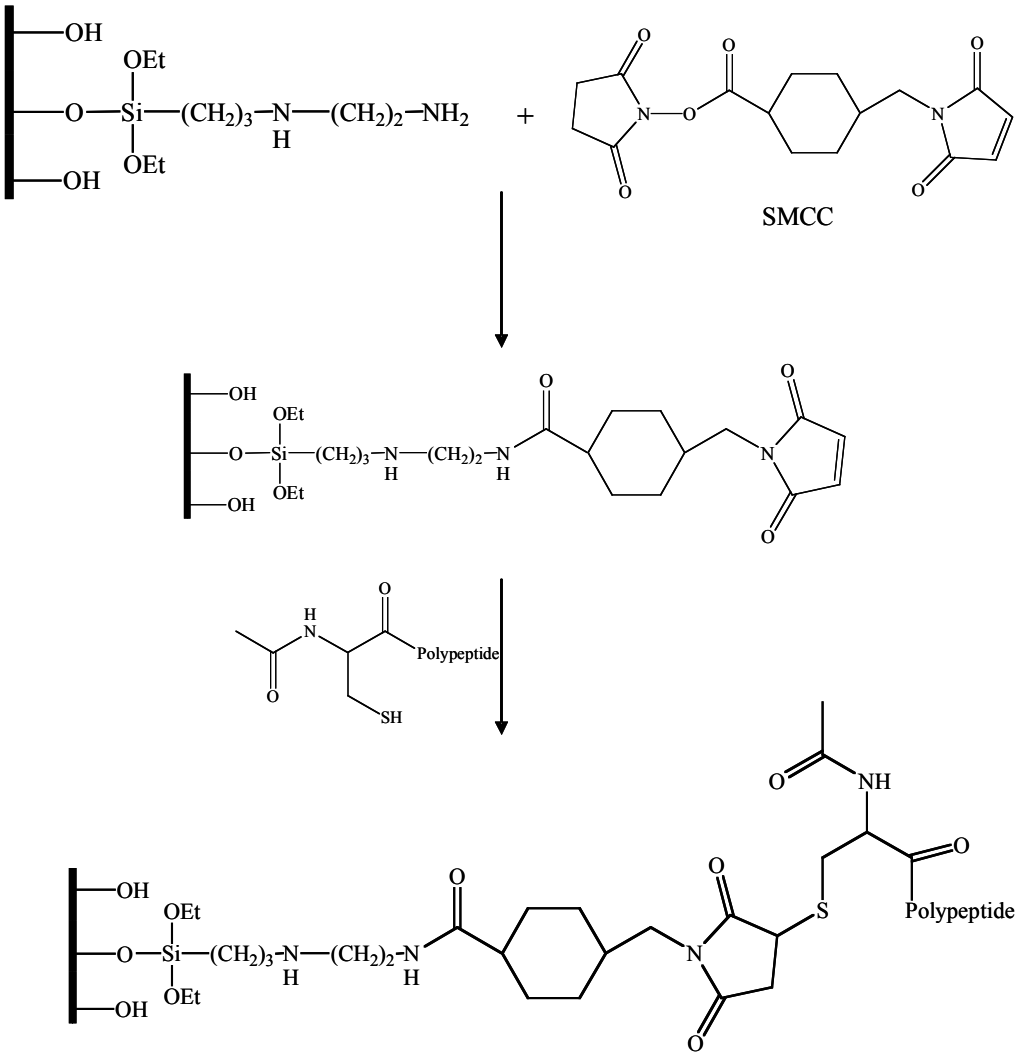

Figure 2.11 Immobilization of polypeptides onto the silica surface through aminoalkylsilane coupling reactions.

2.3.2.2 Core-shell particles developed from surface graft polymerization: amine initiation

Primary amines can serve as initiators for selected ring opening polymerizations. Langer et al. have reported surface initiated polymerization of L-lactide from amine functional silica surfaces using $Sn(Oct)_2$ as a catalyst.[61] They also discussed the polymerization of L-lactide from a carbinol-functional gold surface. The M_n was targeted utilizing the concentration of amines on the silica surface relative to monomer.

Schouten et al. have investigated flat surface graft polymerization of γ-methyl-*L*-glutamate-*N*-carboxyanhydride in the melt from amine-functional silica surfaces.[62] The reaction temperature was maintained above the melting temperature of the monomer (>105 °C). However, these temperatures also allowed for thermal polymerization of the monomer yielding uncontrolled results. The work demonstrated the feasibility of utilizing surface amines as initiators to polymerize grafts of biocompatible polymers from the surfaces of silica substrates. These preliminary results showed feasibility of fabricating a biocompatible proteinaceous coating applicable to other nanoparticle systems.

Surface graft polymerizations of copolyglutamates and copolyaspartates onto silica microparticles have been investigated.[63] It was postulated that surface functionalization of silica microspheres should be more facile than on flat surfaces due to increased surface area. Aminopropyltriethoxysilane was utilized as the coupling agent and served as the primary source of amine surface functionality. *N*-Carboxyanhyrides of glutamate and aspartate were surface-initiated by the amine and polymerized at 40 °C in THF.

2.3.2.3 Polysiloxane grafts

Polymer grafting to the surface may not always occur via covalent interactions. Polydimethylsiloxane (PDMS) has been widely investigated for its ability to hydrogen bond with silanols on silica surfaces to form PDMS-coated silica particles. The propensity to hydrogen bond has been found to be greatest when the degree of hydration is low.[64] The mean number of silanol groups that participate in adsorption is 4 nm^{-2} for specific surface areas equal to 50-150 m^2 g^{-1}. Thomas et al. reported that interactions between PDMS and silica surfaces were greatest when the molecular weights of the polymers were higher.[65] They proposed that some of the PDMS may chemisorb to the surface and the remaining polymer chains irreversibly physisorbed.

2.4 Polysiloxanes

Polysiloxane backbones are comprised of silicon atoms bonded to oxygen. These polymers can be considered as intermediate chemical structures between organic and inorganic compounds, specifically between silicates and organic polymers. The term "silicones" was first coined due to the structural resemblance between R_2SiO and those of "ketones" (R_2CO). However, the Si=O bond is very unstable, unlike the C=O bond in ketones. The term "polysiloxane" was derived from the structure of the repeating unit in the polymer backbone (Si-O-Si).[66] Silicones bring together properties of inorganic and organic materials which give rise to the vast array of industrial applications ranging from aircraft gaskets to auto polishes to construction sealants.[67] Other applications include silicone resins, fluids, room-temperature-vulcanized (RTV's) rubbers, and heat-cured rubbers.

The wide range of applications is attributable to the unique properties of polysiloxanes (table 2.1). These properties result from its inherent chemical structure. The silicon atom possesses *d*-orbitals which are able to accept electron density from other atoms.[68,69] This additional p_π - d_π interaction gives the Si-O bond its partial double bond character, along with its shorter than expected Si-O bond length and the larger than expected (Si-O-Si) bond angle.[69] Organosiloxanes usually have Si-O bond lengths of 1.64 ± 0.03Å, while the interatomic bond length of Si-O is 1.83 Å (calculated from the silicon and oxygen atomic radii) (table 2.2). Thus, the bond lengths are approximately 0.2 Å shorter than expected. The Si-O bond in siloxanes also has a relatively large ionic character of ~40 – 50% with bond orders between 1.2 – 1.5.

Table 2.1 Unique properties of polysiloxanes

Properties
1. Thermal and oxidative stability 2. Low temperature properties. Retention of flexibility, elasticity, or flow at temperatures as low as or even below -110 °C. 3. Low surface tension and high surface hydrophobicity 4. Inertness and biocompatibility 5. Good electrical insulators and resistance.

Table 2.2 Measured siloxane bond lengths

Bond	Mean Distance (Å)
Si-O in PDMS	1.64
Si-O in glass	1.60
Si-O in D_3	1.66
Si-O in D_4	1.65

The bond angle for Si-O-Si varies between 105° and 180° in organosiloxanes. This greatly exceeds the expected valence angle of oxygen in a sp^3 hybridized bond of 109°. The Si-O bond length of PDMS of 1.64 Å allows for the wider valence angles around the Si-O-Si bond due to electron repulsion. This leads to greater flexibility along the polymer backbone and a very low glass transition temperature, T_g, of ~ -123 to -125 °C.[70]

Thermal stability of the Si-O bond is consistent with the high bond strength. The value for the Si-O bond energy has been calculated by Pauling. Table 1.3 lists the values obtained by Pauling for several different Si-X bonds. The heats of formation listed in table 2.3 partially account for the thermal stability of polysiloxanes up to 300 – 400 °C. The p_π-d_π overlap in the Si-O bonds also plays an important role here. The Si-O bond has substantial ionic character and has higher bond strength than that of Si-H or Si-C bonds and more p_π-d_π overlap (more double bond character).[66,71]

Table 2.3 Bond dissociation energies for several Si-X bonds.

Bond	Pauling's Bond Dissociation Values (kcal mol^{-1})
Si-O	88.2
C-O	84
Si-C	69.3
C-C	83.1
Si-H	70.4
C-H	98.8

2.4.1 Polymethylhydrosiloxane: Synthesis

Polymethylhydrosiloxane (PMHS) was first prepared by Sauer et al. in 1946.[72] They reported hydrolysis of methyldichlorosilane in ether yielding a mixture of cyclosiloxanes, primarily containing four to six siloxane units (figure 2.12).[71] The linear

polysiloxanes were synthesized by equilibration polymerization of cyclosiloxane monomers at moderate temperatures (60-150 °C) in the presence of excess hexamethyldisiloxane (figure 2.13).[72,73]

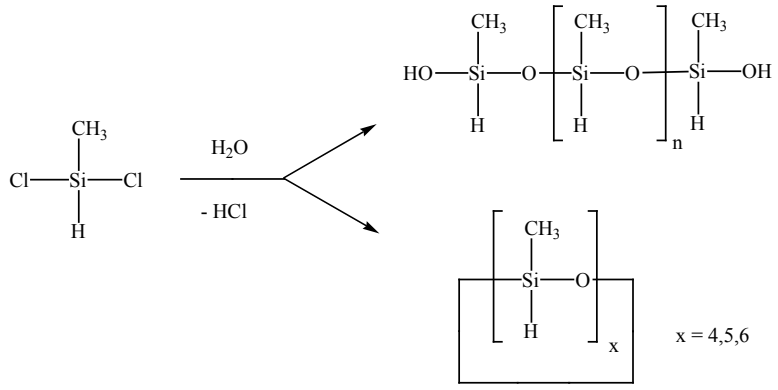

Figure 2.12 Synthesis of cyclic methylhydrosiloxane monomers.[71]

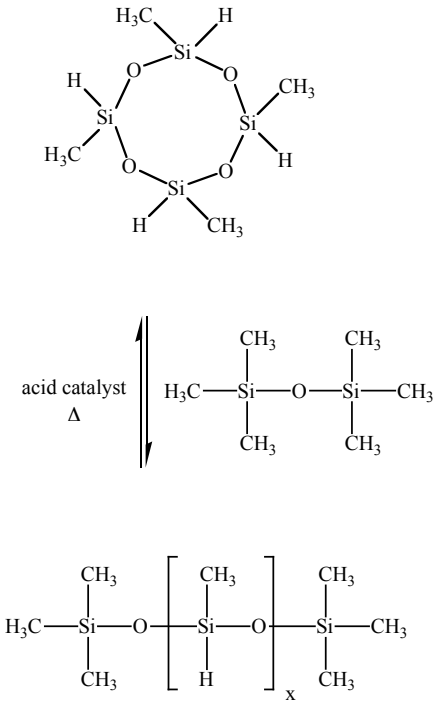

Figure 2.13 Equilibration polymerization of D_4H in the presence of hexamethyldisiloxane to function as an endblocking reagent and catalyst

1,3,5,7-Tetramethylcyclotetrasiloxane (D_4H) can also be copolymerized with 1,1,3,3,5,5,7,7-octamethylcyclotetrasiloxane (D_4) under acidic conditions by cationic ring opening equilibration copolymerization. Hexamethyldisiloxane can be added to function as an endblocking species. Sauvet et al. showed that the thermodynamic equilibrium is established well before any redistribution for certain concentrations of catalyst.[74] They measured M_n and polydispersity indeces at different stages of the reaction in conjunction with measure the persistence ratio. These data suggested that the polymerization rate is much faster than redistribution. Their work illustrated that these copolymers were statistical in chemical sequence due to the rapid redistribution reactions that occurred preventing the formation of block copolymers.

2.4.2 Thermal Stability of Polymethylhydrosiloxane

The thermal stability of alkyl-substituted polysiloxanes is quite high as discussed in section 2.3. Polysiloxanes undergo heterolytic cleavage of the Si-O bonds at high temperatures with a mixture of products obtained from pyrolysis of these polymers. Low molecular weight products of the same composition as the original polymer: six- and eight-membered cyclics that are thermodynamically stable at those temperatures (360 °C for PDMS, onset of degradation) are formed upon thermal degradation.[75] However, it is also possible to cleave the organo-groups bound to the silicon atoms of the backbone. This process usually forms gaseous products accompanied by various crosslinking reactions.[76]

Lenz et al. has proposed three mechanisms for the degradation of PDMS.[77] The first mechanism involved the PDMS chain "unzipping" to monomers. It was recognized that random main chain scission may also occur, and that this could be catalyzed by impurities. However, the mechanistic role in polysiloxane degradation when one methyl group of PDMS is substituted with a hydrido group is largely unknown. Popovic et al. investigated the effect of different substituents on the silicon atom and its correlation to thermal stability.[78] They compared PMHS (M_n 20,000) to PDMS (M_n 20,000). It was found that PMHS begins degradation under inert atmospheres at 320 °C with complete mass loss at 400 °C, much sooner than PDMS (complete mass loss occurs at 650 °C). The work concluded that this earlier degradation was consistent with a depolymerization mechanism.

2.4.3 Chemical Modification of Polymethylhydrosiloxane

2.4.3.1 Hydrosilation Reactions

Chemically modified polysiloxanes play a large role in both academic and industrial sectors. Hydrosilation of vinyl moieties across Si-H bonds is one method to chemically modify polysiloxanes.[79,80] These reactions are usually catalyzed by platinum catalysts or transition metal salts.[81] Hydrosilation results in the formation of new C-C σ-bonds from C=C π-bonds (an exothermic process with a $\Delta H°$ of -33 kcal mol^{-1}).[82] The most common platinum catalysts are H_2PtCl_6 (Speier's catalyst) and $Pt^0 \bullet 1.5[(CH_2=CH(CH_3)_2Si]_2O$ (often marketed with a 2.1-2.4 weight % Pt concentration) (Karstedt's catalyst).[83] Investigations of the catalytic activity of both catalysts found that Speier's catalyst was less reactive than Karstedt's catalyst under similar reaction conditions.[84] The catalytic cycle of a hydrosilation reaction is shown in figure 2.14.

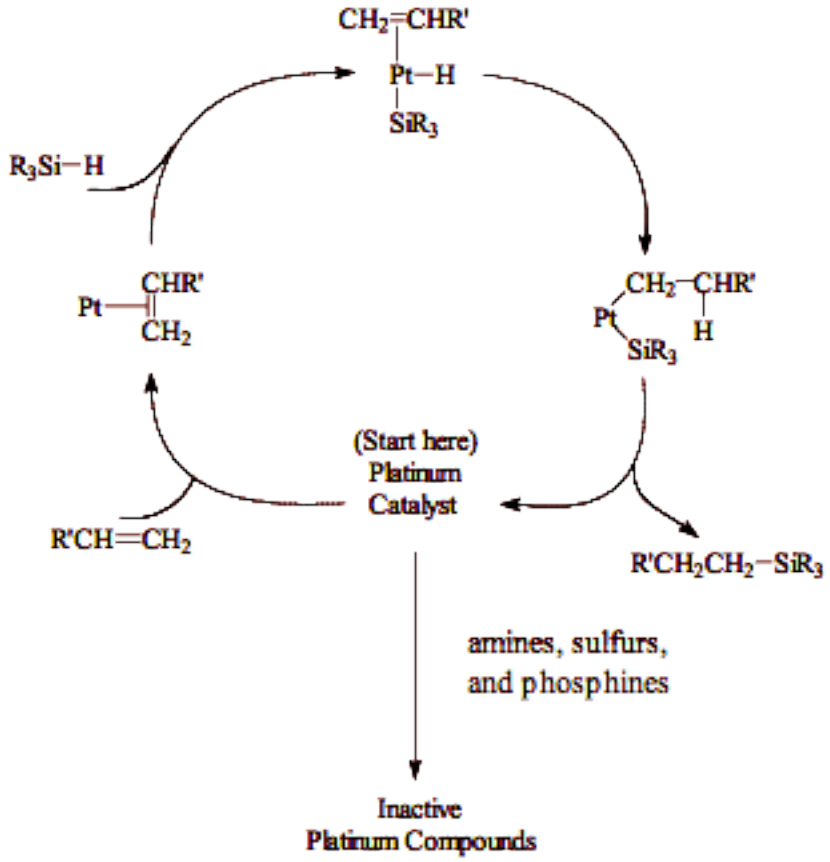

Figure 2.14 The hydrosilation catalytic cycle[83]

The synthesis of hybrid materials is often conducted by the addition of unsaturated derivatives to PMHS. The resultant polymer will have tailored properties which can include increased hydrophilicity, chirality, photo-curable units, or optical activity. Enhanced thermal stability of polysiloxanes has also been reported by hydrosilation of boron containing allyl derivatives.[85] Large groups such as an allyl-derivatized carbohydrates or even polymers lead to increased steric hindrance about the Si-H bond, and this often results in incomplete hydrosilation. Other functional groups including allyl derivatives of nitriles[86] and ethers[87] have been hydrosilated with the Si-H bond of PMHS with complete conversion. Investigations into the most effective

platinum catalyst have also been conducted by Lewandowski et al.[88] Hydrosilations of PMHS with allylchloride and allylnitrile were hydrosilated to PMHS effectively using Karstedt's catalyst. It was found that Speier's catalyst resulted in rearrangement of the allyl bond as well as disruption of the polysiloxane backbone due to the acidic nature of the Speier's catalyst. No change in the average number of repeat units of PMXS was observed using Karstedt's catalyst indicating the hydrosilation reaction did not affect the polymer backbone. This has also been observed by Wnek et al. where functional polysiloxanes were synthesized by hydrosilation of polar groups with pendent Si-H groups on PMHS.[89] These polysiloxanes were fully functionalized leaving no residual Si-H. It is important to note that the PMHS precursors were quantitatively hydrosilated. It is unknown whether partial hydrosilation would lead to subsequent reactions of the hydrosilated nucleophile with remaining Si-H moieties.

Hydrosilation reactions onto PMHS are also useful in fabricating graft copolymers for biomedical applications. Allyl-functional poly(butylene oxide/poly(ethylene oxide) (allyl-PBO-*co*-PEO) has been hydrosilated with PMHS.[90] The presence of allyl-PBO-*co*-PEO copolymer was necessary to decrease the foreign body response *in vivo*. These copolymers showed increased biocompatibility over unfunctionalized PDMS. The hydrosilation reactions were successful and could be tailored to yield a series of graft copolymers with varied concentrations of PMHS:PBO-*co*-PEO.

2.4.3.2 Dehydrogenative Coupling

The unique chemical properties of polymethylhydrosiloxane arise, in part, from the differences in the bond dissociation energies in the backbone of the polymer. The Si-

O bond has much higher bond dissociation energy (88.2 kcal mol^{-1}) than that of Si-H (70.4 kcal mol^{-1}) or Si-C (69.3 kcal mol^{-1}) bonds.[66] The Si atom is less electronegative (1.8) than both H (2.1) and C (2.5) atoms. The Si-H bond is the most polarized in comparison to the Si-C, the Si-O, or even the C-H bond. The polarization of electrons lies towards the more electronegative element: either the H or C in silicon containing compounds, thereby making Si quite susceptible to nucleophilic attack or heteroatom displacement.[66]

The formation of Si-heteroatom bonds via transition metal catalysis is a rapidly emerging field.[91,92] Dehydrocoupling of hydrosilanes with amines in the presence of transition metal catalysts yield linear and/or cross-linked polysilazanes.[93] In addition to amines, hydroxy groups have been utilized to prepare industrial polymers.[94,95] Corey et al. investigated the conversion of n-hexylsilane and dimethylphenylsilane to their respective alkoxysilanes utilizing transition metal catalysis and alcohols (figure 2.15).[94] They reported the effects of steric bulk on the overall reaction. It was generally observed that increasing the steric bulk required longer reaction times and increased reaction temperatures but the alkoxysilane products were still obtained.

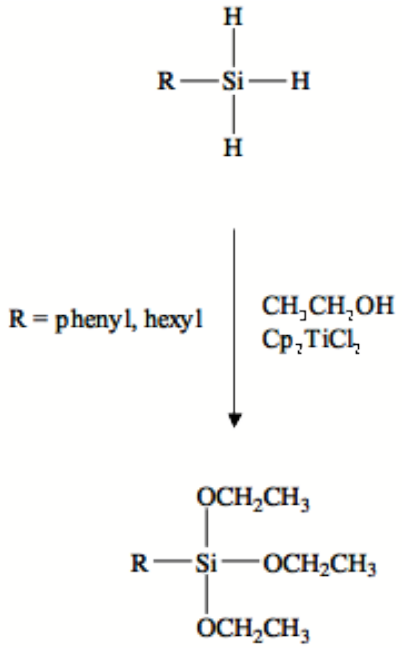

Figure 2.15 Dehydrocoupling via alcoholysis of hydrosilanes to yield alkoxysilanes

Labeling of polymers with fluorescent groups has been of interest for many years, especially for biomedical applications,[58,96] but investigations of fluorescent polysiloxanes have been limited. However, Dias et al. probed the fluorescent properties of the pendent phenyl groups of polymethyphenylsiloxane (PMPS).[97] Fluorescence spectroscopy and ^{1}H NMR were used to investigate fluorescent properties of linear PMPS at temperatures below -50 °C in dilute solution. However, employing the dehydrocoupling reactions explained above, West et al. have synthesized a series of six fluorescent polysiloxanes derived from polymethylhydrosiloxane.[98] Fluorescent alcohols or phenols were utilized in combination with H_2PtCl_6 or Karstedt's catalyst (figure 2.16). These have the potential for use in biomedical applications as fluorescent tags.

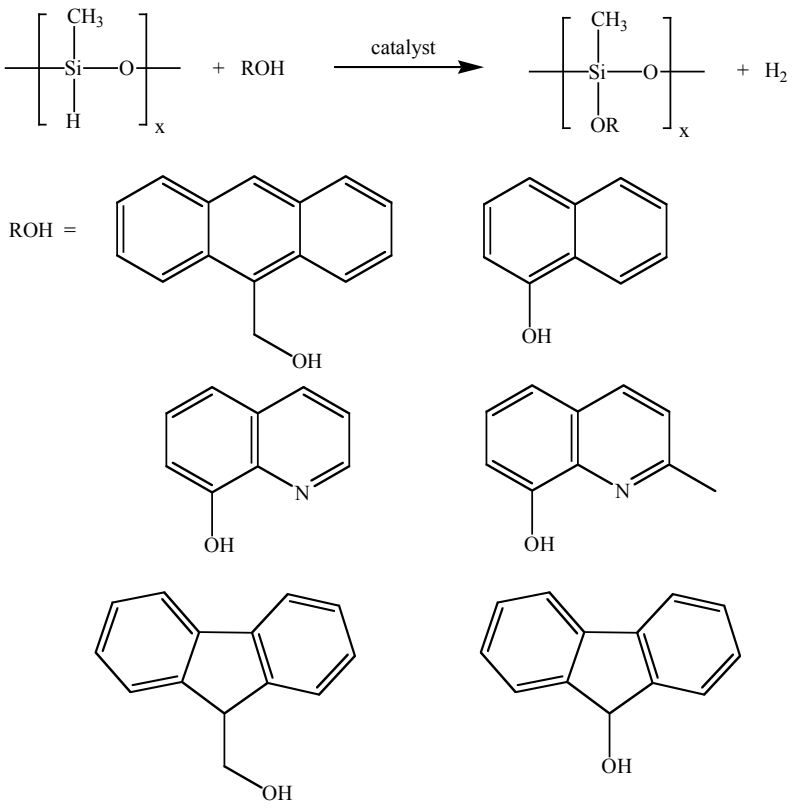

Figure 2.16 Synthesis of fluorescent polysiloxanes

2.5 Poly(ethylene oxide) and applications

Poly(ethylene oxide) (PEO), is a linear or branched polyether typically terminated with hydroxyl groups. It is hydrophilic and biocompatible. The polyether has valuable properties including weak immunogenicity, rapid renal clearance *in vivo*, and resistance to biodegredation. PEO is soluble in both aqueous and organic media. The water solubility is largely due to the binding of 2-3 water molecules to each ethylene oxide unit of the backbone.[99,100]

2.5.1 Ring Opening Polymerization of Poly(ethylene oxide)

Ring opening polymerization (ROP) is a widely used synthetic procedure to prepare homopolymers and random and block copolymers with well-defined molecular weights and architectures. These polymerizations can often be living in nature due to the

relatively stable propagating species relative to carbanions or carbocations. ROP proceeds via three main reaction pathways: cationic, anionic, and coordination insertion mechanisms.[101]

PEO is typically polymerized via anionic ring opening polymerization techniques. These reactions proceed by S_N2 nucleophilic attack of the anionic initiator on the ethylene oxide methylenes. Initiators include hydroxides, alkoxides, oxides, and metal alkyls/aryls such as potassium naphthalene.[101-103] The mechanism for the synthesis of PEO via anionic ring opening polymerization is shown in figure 2.17.

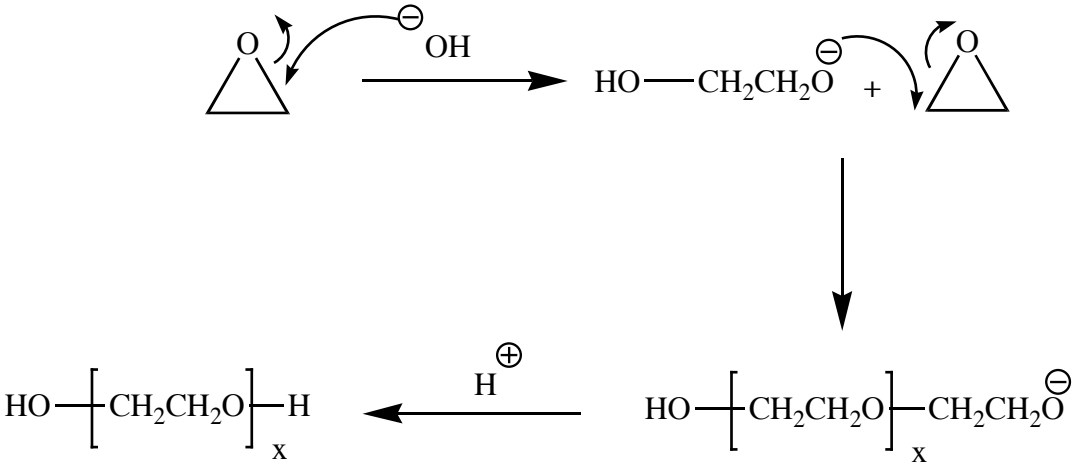

Figure 2.17 Ring opening polymerization of ethylene oxide.

The polymerization of propylene oxide exhibits characteristics of chain growth polymerization in that there can be chain transfer of the propagation center to the monomer and/or solvent (figure 2.18). The propagating alkoxide may occasionally abstract hydrogen from the propylene oxide monomer as depicted in figure 1.18. The resultant species will isomerize to the allyl alkoxide, which leads to polypropylene oxide with only one hydroxy group. This side reaction can hinder the development of a polydiol. This significantly affects the molecular weights and molecular weight

distributions of poly(propylene oxide) oligomers that are initiated by potassium hydroxide.[101]

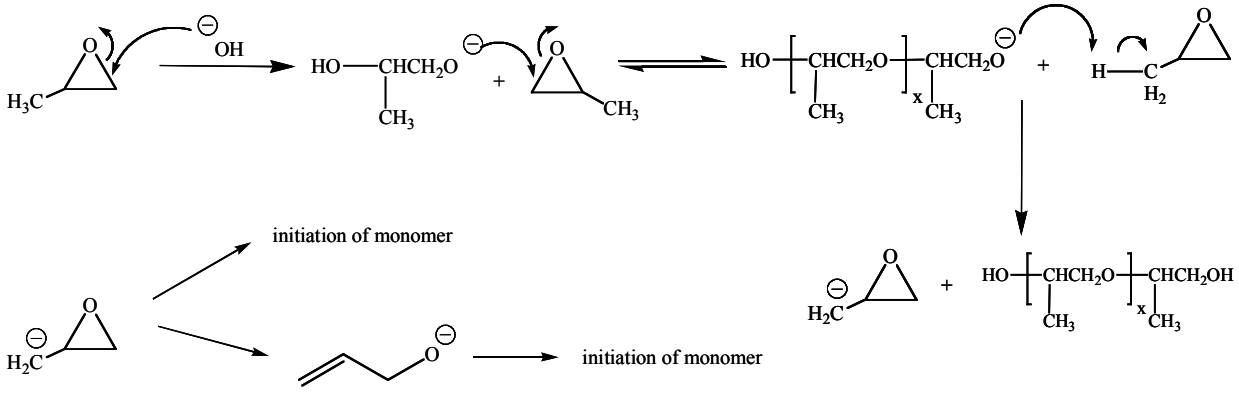

Figure 2.18 Ring opening polymerization and side reactions for propylene oxide.

Epoxide polymerizations can also be conducted utilizing metal catalysts through an anionic coordination mechanism. One example of a class of such catalysts are adducts of zinc such as $Zn(OCH_3)_2$ and $([Zn(OCH_3)_2]_2 \bullet [C_2H_5ZnOCH_3]_6)$.[104] These polymerizations are concerted involving the insertion of the epoxide monomer into a metal-oxygen bond. It is proposed that an alkoxide anion is formed upon cleavage of the oxygen-metal bond (figure 2.19). Thus, the reaction is deemed anionic coordination. These reactions are particulary useful for the polymerization of propylene oxide where the chain transfer to monomer may be avoided and high molecular weight achieved.[104]

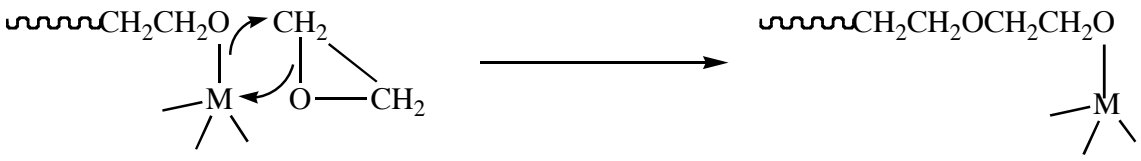

Figure 2.19 Insertion coordination polymerization of ethylene oxide

2.5.2 Poly(ethylene oxide) Derivatization

Poly(ethylene oxide) oligomers and polymers have low immunogenicity and good water solubility, and these properties make it a prime candidate for utilization in biotechnological applications. There are applications in drug delivery, bio-separations, protein modification, and implants (to produce non-fouling surfaces). In order to functionalize a surface or react the PEO with a protein, the PEO is usually derivatized at one or both ends of the molecule. The functional group is tailored to react with the molecule (surface structure or protein amino acid residue) that will be coupled to the PEO. For example, proteins usually contain reactive carboxylic acid or amine functionality in addition to thiol and hydroxyl moieties. Therefore, it is necessary to derivatize the PEO such that the end groups are reactive with these functional groups on the protein.[99] In addition, PEO can be derivatized to contain binding moieties that will interact with metal surfaces.[6]

2.5.2.1 End Group Functionalization of PEO for Amine Conjugation

Conjugation of PEO to biomolecules usually involves an amine group displacing a leaving group located at one terminus of the polymer. These reactions utilize amino acid residues and require mild reaction conditions with the most common coupling reactions involving the alpha or epsilon amine on lysine. A series of different coupling reactions are shown in figure 2.20. Each of these reaction schemes imparts particular leaving groups to the PEO that are tailored for specific amine conjugation or amino acid residues.[99]

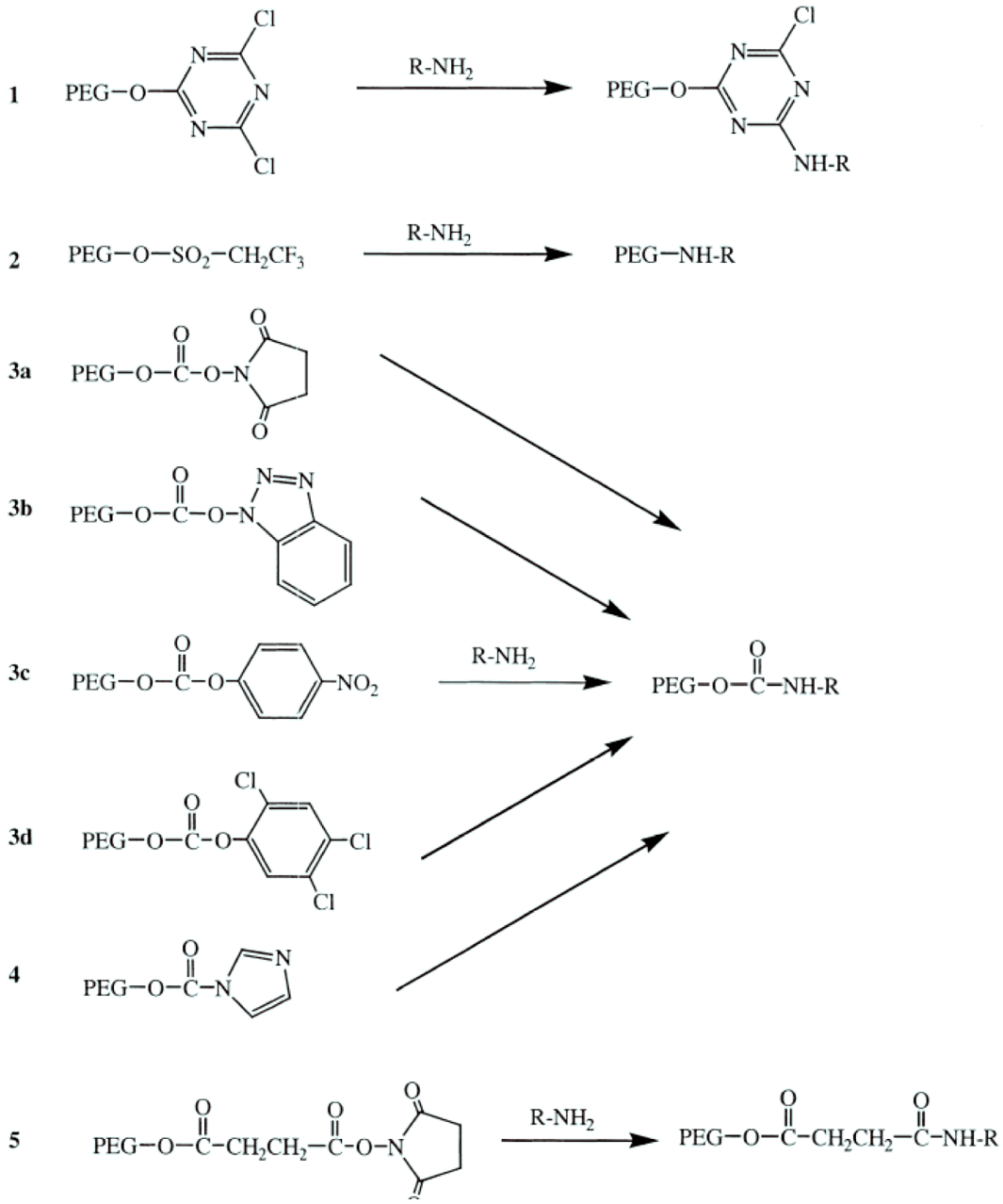

Figure 2.20 End-functional poly(ethylene oxide) and coupling reactions to amines

The derivatization reactions shown in figure 1.20, however, may lack selectivity. For example, the PEO-dichlorotriazine (figure 1.20a) is reactive towards a wide variety of nucleophilic functional groups including lysine, serine, tyrosine, cysteine, and histidine. Reactions with these nucleophiles produce a charged conjugate in the form of a

secondary amine.[105] Cross-linking reactions can also occur with other residues in the protein molecules or with other stronger nucleophiles.[106]

Another methodology of coupling chemistry may be utilized to avoid such reactions as described above. These reactions can be applied to other systems such as amine containing drugs to increase the hydrophilicity of the drug (hydrophobicity is a major problem in drug delivery to date). In addition, the tosylation of the hydroxyl end of PEO can create a substrate that is easily displaced by an amine nucleophile (figure 2.21). The tosylation reaction is more free from side reactions and has been shown to achieve 100% conversion of hydroxyl groups to tosylates.[107]

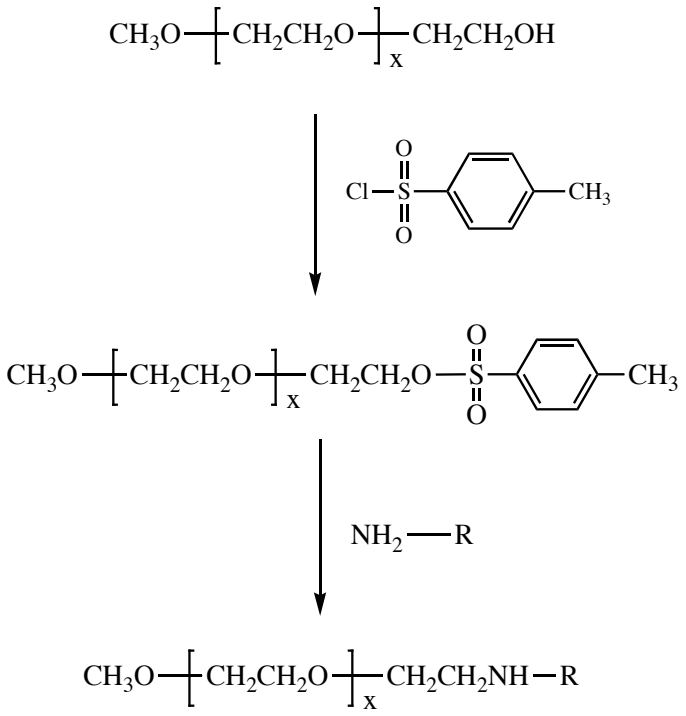

Figure 2.21 Amines can displace the tosyl group on the end of poly(ethylene oxide)

2.5.2.2 Carboxylic Acid Functional Poly(ethylene oxide)

In addition to amine functionality, PEO can be derivatized with terminal carboxylic acid groups via a variety of synthetic methodologies. Jerome et al. functionalized the hydroxy terminus of α-methoxy-ω-hydroxyl poly(ethylene oxide) with fumaryl dichloride.[108] The reaction solution was washed with water to yield the carboxylic acid end group. These functionalization reactions are complicated by the difunctionality of the fumaryl dichloride. The products contained a population of chains that were coupled, a population that had single carboxylic acids, and some unreacted hydroxy PEO.

2.5.3 Functional Poly(ethylene oxide) and Routes to Metal/Metal Oxide Stabilization

Carboxylic acids have been widely utilized as the anchoring unit of a macromolecule to the surface of magnetite nanoparticles.[4,109] Previous investigations have included the use of oleic acid, tricarboxylic acid terminated polydimethylsiloxane, and various other systems. However, these are all hydrophobic systems that do not yield magnetite complexes dispersible in aqueous media. There are a few reports of carboxylic acid containing water soluble polyethers used as stabilizers for metal nanoparticles. These systems will be discussed herein.

2.5.3.1 Diblock Copolymers as Chelating Agents

There have been several reports of utilizing water soluble copolymers that contain carboxylic acid functionality to bind to the surfaces of metals. Zhang et al. utilized a commercial poly(ethylene oxide-*b*-methyl methacrylate) (PEO-*b*-PMMA) diblock copolymer to synthesize silver nanowires in aqueous solutions. The PEO block of the PEO-*b*-PMMA functioned as the tail block whereas the PMMA contained the carboxylic

acid functionality to coordinate with the Ag^{+} ions in solution. The PEO block promoted stabilization or solubilization of these complexes in solution. These polymer-metal complexes were 20-40 nm in diameter as measured by TEM. It was suggested that these silver nanowires form inside carboxylate-rich micellar structures.[110]

Bronich et al. have reported the chelating effects of poly(ethylene oxide-*b*-methacrylate) diblock copolymers where the carboxylic acid methacrylate block forms the micellar core and PEO forms the corona. Divalent ions were utilized to self-assemble these diblock copolymers into micellar structures. The divalent ions, such as Ca^{+2}, coordinated with the carboxylic acids. TEM measurements indicated that these self-assembled structures were approximately 100 nm in diameter, and that the images had in-situ enhanced electron density contrast, presumably from the calcium-rich dispersions. The cores of these micelles were then crosslinked using known reactions between carboxylic acids and amines in the presence of a carbodiimide.[111]

In addition, poly(ethylene oxide-*b*-methacrylic acid) (PEO-*b*-PMAA) diblock copolymers have been shown to bind to metal oxide surfaces. Norwig et al. investigated the stabilization and crystal growth of ZnO in the presence of the PEO-*b*-PMAA where the PMAA adheres to the surface of the ZnO. It was found that solely PEO did not influence the crystal growth of the ZnO crystallites, however, in the presence of the PMAA crystal growth was affected. It was hypothesized that this crystal growth was influenced by the strong adsorption of the PMAA onto the ceramic surface of ZnO. It was also observed that crystal agglomeration was prevented in solution with PEO-*b*-PMAA whereas agglomeration was significant in solutions of solely PMAA.[112]

2.5.3.2 Magnetite Stablization via Dicarboxylic Acid Terminated Poly(ethylene oxide)

Tamaura et al. investigated α,ω-poly(ethylene oxide) dicarboxylic acid as a possible steric stabilizer for magnetite. It was proposed that one terminus of the PEO would complex to the magnetite surface while the free carboxylic acid would couple lipase. Dicarboxypoly(ethylene oxide) (DCPEO) (50 wt. %) magnetite complexes were synthesized in water and bound to lipase utilizing a water soluble carbodiimide. The DCPEO was reported to be irreversibly bound to the surface of magnetite through ionic interactions between the negative carboxylates and positive iron oxide surfaces.[113]

The conjugation of the DCPEO to lipase reduced the enzymatic activity. In an effort to prevent a decrease in K_m, the free carboxylic acid groups of the DCPEO-magnetite complexes were reacted with N-hydroxysuccinimide. The DCPEO-magnetite-NHS material was coupled to the amines of the lipase enzyme. This alternative method prevented crosslinking within the active site of the enzyme.[113]

2.5.3.3 Magnetite Stabilized by Carboxylic Acid Containing Poly(ethylene oxide) Triblock Copolymers

Harris et al. developed a series of triblock copolymers containing PEO tail blocks with carboxylic acid functional polyurethane central anchor blocks (figure 1.22).[6] The research focused on developing magnetite complexes coated with hydrophilic stablizers for dispersion in aqueous media. They investigated various tail and central block molecular weights to obtain the maximum concentration of magnetite in the overall polymer-magnetite complex (figure 2.22).

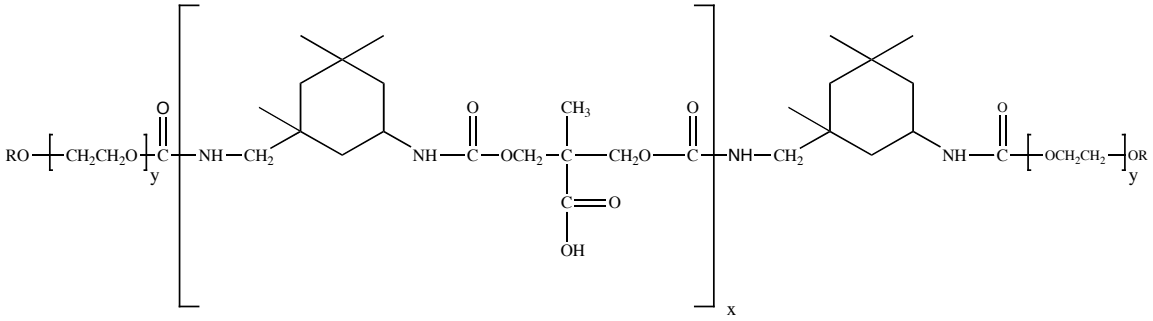

Figure 2.22 A triblock copolymer containing PEO tails and urethane central blocks bind stabilize magnetite nanoparticles in aqueous media.

These complexes were dispersible in aqueous media and transmission electron microscopy demonstrated that the nanoparticles were approximately 8.8 nm in diameter. Their magnetic properties were also examined via vibrating sample magnetometry. These measurements indicated that a sufficient polymer coating was achieved, as evidenced by decreases in the saturation magnetization (reported 34 emu g^{-1} for the complex, 92 emu g^{-1} for pure magnetite).

2.5.3.4 Alternate Routes to Poly(ethylene oxide)-magnetite

Poly(ethylene oxide)s have been investigated as agents to resist protein adsorption, to promote non-antigenicity, and as biocompatible components of many devices or delivery systems. Some studies have shown that this polyether reduces nonspecific protein adsorption in addition to macrophage clearance, thus allowing nanoparticles to traverse cell membranes.[114,115] However, for applications in specific cancer cell recognition and nanoparticle uptake efficiency, folic acid (FA) can be utilized as a low molecular weight targeting agent.

Zhang et al. conjugated folic acid functionalized PEO to the surfaces of magnetite particles through covalent chemical modifications (figure 2.23).[58,116] The PEO prevented nanoparticle agglomeration, increase biocompatibility, and increased their nonspecific

cellular uptake. The folic acid acted as a specific cancer cell target on the distal terminus of the PEO chains. A series of coupling reactions were carried out including silanization of the magnetite surface with 3-aminopropyltrimethoxysilane. Microscopy showed that these FA-PEO modified magnetite nanoparticles were monodisperse. Cell cultures demonstrated that these complexes could be internalized into the BT-20 cancer cell line with higher efficiency of intracellular uptake as compared to PEO-magnetite or FA-magnetite.

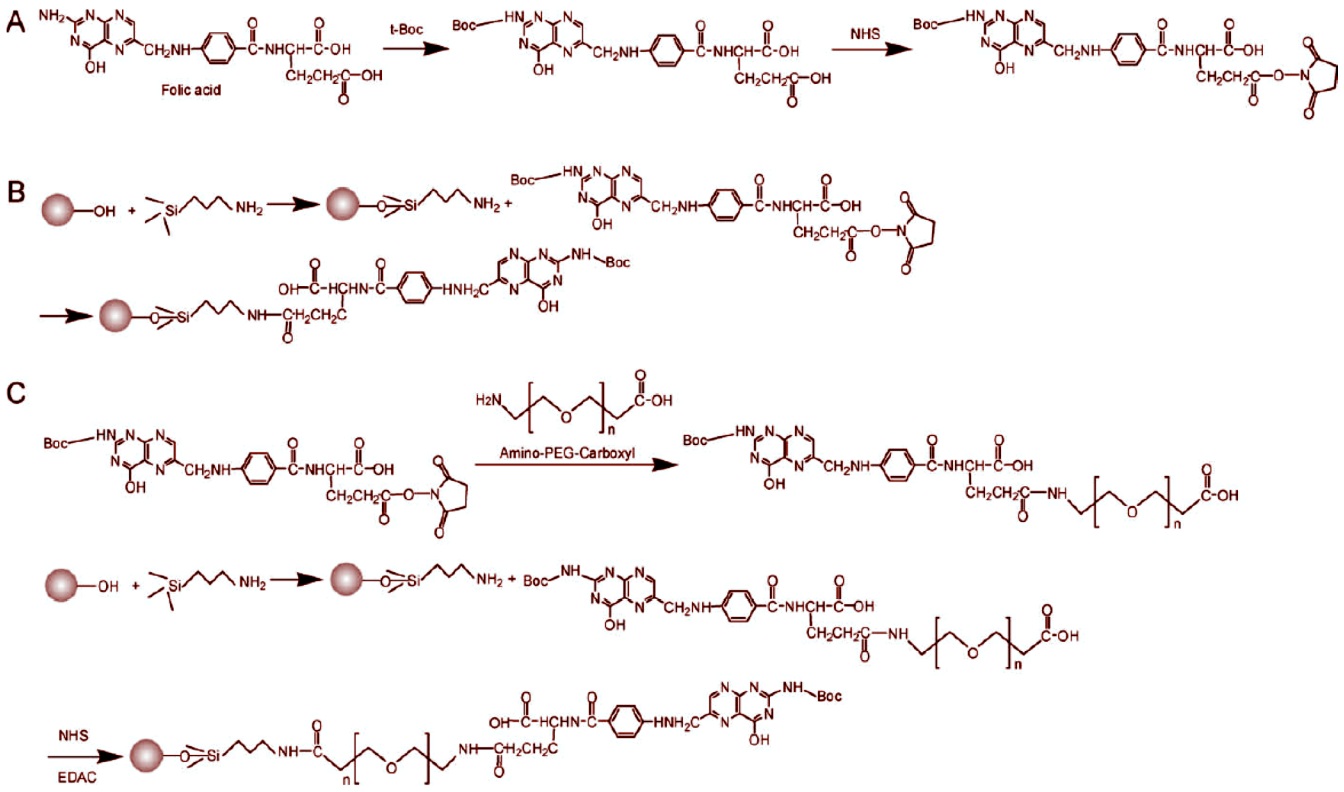

Figure 2.23 Preparation and surface modification of magnetite nanoparticles with PEO-FA conjugates: A) synthesis of FA-NHS, B) silanization of the magnetite surface followed by folic acid attachment, and C) coupling of PEO to the FA magnetite surface

2.6 Conclusions

This literature review describes the essential characteristics of the silica surface that allow for its potential use in the design and synthesis of high moment magnetic drug delivery vehicles coated with biocompatible macromolecules. In addition, an extensive review on the surface functionalization of the silica and magnetite surface has been presented. The functionalization of silica-cobalt and magnetite surfaces with aminoalkyltrialkoxysilane coupling agents as well as a variety of hydrophobic and hydrophilic biocompatible polymers is key to drug delivery technology. Polymethylhydrosiloxanes are one of many biocompatible polymer templates from which polymer-metal nanoparticle complexes can be formed. These polysiloxane-metal complexes are a necessary component of drug delivery vehicles. They possess high magnetic moments and will allow for specific targeting of both the magnetic microspheres and therapeutic agents. They may carry biospecific groups to bind selectively to cells, toxins, etc., to enable their selective removal, and the macromolecules may also be important for protecting biological tissues against toxicity. In addition, bioactive molecules such as drugs, proteins, or genes may be tethered to the ends of the macromolecules that extend from the surface of these magnetic microspheres.

A review of carboxylic acid functional poly(ethylene oxide)s is also provided in this literature review. These polymers are prepared via living anionic polymerizations and the carboxylic acid moiety may be imparted through several chemical modification routes. These polymers are key to preparing aqueous dispersible magnetite complexes for applications in biomedicine.

CHAPTER 3 Synthesis and Characterization of High Magnetic Moment Silica-Cobalt Complexes with Functional Surfaces

3.1 Synopsis

This chapter discusses the synthesis and characterization of siliceous cobalt complexes with high magnetic moments. These complexes have been templated from solutions of PDMS-*b*-[PMVS-*co*-PMTMS] diblock copolymers and annealed at high temperatures. The high temperature treatments afford high magnetic moments in addition to a surface that can easily be functionalized for further modifications. These "silica-like" surfaces can be re-functionalized with amines and isocyanates, as well as with surface-bound polymers such as polylactides, polyethers, and polysiloxanes. Their synthesis and characterization is discussed herein.

3.2 Experimental
3.2.1 Materials

Aminopropyltrimethoxysilane (MW 179.29 g mol^{-1}, d 1.027 g mL^{-1}, BP 80 °C/8 mm HG, Gelest Inc.), stannous 2-ethylhexanoate ($Sn(Oct)_2$, MW 405.12 g mol^{-1}, d 1.251 g mL^{-1}, 95%, Sigma), HCl volumetric standard (0.986N in water, Aldrich), NaOH volumetric standard (1.008N in isopropanol, Aldrich), and trifluoroacetic anhydride (210.03 g mol^{-1}, d 1.487 g mL^{-1}, MP -65 °C, BP 39.5-40 °C, Aldrich) were used as received. Toluene (MW 92.14 g mol^{-1}, d 0.865 g mL^{-1}, MP -63 °C, BP 110 °C, Burdick and Jackson, 99.9 %) was washed twice with conc. H_2SO_4 and neutralized with water. It was dried over $MgSO_4$ for 1 h, then over CaH_2 overnight and distilled just before use. THF (THF, MW 72.11 g mol^{-1}, d 0.889 g mL^{-1}, MP -108 °C, BP 65-67 °C, EM Sciences 99.5%) was dried over CaH_2 overnight, then refluxed over sodium in the presence of benzophenone until the solution was deep purple, and distilled just prior to use. L-lactide (MW 144.13 g mol^{-1}, MP 92-94 °C, 99 %, Pura Biochem) was recrystallized from ethyl acetate, dried under vacuum at 50 °C overnight, and sealed with a septum under nitrogen. PDMS with a tris-trimethoxysilethyl group on one end only was prepared by living anionic polymerization of D_3, terminated with trivinylchlorosilane, then hydrosilated with trimethoxysilane. 3-Isocyanatopropyl)trimethoxysilane was prepared by hydrosilation of allyl isocyanate (MW 83.09 g mol^{-1}, d 0.940 g mL^{-1}, BP 87-89 °C, 98 %, Aldrich) with trimethoxysilane (MW 122.20 g mol^{-1}, d 0.86 g mL^{-1}, MP -114 °C, BP 86-87 °C, 95 %, Gelest). Jeffamine®-2070, kindly donated by Huntsman Corp., is a water soluble, ~2000 g mol^{-1} poly(ethylene oxide-*co*-propylene oxide) oligomer with a primary amine on one end only. It was dried under vacuum overnight at 80 °C.

3.2.2 Preparation of cobalt nanoparticles with surfaces containing silica

Cobalt nanoparticles coated with a 5000–3400 g mol^{-1} PDMS-*b*-[PMVS-*co*-PMTMS] diblock copolymer were prepared as previously described, and dried under vacuum at 80 °C overnight. The dry powders were heated under nitrogen for 2 h at 600 or 700 °C in a quartz tube furnace. The powder was ball-milled using a Puleurisette 7 Ball Mill for 2 h at 700 rpm in anhydrous toluene. The silica-cobalt powders were stored in septum-sealed glass vials under nitrogen.

3.2.3 Functionalization of silica-cobalt particle surfaces with primary amines

A silica-cobalt complex (0.35 g) was quickly charged to a flame-dried, 250-mL, three-neck, round-bottom flask equipped with a condenser, mechanical stirrer with a vacuum ready adapter, and N_2 purge. The apparatus was placed in a temperature controlled silicone oil bath over a hot plate (without a magnetic stirrer). Anhydrous toluene (11 mL), then aminopropyltrimethoxysilane (7×10^{-5} mol, 12 μL), were charged to the reaction vessel via glass syringes. The dispersion was stirred at toluene reflux for 24 h. The functionalized particles were washed 3 times with toluene, dried overnight under vacuum at 80 °C, and stored in a septum-sealed glass vial under N_2.

3.2.4 Titration of aminofunctional silica-cobalt nanoparticles

An aminofunctional silica-cobalt powder (0.03 g, 1.32×10^{-3} eq. amine assuming quantitative functionalization) was charged to a 250-mL, two-neck, round-bottom flask with a condenser, mechanical stirrer with a vacuum ready adapter, and N_2 purge. THF (10 mL), then excess trifluoroacetic anhydride (1.98×10^{-3} mol, 0.413 mL, 0.416 g) were added via glass syringes. The mixture was reacted at 50 °C for 20 min. Water (~12 μL, 6×10^{-4} mol) was added via syringe to hydrolyze the remaining trifluoroacetic anhydride,

and this dispersion was reacted at 50 °C for 20 min. The particles were isolated with a magnet and the THF/trifluoroacetic acid solution was decanted into a beaker. The magnetic powder was washed twice with THF and the extracts were added to the titration solution. The THF/trifluoroacetic acid solution was titrated with NaOH (1.008N in isopropanol). The end-point was determined by pH-meter and the amine concentration was back-calculated. The reported data is an average of 3 titrations.

3.2.5 Polymerization of L-lactide from the surfaces of aminofunctional silica-cobalt particles

A representative preparation of silica-cobalt complexes coated with poly(L-lactide) (target M_n=5000 g mol^{-1}) (50 wt% cobalt-silica and 50 wt% poly(L-lactide)) is provided. Aminofunctional silica-cobalt nanoparticles (0.35 g, 2 x 10^{-4} mol amine per gram of silica-cobalt particles) were charged to a flame-dried, 250-mL, three-neck, round-bottom flask equipped with a condenser, mechanical stirrer with a vacuum ready adapter, and N_2 purge. The apparatus was placed in a temperature controlled silicone oil bath over a hot plate (without a magnetic stirrer). Anhydrous toluene (2 mL) was added via glass syringe. L-lactide (0.35 g) was added and the mixture was stirred for 1 h at 110 °C to initiate the polymerization with the primary amine. $Sn(Oct)_2$ (0.023 mL, 4 x 10^{-4} g, 600 ppm based on the total weight of the reaction solution) was added via glass syringe, and L-lactide was polymerized for 48 h. The poly(L-lactide) coated silica-cobalt complexes were washed twice with toluene, precipitated in methanol, then dried under vacuum at 80 °C for 24 h.

3.2.6 Functionalization of silica-coated cobalt particles with PDMS

Silica-cobalt nanoparticle powder (0.3 g) was charged to a flame-dried, 250-mL, two-neck, round-bottom flask with a condenser, mechanical stirrer with a vacuum ready

adapter, and N_2 purge. A 10,000 g mol^{-1} tris-trimethoxysilethyl terminated PDMS (0.1 g, 1 x 10^{-5} mol, 3 x 10^{-5} eq. trimethoxysilyl groups) was charged to the reaction vessel. Anhydrous toluene (10 mL) was added via glass syringe followed by water (~0.81 μL, ~4.5 x 10^{-5} mol). The reaction was stirred at toluene reflux for 24 h, then the PDMS-silica-cobalt complex was collected with a magnet and the toluene was decanted. The magnetic powder was washed several times with toluene to remove any adsorbed PDMS, dried under vacuum at 80 °C overnight, and stored in a septum-sealed vial under N_2.

3.2.7 Functionalization of the silica-cobalt powder with isocyanates

A silica-cobalt complex (0.1 g) was charged to a flame-dried, 250-mL, three-neck, round-bottom flask with a condenser, mechanical stirrer with a vacuum ready adapter, and N_2 purge. The apparatus was placed in a temperature controlled silicone oil bath over a hot plate (without a magnetic stirrer). Anhydrous toluene (10 mL) was added via glass syringe, then (3-isocyanatopropyl)trimethoxysilane (0.14 g, 7 x 10^{-4} mol) was added via cannula and the reaction was stirred at toluene reflux for 24 h. The magnetic powder was collected with a magnet, washed several times with toluene to remove excess isocyanate, then dried under vacuum at 80 °C overnight taking care to avoid exposure to moisture.

3.2.8 Titration of isocyanate groups on the surfaces of silica-cobalt nanoparticles

An isocyanate-functional silica-cobalt complex (0.03 g, 2.21 x 10^{-4} eq. isocyanate assuming quantitative functionalization) was added to a flame-dried, 250-mL, two-neck, round-bottom flask with a condenser, mechanical stirrer with a vacuum ready adapter, and N_2 purge. The apparatus was placed in a temperature controlled silicone oil bath over a hot plate (without a magnetic stirrer). Anhydrous THF (10 mL), then dry

Jeffamine®-2070 (0.63 g, 3 x 10^{-4} eq. amine) were added via syringes, and the mixture was reacted for 20 min at 50 °C. The magnetic powder was collected with a magnet, and the THF-Jeffamine® solution was decanted into a beaker. The powder was washed twice with THF to remove any residual Jeffamine® and the extracts were added to the titration beaker. Bromophenol blue was added to the THF-Jeffamine® solution until it was deep purple, and the solution was titrated with aq HCl (0.986N) until it was bright yellow. The reported data is an average of 3 titrations.

3.2.9 Instrumentation

A Standard 7300 Series Lakeshore vibrating sample magnetometer was used to determine magnetic properties of the cobalt. The magnetic moment of each dried sample was measured over applied fields from -8000 to +8000 Oe with a sensitivity of 0.1 emu. A Quantum Design magnetic properties measurement system (MPMS-7) using a SQUID sensor was used to make measurements of cobalt specific magnetization (σ) in applied magnetic fields (H) over the range from –70,000 to +70,000 Oe at room temperature and 5 K. Low temperature measurements were made both after cooling the sample in zero applied field and in an applied field at 70,000 Oe. Elemental analyses for cobalt were performed by Desert Analytics Laboratory (Tucson, AZ) by treating the samples with hot conc. nitric acid followed by conc. perchloric acid until complete dissolution was achieved. The solutions were analyzed by inductively coupled plasma optical emission spectroscopy (ICP-OES), and cobalt concentrations were calculated from the sample responses relative to standards and blanks. Transmission electron micrographs were acquired using a Philips 420T TEM at 100kV. Samples were prepared by syringing a drop of a dilute toluene dispersion of cobalt-copolymer particles onto a carbon-coated

copper grid and the toluene was evaporated. Weight loss profiles were analyzed with a TA Instruments TGA Q0500 under N_2. XPS was performed with a Perkin-Elmer 5400 with a Mg X-ray source at 1253.6 eV.

3.3 Results and discussion

Design and synthesis of discreet magnetic nanoparticles where each particle is coated with a biocompatible macromolecule are keys to obtaining magnetic materials for biotechnological applications. The organic components of polymer-metal nanoparticle complexes can stabilize their dispersions in biological fluids by enhancing steric or electrostatic repulsions between particles. They may carry biospecific groups to bind selectively to cells, toxins, etc., to enable their selective removal, and the macromolecules may also be important for protecting biological tissues against toxicity.

Most of the research on magnetic nanoparticles for clinical applications has focused on iron oxides such as magnetite (Fe_3O_4) or maghemite (γ-Fe_2O_3) due to their oxidative stability and biological compatibility.[117-119] Cobalt metal nanoparticles have the potential for three to four times the saturated magnetization of the iron oxides. A major challenge, however, is that cobalt nanoparticles oxidize in air (even when they are well-coated with a surfactant or polymer), forming non-magnetic cobalt oxides.[120,121] Thus, methodologies that afford surface protection to prevent oxidation of these particles are important for their consideration in biotechnological applications.

Previous investigations of dicobalt octacarbonyl reactions in our laboratories utilized poly(dimethylsiloxane-*b*-(3-cyanopropyl)methylsiloxane-*b*-dimethylsiloxane) (PDMS-*b*-PCPMS-*b*-PDMS) triblock copolymers in toluene, D_4, or PDMS solvents to generate cobalt nanoparticles.[1,2,120] The nitrile block of the polymer (the so-called anchor

block) coordinated with the cobalt metal, and the PDMS (tail block) extended into the non-polar solvent to sterically stabilize dispersions of these complexes. While these systems produced discreet cobalt nanoparticles, aging studies under ambient conditions revealed a slow loss in magnetization, and this was attributed to oxidation of the nanoparticle surfaces.[120] Copolysiloxanes with alkoxysilane-functional blocks were later explored as dispersion stabilizers for cobalt in efforts to develop cobalt-polymer complexes which could be post-reacted to form protective coatings around the particles comprised of crosslinked Si-O chemical structures.[120]

This research builds on previous work describing the formation of cobalt nanoparticles encased in poly(dimethylsiloxane-*b*-(methylvinylsiloxane-*co*-methyltrimethoxysilethylsiloxane)) (PDMS-*b*-[PMVS-*co*-PMTMS]) copolymers.[3] The PDMS serves as the tail block and the randomly sequenced PMVS-*co*-PMTMS is the anchor block. The complexes were heated at 600-700 ^{o}C to condense pendent trimethylsiloxy groups on the anchor block into protective silica-containing shells around the cobalt. The heat treatments essentially pyrolyze the copolymers on the nanoparticle surfaces to form the protective shells. In addition, to utilize these cobalt-silica nanoparticle complexes in biomedical applications, their surfaces must be re-functionalized with appropriate organic components. The methods to re-functionalize the "silica-like" surfaces of the cobalt nanoparticles with amine and isocyanate groups, and with poly(L-lactide) and polydimethylsiloxane are discussed herein.

Copolymer-cobalt complexes were prepared by thermolysis of dicobalt octacarbonyl in toluene solutions of PDMS-*b*-[PMVS-*co*-PMTMS] block copolysiloxanes as described previously (Figure 3.1).[3] The anchor block on the

copolymer was designed to (1) complex with the cobalt nanoparticle surfaces, and (2), form a shell containing silica around the nanoparticles in a subsequent elevated temperature step. The tail PDMS block extended into the thermolysis solvent (toluene) to sterically stabilize nanoparticle dispersions of the complexes. Cobalt nanoparticles coated with the copolymers resulted, with particle diameters of ~10-15 nm.[3] Specific saturation magnetizations of these copolysiloxane-cobalt complexes ranged from about 15-17 emu g^{-1} (17-21 wt% cobalt). Thermal analyses show the presence of copolysiloxanes on the surfaces of the copolysiloxane-cobalt complexes (figure 3.1).

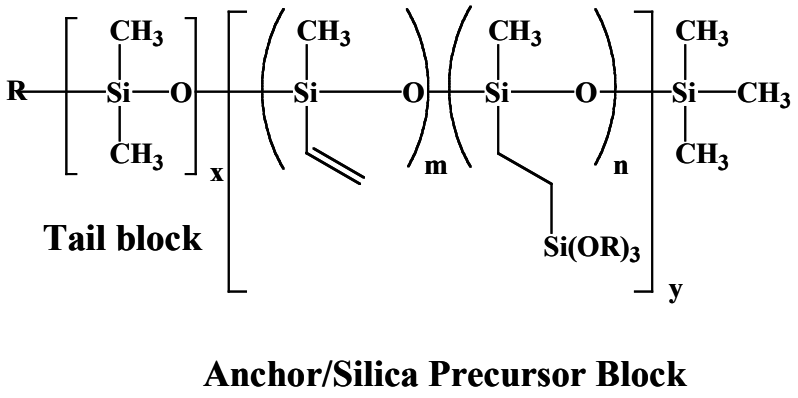

Figure 3.1 PDMS-*b*-[PMVS-*co*-PMTMS] diblock copolymer templates utilized for the formation of copolysiloxane coated cobalt nanoparticles.

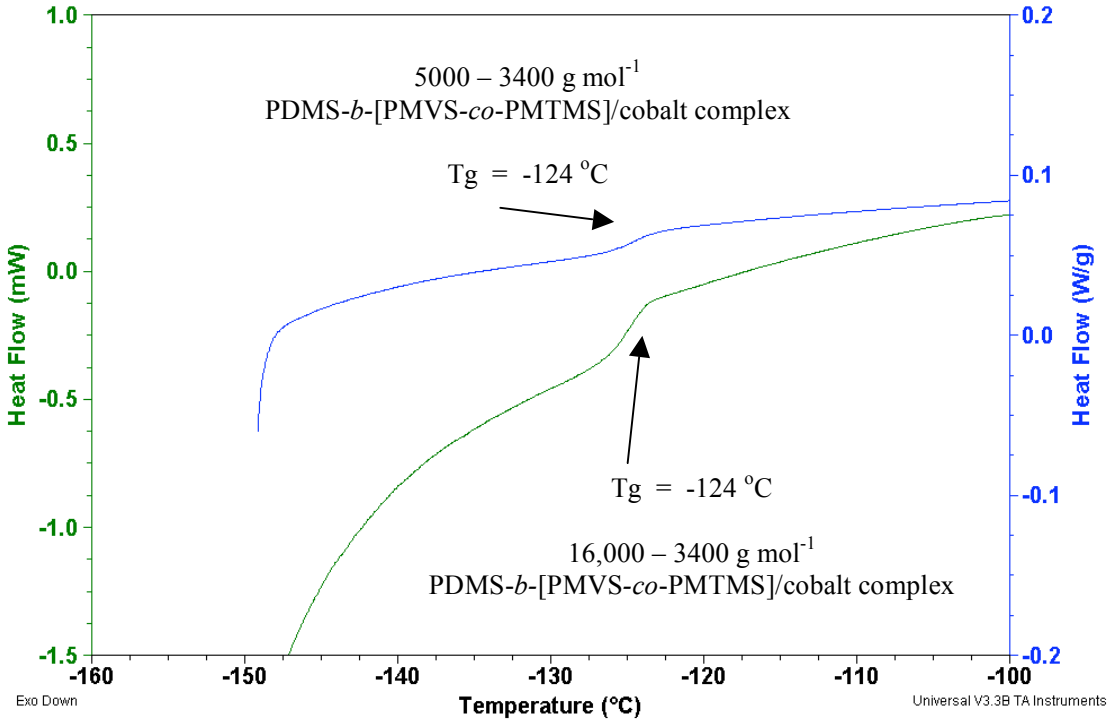

Figure 3.2 Differential scanning calorimetry shows the presence of copolysiloxanes on the surfaces of the cobalt complexes.

3.3.1 Elevated heat treatments form shells around cobalt nanoparticles which contain silica

Silica formation from alkoxysilane copolymers at elevated temperatures has been previously reported.[28,33] Pyrolyses at 300-1000 °C of polymeric silica precursors have been investigated to form crosslinked matrices containing silicon and carbon. In the present work, PDMS-*b*-[PMVS-*co*-PMTMS]-cobalt complexes were heated under nitrogen to form protective shells around the nanoparticles. TGA weight loss profiles of the resultant complexes and of model polysiloxanes were helpful for defining appropriate annealing/pyrolysis conditions. The materials were ramped at 20 °C per minute from room temperature to designated isothermal "holding" temperatures under nitrogen (Fig.

2). PDMS exhibited almost quantitative weight loss at ~450 °C, suggesting that the tail blocks in the cobalt-copolymer complexes may not contribute to the residual coating around the cobalt upon pyrolysis at high temperatures. Poly(dimethylsiloxane-*b*-methylvinylsiloxane) (PDMS-*b*-PMVS) diblock copolymers retained ~30% of the original weight and PDMS-*b*-[PMVS-*co*-PMTMS] diblock copolymers which contained the alkoxysilane silica precursor exhibited 70 weight percent char after heating at 700 ^{o}C. This suggests that both the vinylsiloxane and the alkoxysilane pendent groups may contribute significantly to protective silica-containing coatings. Cobalt-copolymer complexes containing alkoxysilane-functional anchor blocks were heated at temperatures ranging from 300–700 °C (figure 3.3). The complexes retained substantial weight fractions even after heating at the higher temperatures. A plateau in the weight loss profile was observed with each copolysiloxane-cobalt complex after ~40 minutes suggesting formation of stable shells. The complexes treated at 600 and 700 °C retained similar weight fractions, but there was a significant change in retained weight between complexes heated at or below 500 °C versus those treated at 600 or 700 °C. Cobalt concentrations in the complexes after heating at 600 or 700 °C for two hours were calculated from both elemental analysis and TGA, and the values were in good agreement (table 3.1).

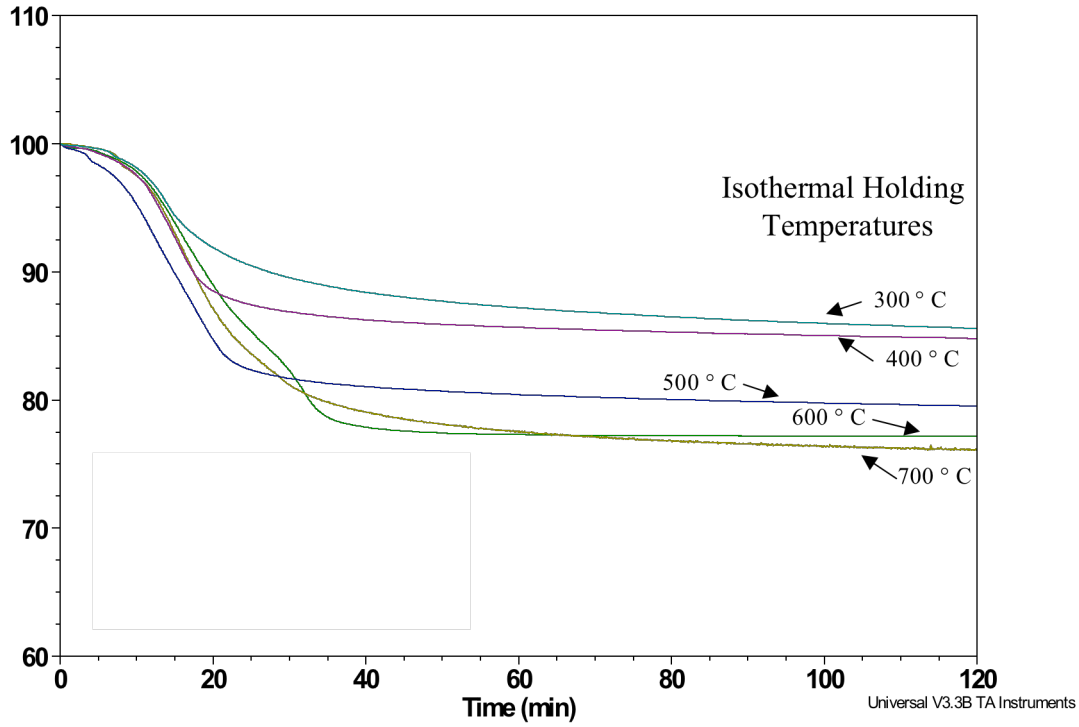

Figure 3.3 Weight loss profiles of cobalt-copolysiloxane complexes prepared with a 5000-3400 g mol^{-1} PDMS-b-[PMVS-*co*-PMTMS] copolymer suggest that substantial residual weight is retained even at high temperatures. The complexes were ramped from 20 ^{o}C at 20 ^{o}C per minute to the designated "holding" temperature, then held isothermally at the designated temperature.

Table 3.1 Cobalt concentrations in the cobalt-silica complexes after pyrolysis

Pyrolysis Temperature (°C)	Cobalt Concentration from Elemental Analysis (%)	Cobalt Concentration from TGA* (%)
600	28	27
700	29	30

*Calculated from the data in figure 3.3 by assuming quantitative retention of cobalt during pyrolysis

Cobalt-copolysiloxane complexes that had not been heated to elevated temperatures had surface compositions similar to PDMS (table 2). They also showed thermal transitions typical of PDMS where the glass transition temperatures were 124 °C for both systems investigated (figure 3.2). By contrast, complexes which were heated at 600 or 700 °C for two hours had surface Si:O atomic ratios of 1:2, suggesting that networks with chemical compositions similar to silica had formed on the cobalt surfaces.

Table 3.2 XPS atomic compositions of the surfaces of copolymer-cobalt complexes prepared with a 16,000–3400 g mol^{-1} PDMS-*b*-[PMVS-*co*-PMTMS]

Temperature (°C)	Silicon (%)	Oxygen (%)	Carbon (%)	Cobalt (%)
Not heat-treated	22	27	49	0
600	22	44	29	3
700	20	48	25	5

3.3.2 Particle size and distribution analysis after elevated heat treatments

The bulk pyrolysis process employed for collapsing the silica-containing shells onto the cobalt nanoparticles resulted in brittle materials adhered together. These complexes were imaged by electron microscopy to assess particle sizes and whether any particle sintering had occurred during pyrolysis.

3.3.2.1 Silica-cobalt complexes after heat treatment at 600 °C

The particle size distribution for the material before the heat treatment ranged from 8 to 38 nm with a mean of 14.1 nm and mode of 12.5 nm (sample population = 536 particles) (figure 3.4a). The mean aspect ratio was 1.51 with a standard deviation of 0.46. The particle size and size distribution was altered dramatically after elevated heat treatments at 600 °C. A bimodal particle size distribution (modes at ~ 10 and 120 nm) was observed for these systems. The particle size distribution ranged from 4 to 750 nm

with a mean of 91 nm (sample population = 399 particles) (figure 3.4b). The mean aspect ratio for the smaller particles was 1.61 with a standard deviation of 0.5, while the mean aspect ratio for the larger particles was 2 with a standard deviation of 0.9.

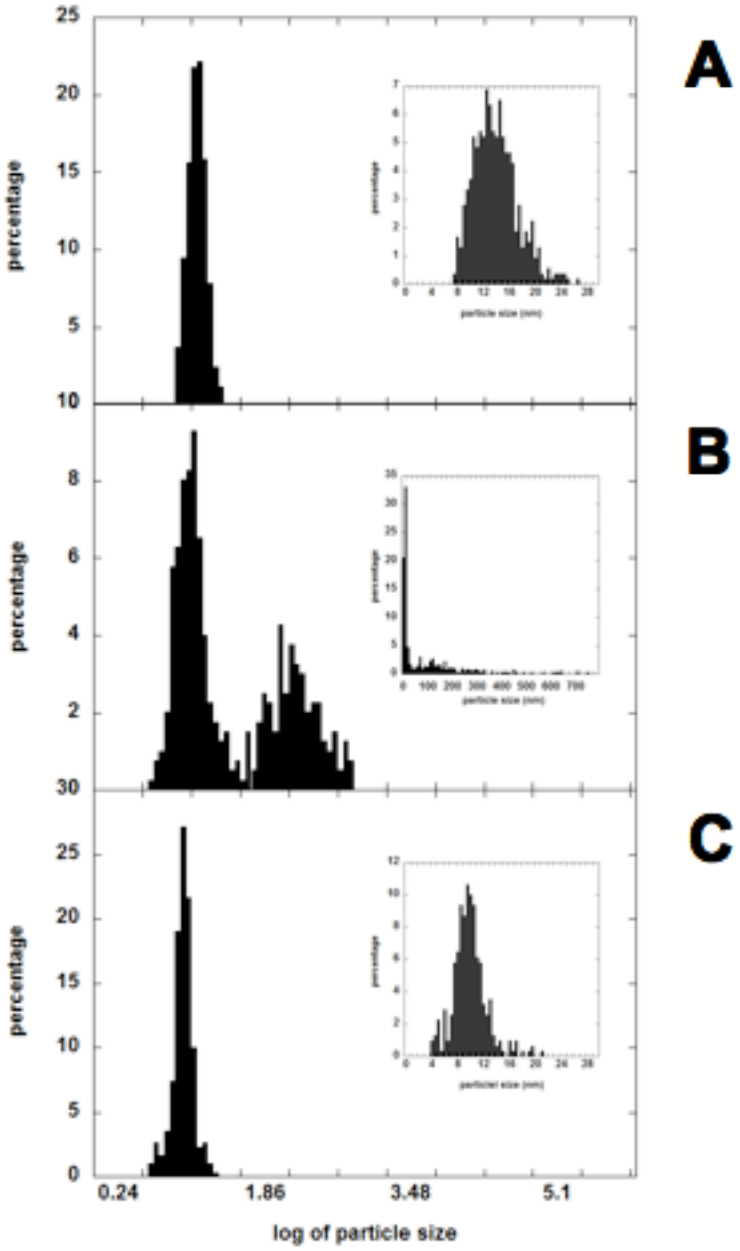

Figure 3.4 Logged particle size histograms for: a.) pre-heat-treated sample, b.) sample heated at 600 °C, and c.) sample heated at 700 °C. Insets show particle size histograms in nm. Note: The raw data was logged and re-binned to generate the logged particle histograms.

Transmission electron microscopy showed that thermal treatment at 600 ^{o}C produces some cobalt nanoparticle sintering in addition to the pyrolysis of the polymer (figure 3.5). It was reasoned that particle sintering occurred before the polymer was completely pyrolyzed to form a protective inorganic shell, and that this led to aggregates of fused cobalt nanoparticles. Jacobsohn *et al.* reported the increase in size of ion-implanted cobalt nanoparticles in a fused silica matrix after annealing at 900 ^{o}C under vacuum for 10 hours.[122] The system reported by Jacobsohn *et al.* is different from the system discussed here; nevertheless, the particle growth mechanism appears similar.

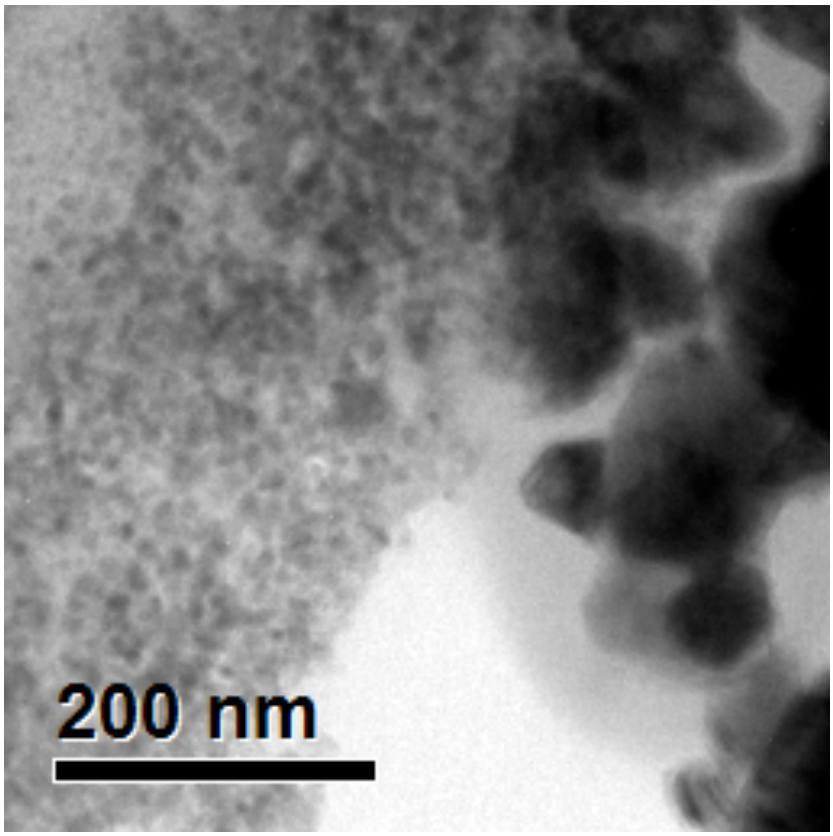

Figure 3.5 HRTEM image of the 600 °C silica-cobalt complexes show two particle size distributions and sintering.

3.3.2.2 Silica-cobalt complexes after heat treatment at 700 °C

Thermal treatment at 700 ºC resulted in a narrow particle size distribution, similar to that of the material that had not been subjected to the high temperature. The particle sizes ranged from 4 to 21 nm with a mean of 10.1 nm and a mode of ~9.5 nm (sample population = 310 particles) (figure 3.4c). The mean aspect ratio was 1.37 with a standard deviation of 0.34.

High resolution transmission electron microscopy of thin sections of 700 °C sample showed both the narrow population size distribution as well as ordered nanoscale coatings surrounding many of the cobalt particles (figure 3.6). It may be that this ordered coating prevents cobalt sintering during the heat treatment. Thus, the particles are separated by a 'silica' matrix and the average particle size and size distribution remain narrow as in the pre-heat-treated sample. In addition, it appears that a more rapid pyrolysis of the polymer, such as may be achieved at 700 ^{o}C, may prevent the cobalt particles from coming into contact with one another and sintering.

Moreover, the data suggests that the mean particle sizes and size distribution of the 700 °C sample (10.07 ± 2.61 nm) may be smaller and narrower than for the non-treated sample (14.14 ± 3.37 nm), although these values are within the standard deviations of the measurements (figure 3.4). It is recognized, however, that the block lengths and concentrations of copolysiloxane in the thermolysis and subsequent pyrolysis reactions may correlate with morphologies of the materials, and that this warrants further investigation.

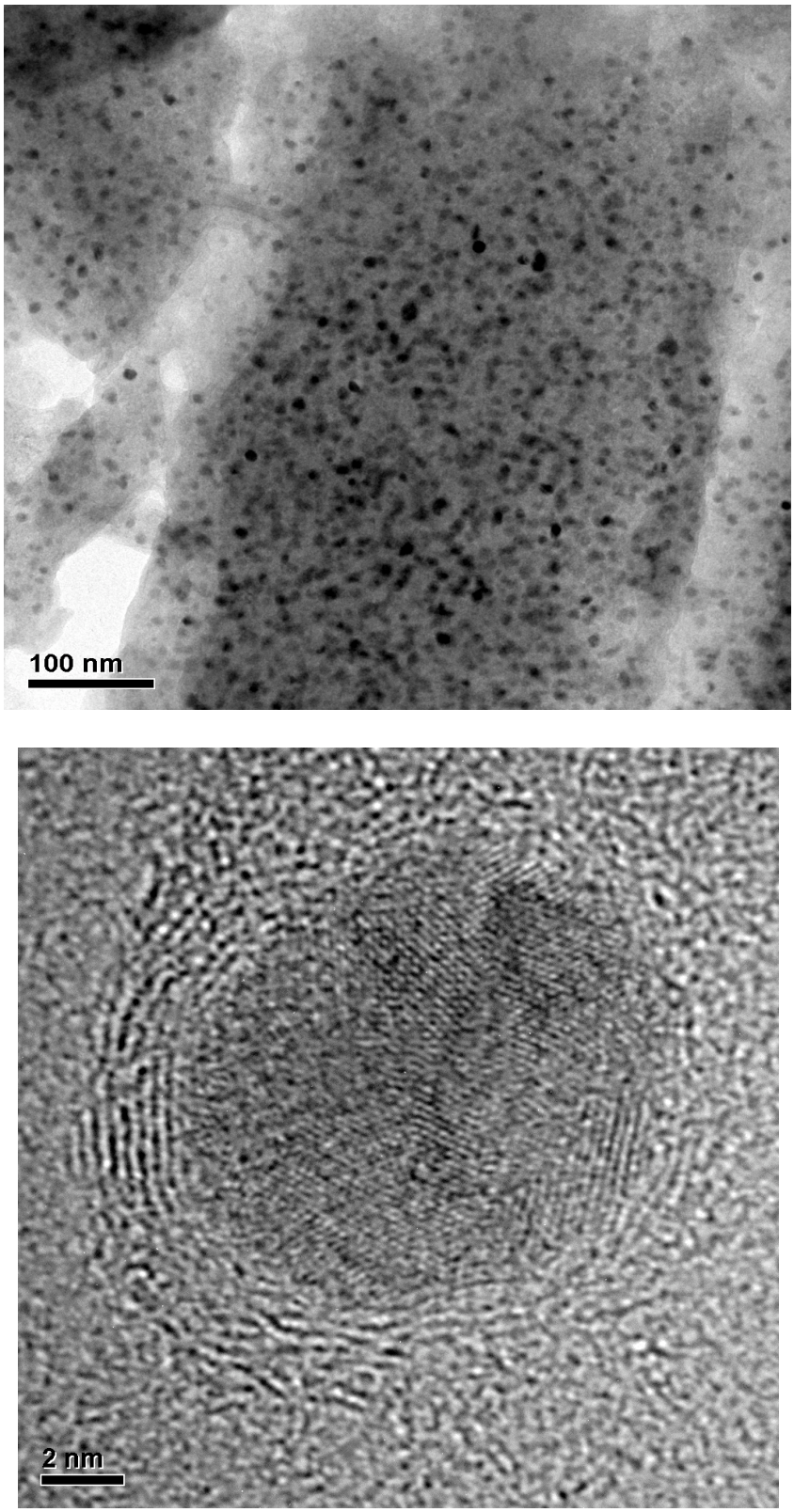

Figure 3.6 a.) TEM micrograph of silica-cobalt nanoparticles treated at 700 °C b.) a high resolution TEM image showing the ordered silica coating encasing the particle

3.3.3 Formation of high moment silica-cobalt nanoparticles

Specific saturation magnetizations of silica-cobalt nanoparticle complexes, which had been heated at a series of temperatures increased substantially with the pyrolysis temperature (figure 3.7). It was expected that weight loss of the polymer upon pyrolysis would lead to complexes with higher cobalt concentrations, and thus increased magnetic susceptibility. Room temperature magnetic measurements conducted on a SQUID magnetometer showed an increase of cobalt specific magnetization from 48 emu g^{-1} Co (for a sample prior to pyrolysis) to 141 emu g^{-1} Co (for a sample pyrolyzed at 600 ºC for two hours). However, the magnitude of increase in magnetic susceptibility after treating these materials at 600 and 700 ° C could not be wholly attributed to weight loss of the non-magnetic portion. X-ray diffraction and high resolution TEM were utilized to probe the underlying reasons behind this drastic increase in magnetization.

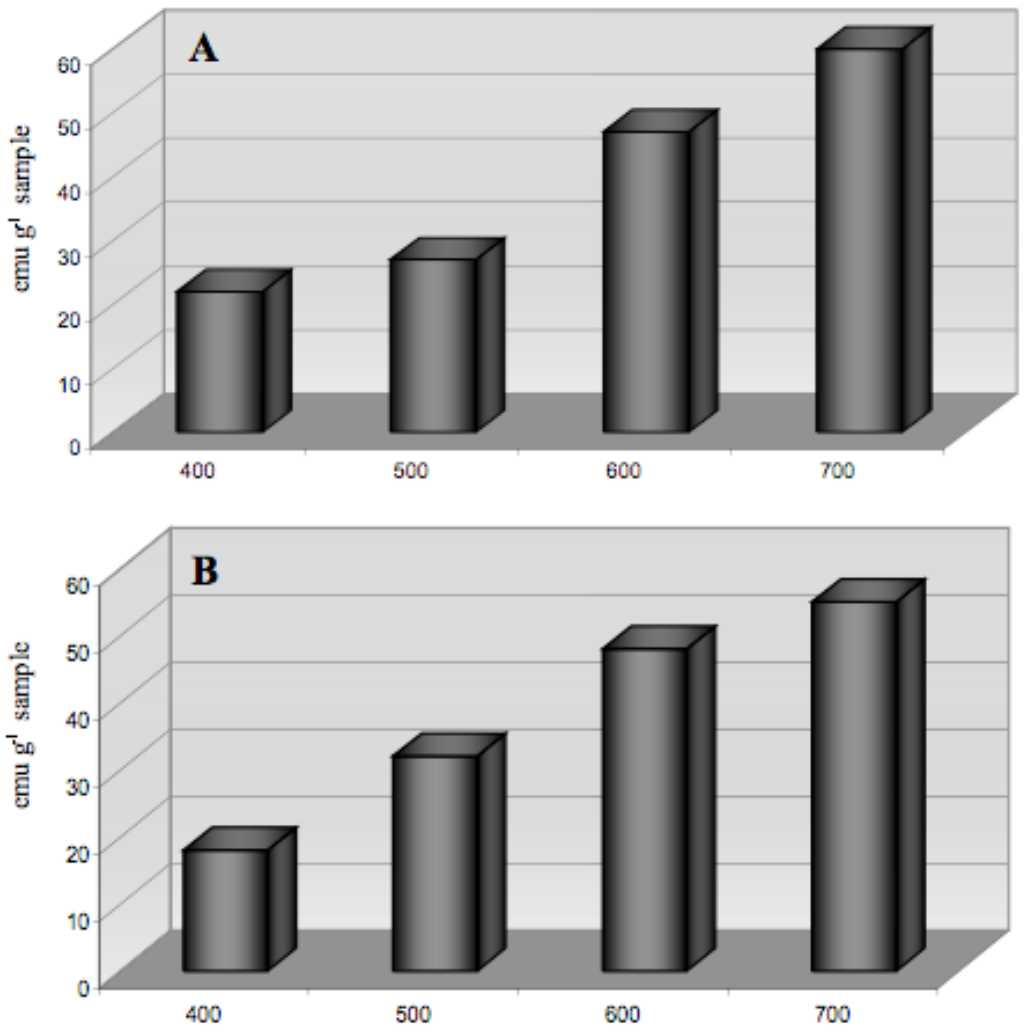

Figure 3.7 Specific saturation magnetizations of silica-cobalt nanoparticle complexes after pyrolysis for two hours at the designated temperature. (A: complexes formed from 5000 – 3400 g mol^{-1} PDMS-*b*-[PMVS-*co*-PMTMS] copolymers, B: complexes formed from 16, 000 – 3400 g mol^{-1} PDMS-*b*-[PMVS-*co*-PMTMS] copolymers)

3.3.3.1 X-ray diffraction and high resolution transmission electron microscopy examine particle crystallinity

Increased diffraction contrast was observed when the samples when analyzed by TEM implying increased crystallinity due to thermal treatment. High-resolution transmission electron microscopy (HRTEM) and x-ray diffraction were implemented to evaluate the crystallinity of the cobalt nanoparticle complexes with and without the high

temperature heating (annealing) steps. Although the samples prior to pyrolysis were only weakly crystalline, several high-resolution images were obtained. Figure 3.8 shows a crystalline particle before pyrolysis with measured lattice spacings of ~2.01 Å, which are consistent with the {111} plane of fcc cobalt (2.05 Å), but these could also be attributed to the {002} plane of hcp cobalt (2.02 Å).

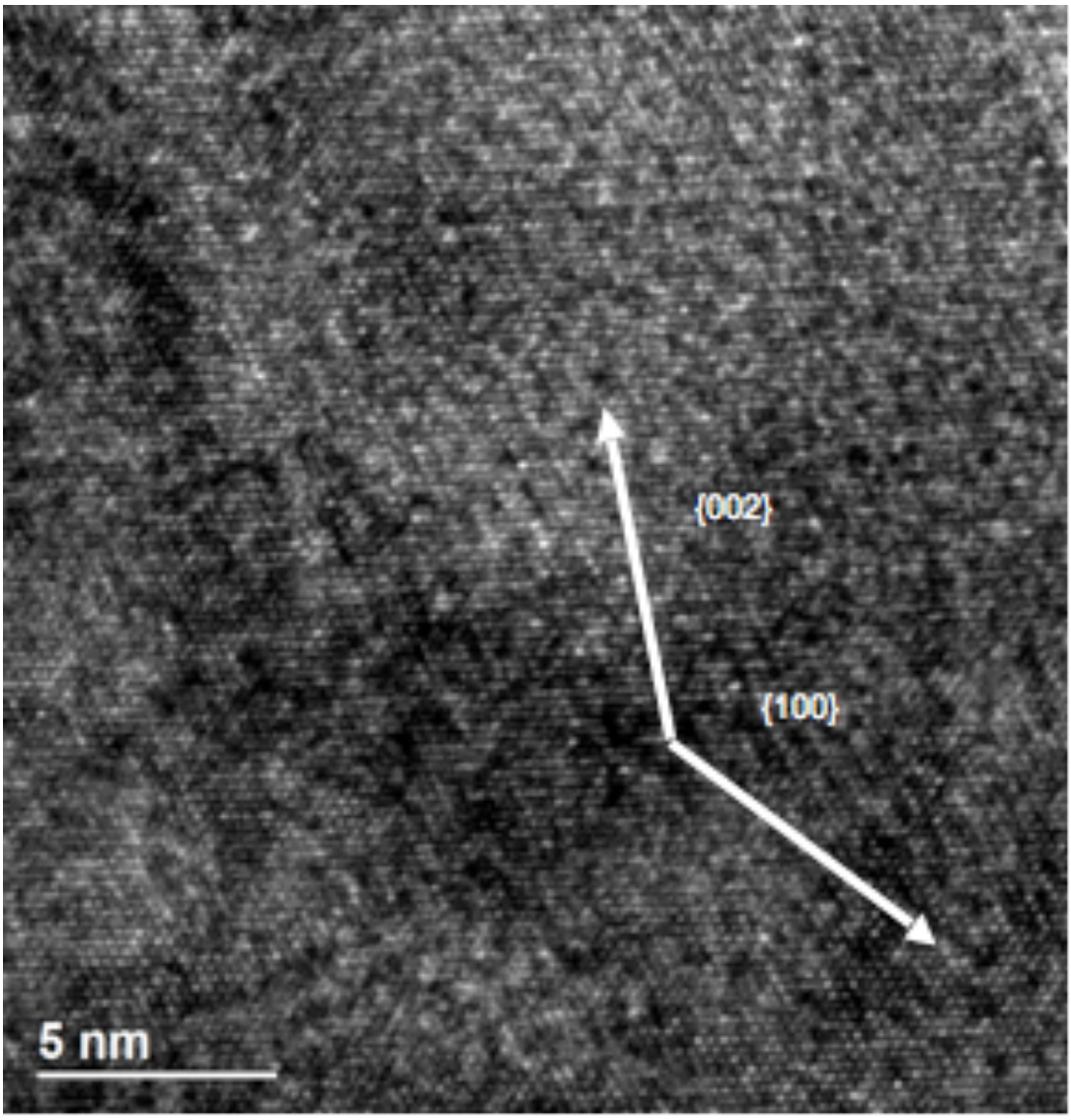

Figure 3.8 A HRTEM image of a pre-pyrolyzed copolysiloxane-cobalt complex.

The x-ray diffraction data shows the predominance of fcc cobalt for the materials treated at the elevated temperatures for both the 600 °C and 700 °C samples, but the HRTEM images cannot distinguish the dominance of the fcc phase over hcp. X-ray diffraction was used to complement electron diffraction as it provides crystallographic information on macroscopic quantities of sample. X-ray diffraction of the material that had not been heated at the elevated temperatures showed that it was only weakly crystalline, in agreement with the HRTEM data (Figure 3.7). Some intense reflections were present at 2θ values of 41.3, 44.7 and 47.4° corresponding to experimental d-spacings of 2.19, 2.03 and 1.92 Å respectively (figure 3.9a). These values match well with literature d-spacings for hexagonal close packed (hcp) cobalt of 2.17, 2.04 and 1.92 Å respectively; however, the experimental intensities do not follow the same trend as the intensities previously reported in the literature.[123] The energetic difference in atomic stacking between the three known phases of cobalt (fcc, hcp and epsilon) is low; therefore, having multiple phases of cobalt is possible.[123,124]

From the x-ray diffraction data, it is clear that the dominant phase of the cobalt after being heat treated at 600 °C is fcc. Intense reflections were present at 2θ values of 44.1, 51.5, 75.7 and 92.1° corresponding to d-spacings of 2.05, 1.77, 1.25 and 1.07 Å respectively. These experimental values match well with the literature values for the {111}, {200}, {220} and {311} lattice planes of fcc cobalt (figure 3.9b).[125] Other less intense peaks were also present, and this suggests the minor presence of other phases. The data for the 700 °C sample was similar to the 600 °C sample with major reflections at 2θ values of 44.4, 52, 76 and 92° corresponding to d-spacings of 2.03, 1.76, 1.25 and 1.07 Å respectively. These reflections, although broader than for the 600 °C matched the

literature values for fcc cobalt (figure 3.9c).[125] Qualitative peak broadening calculations were performed for the materials which had been subjected to heating at 600 and 700 ºC using the Scherrer equation. The increased breadth of the 700 °C peaks compared with 600 °C is consistent with particle size data obtained from TEM, which indicated a smaller mean particle size for the 700 °C sample.

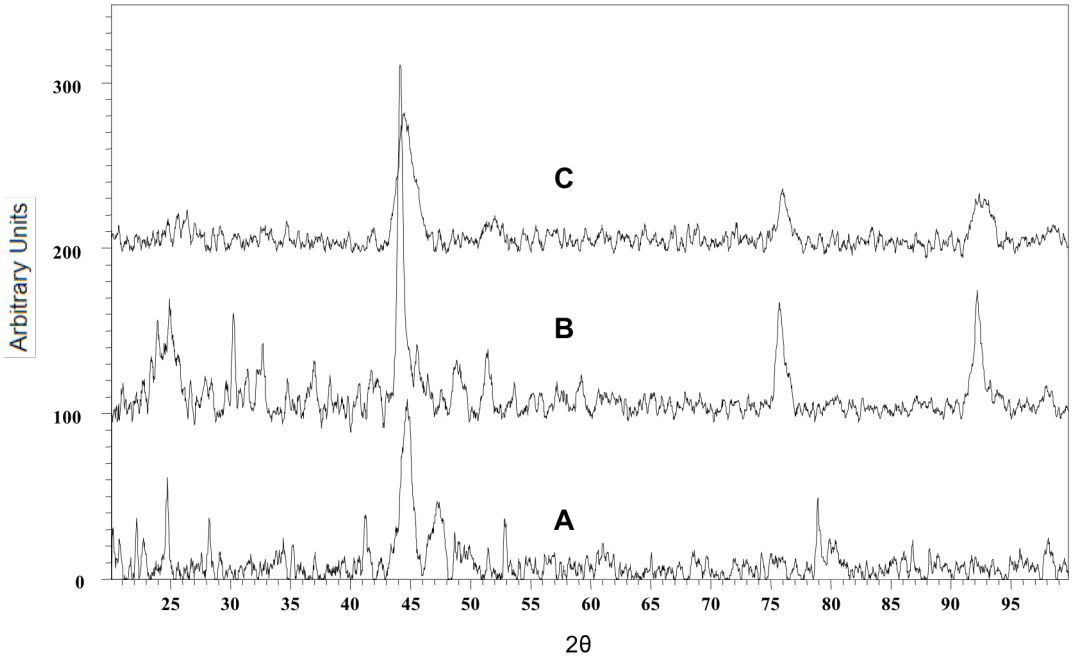

Figure 3.9 X-ray powder diffraction patterns for a.) non-heat treated b.) 600 °C and c.) 700 °C

3.3.4 SQUID magnetometry measurements evaluate the oxidative stability before and after elevated heat treatments of the cobalt complexes

3.3.4.1 Magnetic measurements and oxidative stability of complexes that were not mechanically ground

The magnetic properties and oxidative stability of these complexes before and after mechanically grinding these materials was evaluated via SQUID magnetometry (figure 3.10). Room temperature measurements σ vs. H measurements of the material

without high temperature heat treatment after being exposed to air revealed cobalt specific saturation magnetizations (σ_s) of 48 (aged for 4 months) and 47 emu g^{-1} (aged for 15 months), and these values are significantly less than the 161 emu g^{-1} value of bulk cobalt.[126] The low magnetizations suggest that an oxide layer had formed on both materials. The similarity of these values suggests that the cobalt-copolymer complexes reached the maximum extent of oxidation within 4 months, and the prolonged 15-month exposure did not oxidize the materials further. In addition, the unpyrolyzed samples did not display any significant remanence or coercivity. Room temperature magnetization curves almost saturate in high-applied fields, while 5 K magnetization curves have a positive slope in high-applied fields. The positive slope in the low temperature magnetization curves suggests the presence of a residual paramagnetic component. The paramagnetic component is believed to be unreacted cobalt carbonyl species that were not incorporated into the cobalt nanocrystals during their synthesis.

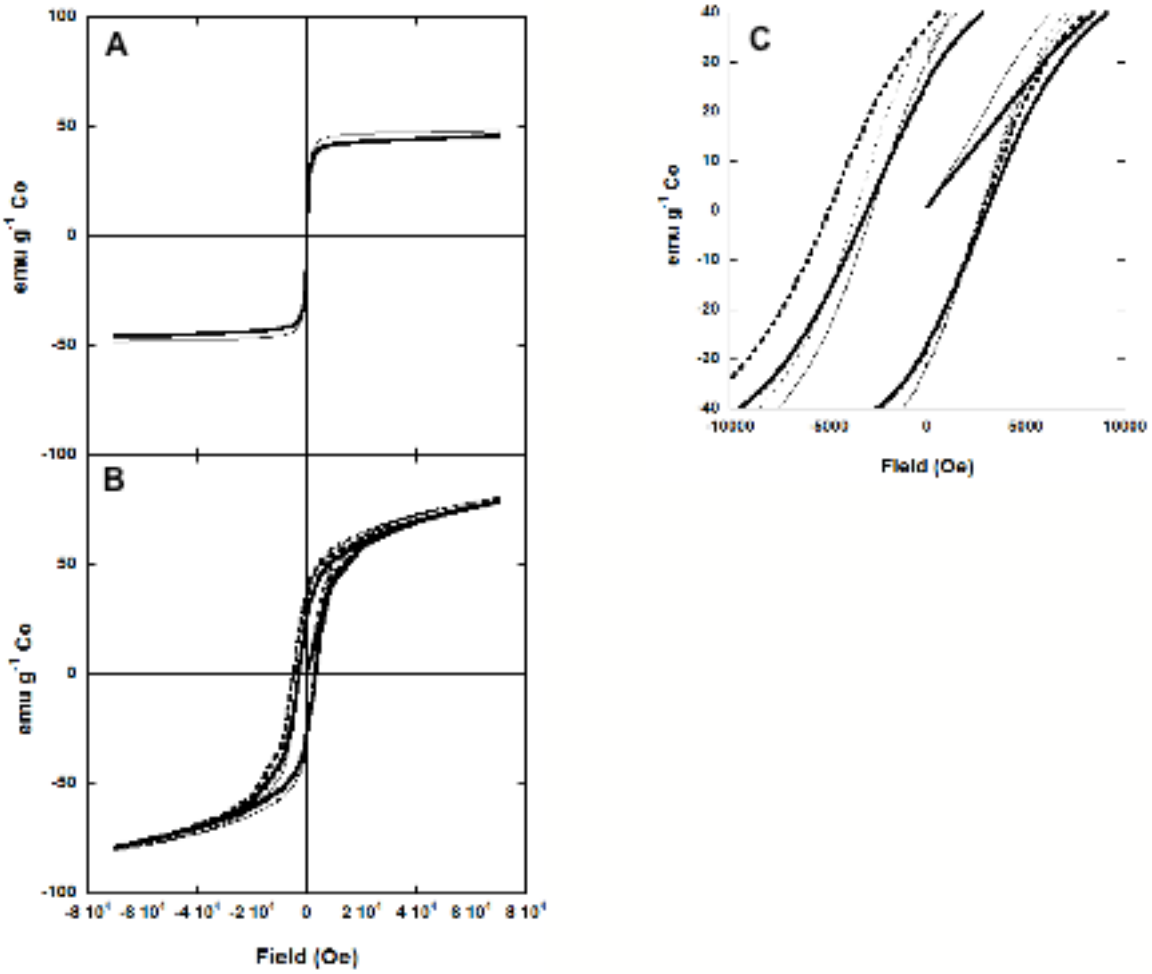

Figure 3.10 σ vs. H measurements conducted on the non-heat treated sample at a.) 300 K b.) 5 K zero-field cooled hysteresis loop, and c.) shows enlarged region around the origin for the 5K hysteresis loop showing asymmetric field-cooled hysteresis loop shift.

A cobalt-copolymer complex was heated at 600 ºC for two hours, then aged in ambient air for 200 days. This material was not mechanically ground. The cobalt nanoparticles were adequately protected against oxidation as evidenced by the long-term oxidative stability of the materials (figure 3.11). The data indicated that the intact silica coating prevented the formation of cobalt oxide on the surfaces of these silica-cobalt nanoparticle complexes.

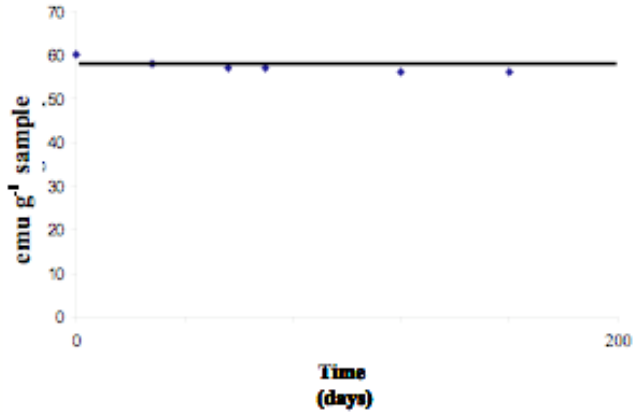

Figure 3.11 Aging results of silica-cobalt nanoparticles after pyrolysis at 600 °C for two hours demonstrate their oxidative stability in ambient air for at least 200 days.

Magnetizations of the materials that had been heated at the elevated temperatures were much higher than those without the heat treatments. Room temperature σ vs. H measurements for the 600 °C sample indicated a σ_s of 174 emu g^{-1} Co. This is above the reported σ_s for bulk cobalt (161 emu) by 8.75%. This error may be within the reproducibility limits for the elemental analysis measurements. The magnetization curves for 600 °C saturate at high-applied fields at room temperature and 5K (figure 3.12a). These data suggest that the heat treatment had eliminated any remaining carbonyl ligands and the paramagnetic cobalt atoms had been incorporated into cobalt nanocrystal lattices. Room temperature σ vs. H measurements for the 700 °C sample yielded a σ_s of 136 emu g^{-1} Co (Figure 3.12b). There is a reasonable decrease of σ_s from 600 ° to 700 °C (38 emu). Although it is unclear why this is so, it may be related to the crystallization process and rate of crystallization of the cobalt nanoparticles. The magnetization curve for 700 °C saturates in high-applied fields at room temperature and at 5K (figure 3.12 a and b). This is consistent with the hysteresis loops for the material that was heated at 600 °C.

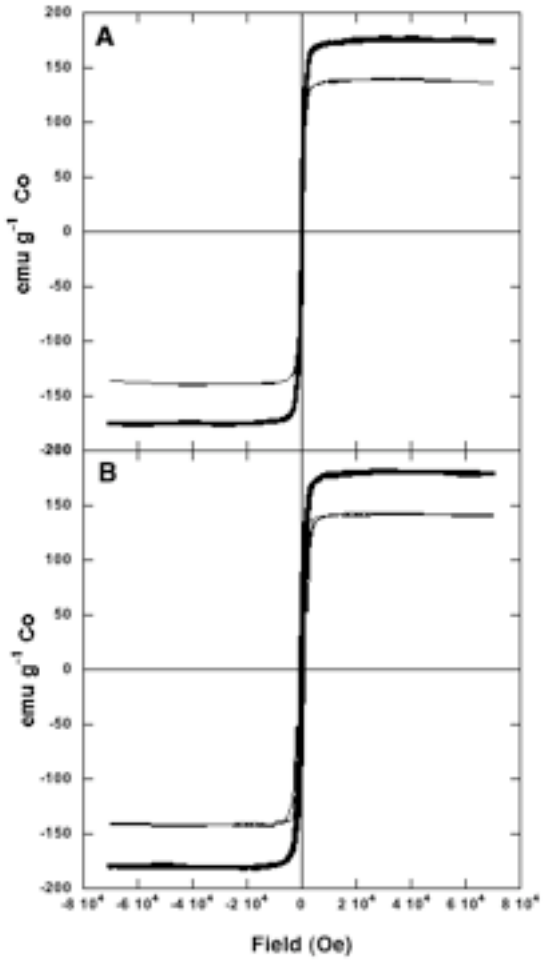

Figure 3.12 σ vs. H measurements conducted the 600 °C and 700 °C samples at a.) 300 K and b.) 5 K

3.3.4.2 Magnetic measurements and oxidative stability of these materials after mechanically grinding

The oxidative stability of the heat-treated cobalt complexes after being mechanically ground were evaluated over an exposure period of 180 days to ambient conditions. The material that had been heated at 700 ^{o}C, then mechanically ground and aged in air over 180 days had a much larger decrease in σ_s from 136 to 31 emu g $^{-1}$, with an increase in H_e from 0 to 156 Oe (figure 3.12). One possible cause for the drastic decrease of σ_s for the material heated at 700 vs. 600 ^{o}C may be related to the much

smaller particle size of the cobalt heated at the higher temperature. The 700 °C sample is comprised of cobalt nanoparticles having a small mean particle size of 10.1 nm, while the 600 °C sample has a bimodal particle size distribution comprised of small and large particles, likely attributable to sintering. Thus, 600 °C has more surface area than 700 °C and more oxidation per unit volume would be expected.

Over the 180 days, σ_s for the material that had been heated at 600 °C and ground decreased from 174 to 143 emu g^{-1} Co (figure 3.13). In addition, the exchange bias field (H_e) increased from 40 to 153 Oe (figure 3.13). The decrease of σ_s and the increase of H_e over time suggest that cobalt oxide had formed on the surfaces of the cobalt nanoparticles. This implies that mechanically grinding this material may fracture the silica shell around the nanoparticles, thus exposing bare cobalt. From days 80 to 180, a slight increase in H_e was observed without a decrease in σ_s, and it was reasoned that this might be due to an increase in interfacial order of the antiferromagnetic cobalt oxide layers in contact with the ferromagnetic cores of the cobalt nanoparticles.

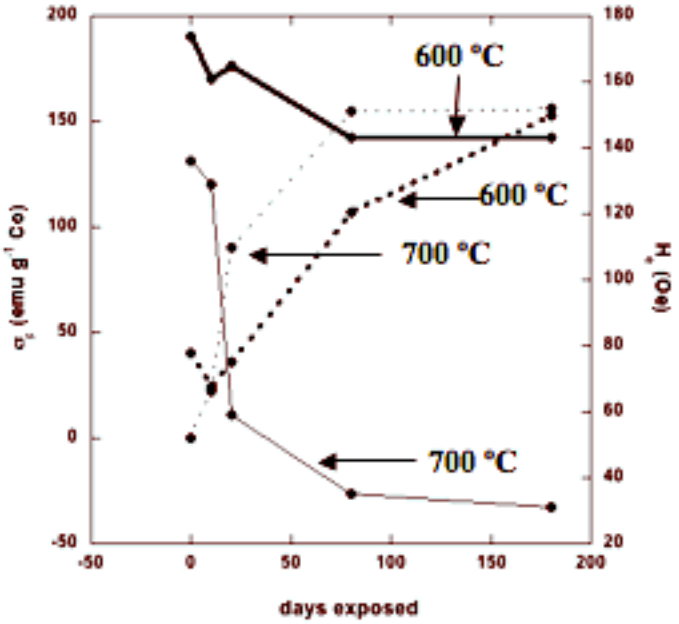

Figure 3.13 Magnetic susceptometry measurements conducted on the 600 ° and 700 °C samples while exposing them to air for 180 days indicated that oxidation was taking place as evidenced by a decrease in σ_s and an increase in H_c over time. The solid lines represent the saturation magnetization whereas the dotted lines represent the coercivity.

3.3.5 Re-functionalization of the surfaces of silica-cobalt complexes

In addition to forming protective shells around the cobalt nanoparticles, a methodology to prepare complexes with appropriate organic components tethered to their surfaces was investigated. The methods to re-functionalize the "silica-like" surfaces of the cobalt nanoparticles with amine and isocyanate groups, and with poly(L-lactide) and polydimethylsiloxane will be discussed.

3.3.5.1 Functionalization of the silica-cobalt complex surfaces with aminosilane coupling agents

Functionalization of silica surfaces with aminofunctional alkoxysilanes has been reported.[48,62,127,128] Schouten et al. reacted (4-aminobutyl)dimethylmethoxysilane with silicon wafers forming a silanized surface with amine groups. These amines served as initiators for polymerization of N-carboxyanhydrides directly from the surface. Vrancken et al. condensed various aminopropyltrialkoxysilanes onto silica surfaces in the absence of water. In this research, silica-cobalt nanoparticles were re-functionalized with aminopropyltrimethoxysilane by condensing the coupling agent onto the nanoparticle surfaces in anhydrous refluxing toluene.

The surfaces of the silica-cobalt complexes were examined before and after treatment with aminosilane coupling agent utilizing XPS.[128] The untreated material showed surface atomic ratios similar to that of silica where the Si:O ratio was approximately 1:2. It is important to note that there was no nitrogen present on the surface. The atomic concentration of cobalt was 3% before treating the surfaces of the silica-cobalt complexes. This may be due to the surface penetration depth of the electrons utilized in the surface analysis method. The atomic ratios were changed after treating the surfaces with the aminosilane coupling agent. Importantly, the surface compositions were rich in nitrogen resultant from the coupling agent. In addition, the cobalt concentration decreases likely due to a thicker coating on the surfaces of the complexes.

Table 3.3 X-ray Photoelectron Spectroscopy examines the surfaces of the cobalt complexes before and after treating with 3-aminopropyltrimethoxysilane. The surfaces are nitrogen rich after functionalization.

Sample	Silicon (%)	Oxygen (%)	Nitrogen (%)	Cobalt (%)	Carbon (%)
Untreated	29	44	0	3	22
Treated	18	31	7	1	42

Quantifying the surface concentration of the coupled amines was important for utilizing the amines in any further reactions. XPS only yields atomic surface ratios and not exact molar quantities. Therefore, the surface-bound amines were quantified by derivatizing the aminofunctional particles with trifluoroacetic anhydride, hydrolyzing excess anhydride, then back-titrating the resultant acids. The titration procedure was verified using Jeffamine-2070® (a mono-amine terminated poly(ethylene oxide-*co*-propylene oxide) oligomer) as a model primary amine (table 3.4).

Table 3.4 Average surface amine concentrations determined by titration.

Sample	Theoretical Amine Concentration (mol g^{-1})	Average Amine Concentration Determined By Titration (mol g^{-1})
Jeffamine-2070®	2×10^{-4}	$1.9 \times 10^{-4} \pm 1 \times 10^{-5}$
amine-silica-cobalt	0.044	0.038 ± 0.0075
amine-silica-cobalt	0.024	0.022 ± 0.0055
amine-silica-cobalt	0.0024	0.0012 ± 0.0004

The concentrations of primary amine on the surfaces were quantified after establishing effectiveness of the procedure. Surface analysis was employed to verify the presence of fluorine on the surface of the particles. Atomic surface compositions derived from XPS of the silica-cobalt nanoparticles before functionalization did not contain fluorine, whereas fluorine was prominent after reacting the aminofunctional surfaces with trifluoroacetic anhydride (table 3.5).

Table 3.5 X-ray photoelectron spectroscopy showed the presence of fluorine after titration of the surface amines.

Sample	Silicon (%)	Oxygen (%)	Nitrogen (%)	Fluorine (%)
control	18	31	7	0
titrated	18	26	6	12

Three separate concentrations were targeted and measured. The concentrations achieved were in reasonable agreement with the charged concentrations (table 3.4), signifying that the amine concentrations can be qualitatively controlled. This is important because the primary amines can serve as initiators for polymerizing L-lactide directly from the surfaces of the particles, and it is expected that this allows for controlling the poly(L-lactide) molecular weights.

It was also important to analyze whether the aminosilane coupling reaction had any effect on the magnetic properties of the silica-cobalt complexes. Vibrating Sample Magnetometry (VSM) measurements before and after silane treatment indicate that the magnetic susceptibility of these complexes remained unchanged after reaction. Table 3.6 shows the values obtained in emu g^{-1} sample of complex.

Table 3.6 Magnetization remains unchanged after coupling the aminosilane to the surface of the silica-cobalt complexes.

Sample	M_s (emu g^{-1} sample)
untreated	60
amine-treated	60

3.3.5.2 Polymerization of L-lactide directly from the surfaces of silica-cobalt nanoparticles

Polymerization of L-lactide from the surface of amine modified self-assembled monolayers (SAM's) has been reported.[127] Langer et al. formed a SAM of *N*-(2-aminoethyl)-3-aminopropyltrimethoxysilane on a Si/SiO_2 surface for subsequent surface initiated polymerization of L-lactide. In this research, the surface-bound amines initiated L-lactide and the biodegradable polymer, poly(L-lactide), was polymerized directly from the surfaces of the silica-cobalt nanoparticles (figure 3.14).

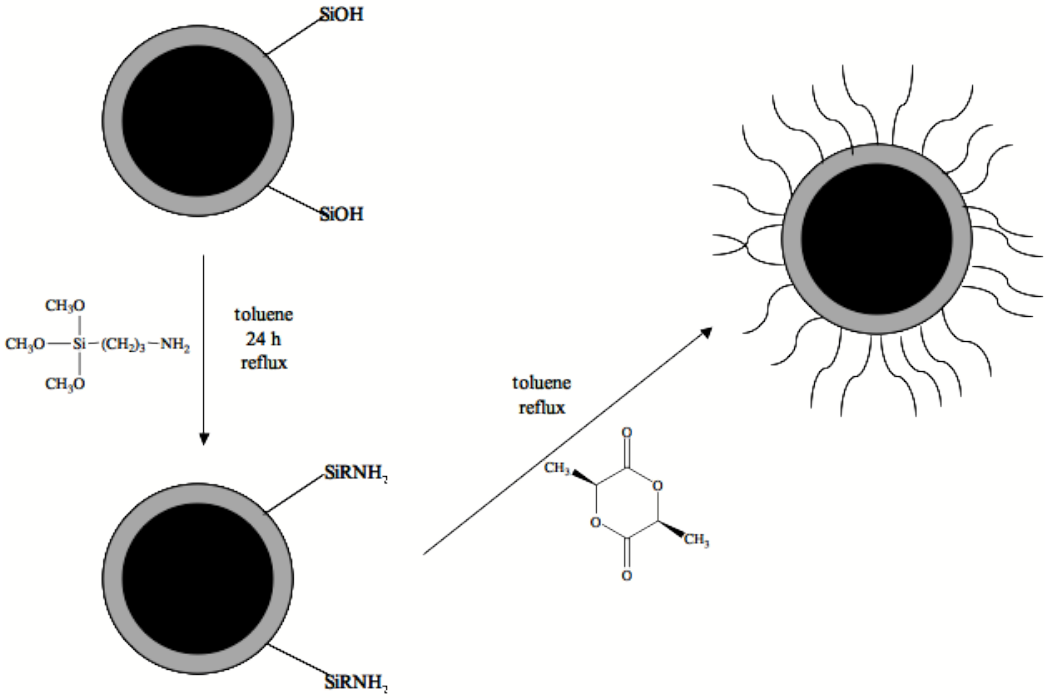

Figure 3.14 Silica-protected cobalt nanoparticles can be re-functionalized with amines, then the amine groups can initiate poly(L-lactide) oligomers directly from the particle surfaces.

It is important to note that the average molecular weights of the poly(L-lactide) tails should be related to the amine initiator concentration (i.e., M_n equals (grams of L-

lactide)/(moles of amine)). A series of poly(L-lactide)-cobalt-silica complexes were synthesized, and magnetic measurements obtained from VSM were utilized to verify the weight fractions of poly(L-lactide) on their surfaces (table 3.7).

Table 3.7 Concentrations of poly(L-lactide) on the surfaces of the silica-cobalt nanoparticles

Poly(L-lactide) Fractions in PLLA-Silica-Co Complexes	**Specific Saturation Magnetization* (emu g^{-1})**
0.3	40
0.5	32

***** The saturation magnetization was 60 emu g^{-1} prior to adding the poly(L-lactide).

In addition, the surface compositions were analyzed by Thermal Gravimetric Analysis and XPS. The samples were heated from 25 °C to 700 °C at 10 °C min^{-1}. The major weight loss for all three concentrations occurred at 330 °C comparable to literature values for the decomposition temperature of poly(L-lactide). For each composition, the weight loss correlated well with the theoretical weight fraction of poly(L-lactide) on the surfaces of the complexes (figure 3.15). XPS also indicated the presence of carbonyls at 290 eV (the binding energy for C=O) on the surfaces resultant from the carbonyl rich backbone of poly(L-lactide) (figure 3.16).

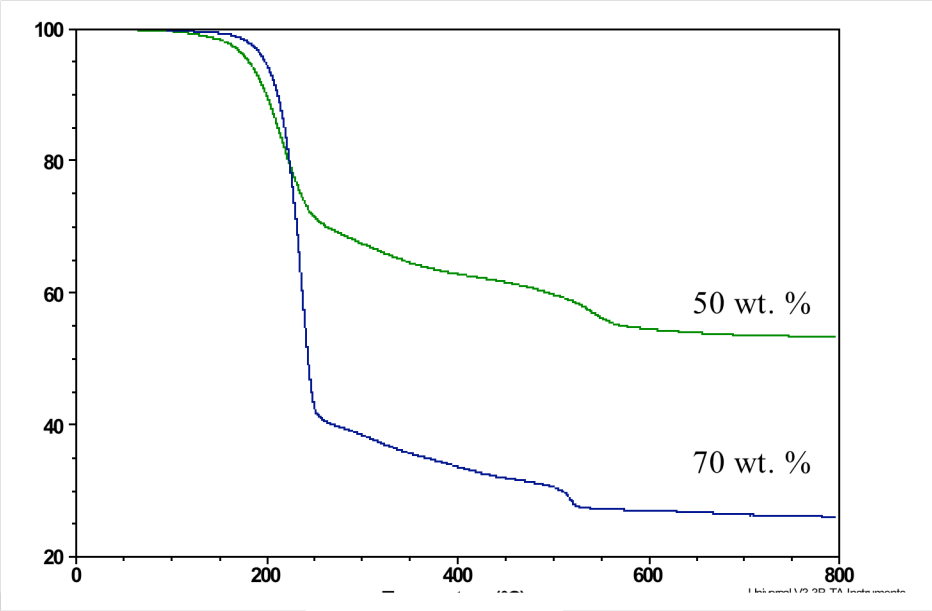

Figure 3.15 Weight loss profiles of three compositions of poly(L-lactide)-silica-cobalt complexes demonstrating the controllability of these surface initiated polymerizations.

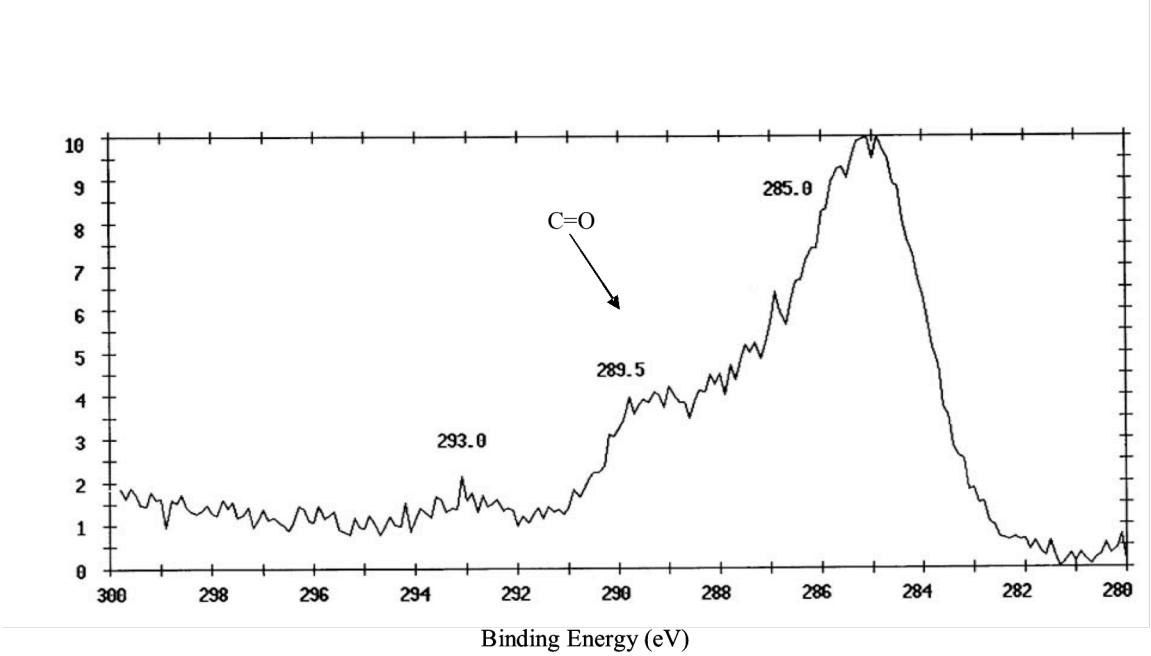

Figure 3.16 XPS binding energy indicative of C=O resultant from the poly(L-lactide) backbone.

3.3.5.3 Functionalization of silica-cobalt nanoparticles with PDMS

A 10,000 g mol^{-1} PDMS with trivinylsilane on one end only was hydrosilated with trimethoxysilane and reacted with the surfaces of silica-cobalt complexes. These functionalization reactions carried out in the absence of water afforded complexes with only small amounts of PDMS tethered to the silica-cobalt complex as evidenced by magnetic measurements (table 3.8). However, if small amounts of water were added to the reactions, substantial differences in saturation magnetizations were observed. This suggests that the water aided in hydrolysis and condensation of the trimethoxysilyl groups on the particle surfaces.

Table 3.8 Magnetic measurements suggest that the silica-cobalt complex surface is functionalized with PDMS.

Sample	Silica-Cobalt Complex Charged (g)	PDMS Charged (g)	Saturation Magnetization (emu g^{-1})
No water	0.03	0.3	49
Water (~1:2– water:methoxy)	0.03	0.1	27

3.3.5.4 Functionalization of silica-cobalt nanoparticles with isocyanate groups

For certain biotechnological applications, the silica-cobalt nanoparticles should be coated with a hydrophilic polymer such as poly(ethylene oxide). Water soluble oligomers bound to the particle surfaces can provide dispersive capabilities in aqueous media such as blood. Amines and alcohols react readily with isocyanates forming urea and urethane bonds, respectively. These silica-cobalt nanoparticles were re-functionalized with (3-isocyanatopropyl)trimethoxysilane under similar reaction conditions to those discussed for functionalization with aminopropyltrimethoxysilane.

Surface-bound isocyanates were further reacted with a mono-amine terminated poly(ethylene oxide-*co*-propylene oxide) copolymer. Titrations with the hydrophilic copolymer were also utilized to quantify the isocyanate concentration on the silica-cobalt surface (table 3.9). Although the charged concentrations differed from the final compositions, it is clear that hydrophilic oligomers can be reacted onto the particle surfaces by this method.

Table 3.9 Titrations suggest that the silica-cobalt complex surface can be re-functionalized with isocyanates, then further reacted with monoamine-terminated copolymers containing poly(ethylene oxide).

Theoretical Surface-bound Isocyanates (moles charged)	**Actual Surface-bound Isocyanates via Titration (mol)**	**Surface Jeffamine-2070® (g)**
2.73×10^{-5}	$(1.14 \pm 0.09) \times 10^{-5}$	0.024
2.2×10^{-4}	$(5.29 \pm 1) \times 10^{-5}$	0.111

CHAPTER 4 Synthesis and Characterization of Polysiloxanes with Pendent Phthalonitrile Groups

4.1 Synopsis

This chapter describes the synthesis and characterization of copolysiloxanes comprised of poly(dimethylsiloxane-*co*-methylhydrosiloxane) or poly(methylhydrosiloxane) and graft copolymers from these materials with an average of one polystyrene graft per copolymer. These random copolymers and homopolymers with pendent polystyrene grafts served as precursors for polymer modifications with pendent phthalonitriles. The modified polymers were used as dispersion stabilizers for preparing cobalt nanoparticles.

Cationic ring opening equilibration copolymerizations to form random copolysiloxanes were carried out utilizing D_4 and D_4H. In addition, cationic ring opening equilibration polymerization of D_4H was utilized to form the polymethylhydrosiloxane homopolymer. Characterization methods have included ^{1}H and ^{29}Si Nuclear Magnetic Resonance Spectroscopy (NMR), Thermal Gravimetric Analysis (TGA), and Differential Scanning Calorimetry (DSC).

These polysiloxane copolymers were functionalized with 2-allylphenoxyphthalonitrile and monovinyl terminated polystyrene oligomers to form the dispersion stabilizers. Their synthesis and properties are discussed herein.

4.2 Experimental
4.2.1 Materials

1,1,3,3,5,5,7,7-Octamethylcyclotetrasiloxane (D_4, MW 296.61 g mol^{-1}, d 0.956 g mL^{-1}, BP 104°C/2.5 mm Hg, Gelest Inc., 95 %) and 1,3,5,7-tetramethylcyclotetrasiloxane (D_4H, MW 240.51 g mol^{-1}, d 0.9912 g mL^{-1}, MP -69 °C, BP 134-135 °C, Gelest Inc.) were dried over calcium hydride for 24 h and distilled prior to use. Hexamethyldisiloxane (MW 162.38 g mol^{-1}, d 0.7636 g mL^{-1}, MP -67 °C, BP 99-100 °C, Gelest Inc.) was distilled prior to use. Trifluoromethanesulfonic acid (MW 150.07 g mol^{-1}, d 1.708 g mL^{-1}, BP 162 °C, Aldrich, 99%) was used as received. Toluene (MW 92.14 g mol^{-1}, d 0.865 g mL^{-1}, MP -63 °C, BP 110 °C, Burdick and Jackson, 99.9 %) was washed twice with concentrated sulfuric acid and neutralized with water. It was dried over $MgSO_4$ for one h, then over calcium hydride overnight and fractionally distilled just before use. The first fraction which contained the toluene-water azeotrope was discarded, then the fraction with a constant boiling of 110 ^oC was collected. A Pt^0(1,3-divinyl-1,1,3,3-tetramethyldisiloxane)$_{1.5}$ complex catalyst in xylene (2.1 – 2.4 wt % Pt^0, Karstedt's catalyst, Gelest Inc.) was used as received. 4-Nitrophthalonitrile (MW 173.13 g mol^{-1}, MP 142-144 °C, kindly donated by Bayer, Inc.) was recrystallized from ethanol then dried *in vacuo* at 100 °C overnight. 2-Allylphenol (MW 134.18 g mol^{-1}, d 1.028 g mL^{-1}, BP 220 °C, 98%), 1-methyl-2-pyrrolidinone (NMP, MW 99.13 g mol^{-1}, d 1.028 g mL^{-1}, MP -24 °C, BP 81-82/10 mm Hg, 99 %) and K_2CO_3 (MW 138.21 g mol^{-1}, d 2.430 g mL^{-1}, MP 891 °C, 99 %) were purchased from Aldrich and used as received. Styrene (MW 104.15 g mol^{-1}, d 0.909 g mL^{-1}, MP -31 °C, BP 145-146 °C, Aldrich, 99%) was stirred over calcium hydride for 24 h and distilled prior to use. *N*-Butyllithium (2.0 M in cyclohexane, Aldrich) was used as received. Vinyldimethylchlorosilane (MW 120.65 g

mol^{-1}, d 0.884 g mL^{-1}, BP 82-83 °C, Gelest Inc.) was vacuum distilled prior to use. Tetrahydrofuran (THF, EM Science 99.5%) was dried over calcium hydride and refluxed over sodium with benzophenone until the solution was deep purple. It was fractionally distilled into a flame-dried, round bottom flask prior to each reaction.

4.2.2 Synthesis of 2-allylphenoxyphthalonitrile

2-Allylphenol (5.0 g, 0.042 mol), potassium carbonate (K_2CO_3) (13.821 g, 0.100 mol), 4-nitrophthalonitrile (7.570 g, 0.0438 mol), and ~30 mL of N-methylpyrrolidone (NMP) were charged to a one-neck, 250-mL, round bottom flask. Small amounts of water were added to aid the dissolution of the K_2CO_3. The reaction was conducted for 24 h at room temperature. The 2-allylphenoxyphthalonitrile was precipitated by slowly adding the reaction solution to rapidly stirring (stirred with a blender) water at room temperature, then the precipitate was stirred for an additional 10 min. The 2-allylphenoxyphthalonitrile was collected via vacuum filtration. The product was dried under vacuum at 70 °C overnight. The 2-allylphenoxyphthalonitrile was kept in a sealed amber bottle and stored in a glass vial until use.

4.2.3 Synthesis of Poly(dimethyl-*co*-methylhydro)siloxane (PDMS-*co*-PMHS)

A synthesis procedure for PDMS-*co*-PMHS (50:50 composition, 2000 g mol^{-1}) is provided. A series of copolymers with systematically varied compositions was synthesized utilizing this same procedure, but with appropriate relative concentrations of D_4 and D_4H. D_4 (5.6 g, 5.91 mL, 0.019 mol) and D_4H (4.81 g, 4.85 mL, 0.020 mol) were added via syringe to a septum-sealed, flame-dried flask under nitrogen. Hexamethyldisiloxane (0.81 mL, 0.6 g, 0.004 mol) was added via syringe to the reaction

vessel. The reaction solution was allowed to stir for 10 min at 65 °C. Triflic acid (0.1 wt% of polymer, 0.01 mL, 0.011 g, 7.79 x 10^{-5} mol) was cautiously added via syringe. The polymerization was carried out under nitrogen at 65 °C for 3 days. The polymer was dissolved in dichloromethane and washed with water several times to neutralize the acid. The dichloromethane was evaporated and cyclics were removed by vacuum distillation at 100 °C.

4.2.4 Synthesis of poly(dimethyl-*co*-methyl-3-propylphenoxyphthalonitrile)siloxane (PDMS-*co*-PHTH)

A synthetic procedure for the hydrosilation of a PDMS-*co*-PMHS (50:50 eq:eq composition, 2000 g mol^{-1}) is provided. All hydrosilated copolymers in the series were prepared utilizing this procedure. 2-Allylphenoxyphthalonitrile (1.148 g, 0.004 mol) was dissolved in 20 mL of anhydrous toluene in a flame-dried, round-bottom flask sealed with a septum under nitrogen. The solution was stirred at 50 °C for 10 min. Karstedt's catalyst (0.0363 mL, 8.35 x 10^{-4} g, 4.28 x 10^{-6} mol, 1 eq platinum per 1000 allyl groups) was added and allowed to stir for another 10 min. PDMS-*co*-PMHS (0.5 g, 0.0035 eq Si-H) was added via syringe. The reaction was conducted at 50 °C until reaction completion was achieved as monitored by ^{1}H NMR.

4.2.5 Synthesis of a vinyldimethylsilyl terminated polystyrene oligomer

A procedure for preparing a 7000 g mol^{-1} monovinyl functional polystyrene is provided. A series of vinyl functional polystyrenes were synthesized utilizing this procedure. Styrene (15 g, 16.5 mL) was charged via glass syringe to a flame-dried, 250-mL, round bottom flask equipped with a magnetic stir bar. Anhydrous toluene (10 mL) was added to the reaction vessel via glass syringe and the solution was allowed to stir at room temperature for 10 min to ensure a homogeneous solution. *N*-Butyllithium (0.0021

mol, 1.05 mL) was added via glass syringe. Anhydrous THF (10 mL) was added to the reaction vessel via glass syringe. The reaction turned a bright red-orange color indicating the presence of the styrenic anion. The reaction progress was monitored via ^{1}H NMR. The reaction temperature was decreased to -78 °C. The polymerization was terminated with vinyldimethylchlorosilane (0.25 g, 0.0021 mol, 0.29 mL) which was added via glass syringe. The solution turned hazy indicating the presence of LiCl salts. The polystyrene was washed with water several times to remove salts, precipitated into methanol, and dried under vacuum. The molecular weights were determined by GPC and ^{1}H NMR.

4.2.6 Synthesis of poly(dimethyl-*co*-[methyl-3-propylphenoxyphthalonitrile]-*g*-styrene) ([PDMS-*co*-PHTH]-*g*-PS)

PDMS-*co*-PHTH-*g*-PS graft copolymers were synthesized via a series of hydrosilation reactions. PDMS-*co*-PMHS, with a backbone molecular weight of 9800 g mol^{-1} wherein there were 25 % Si-H repeat units and 75 % dimethylsiloxane repeat units, (2 g, 0.0067 eq Si-H) was added to a 100-mL, round bottom flask equipped with a magnetic stir bar. Monovinyl-functional polystyrene (6900 g mol^{-1}, 1 graft per PDMS-*co*-PMHS chain, 1.408 g, 2.04 x 10^{-4} mol vinylsilyl end group) was pre-weighed and added to the reaction vessel. Anhydrous toluene (10 mL) was added via glass syringe and the solution was allowed to stir for 10 min. Karstedt's catalyst solution in xylenes (0.020 mL) was added via syringe. The reaction was conducted for 4 h at 50 °C. ^{1}H NMR was utilized to monitor the progress of the reaction. A slight excess of 2-allylphenoxyphthalonitrile (0.0070 mol, 1.736 g) was dissolved in a separate toluene solution and added to the reaction vessel drop-wise over 10 min. The solution turned golden brown. The graft copolymer with phthalonitrile pendent groups was precipitated

into cold methanol and dried under vacuum. ^{1}H NMR was utilized to characterize the copolymer composition.

4.2.7 Synthesis of poly(methyl-3-propylphenoxyphthalonitrile-*g*-styrene) (PHTH-*g*-PS)

A similar procedure as described in 4.2.7 was utilized to prepare graft copolymers consisting of an average of one polystyrene graft per PMHS chain. The PMHS-*g*-PS was further hydrosilated with 2-allylphenoxyphthalonitrile to form the final composition. PMHS (2 g, 0.001 mol chains) was charged to a 100-mL, round bottom flask. Polystyrene (0.001 mol, 0.001 eq vinyl, 6.9 g) was charged to the reaction vessel. Anhydrous toluene (10 mL) was added via syringe to dissolve the oligomer. Karstedt's catalyst (0.010 mL, 1 mol Pt^0:1000 mol vinyl) was added via syringe. The reaction solution was stirred for 4 h at 50 °C. 2-Allylphenoxyphthalonitrile (0.033 mol, 8.18 g) was dissolved separately in anhydrous toluene and added via syringe to the reaction vessel. The reaction was monitored by ^{1}H NMR until reaction completion. The graft copolymer was precipitated from cold methanol. The final composition was determined by ^{1}H NMR.

4.3 Copolymer characterization

4.3.1 ^{1}H nuclear magnetic resonance spectroscopy

All ^{1}H NMR spectra were obtained on a Varian Unity 400 MHz NMR spectrometer operating at 400 MHz. The NMR parameters included a pulse width of 28.6° and a relaxation delay of 1.000 sec at ambient temperature. The samples were dissolved in *d*-$CHCl_3$ for obtaining the spectra.

4.3.2 ^{29}Si nuclear magnetic resonance spectroscopy

All ^{29}Si NMR spectra were obtained on a Varian Unity 400 MHz NMR spectrometer operating at 80 MHz. The samples for ^{29}Si NMR were prepared with 0.63g copolymer, 0.52g $Cr(Acac)_3$, and 2.4 mL *d*-$CHCl_3$. Quantitative silicon NMR spectra were obtained with the aid of the relaxation agent, $Cr(Acac)_3$, with a pulse width of 168.0° and a relaxation delay of 10 sec. Six hundred fifty scans were accumulated for each spectrum.

4.3.3 Gel permeation chromatography

Gel permeation chromatograms were obtained in chloroform at 30 °C on a Waters Alliance Model 2690 chromatograph equipped with a Waters HR 0.5 + HR 2 + HR 3 + HR 4 styragel column set. A Viscotek viscosity detector and a Waters refractive index detector were utilized with polystyrene calibration standards to generate a universal molecular weight calibration curve for absolute molecular weight analyses. Samples were prepared by dissolving 15-20 mg of sample in 10 mL of HPLC grade chloroform.

4.3.4 Thermal properties

4.3.4.1 Differential scanning calorimetry

Thermal properties of the copolymers were analyzed by differential scanning calorimetry using a TA Instruments DSC Q1000 under a constant flow of helium. The samples (10-15 mg) were cycled from -150 to 120 °C using hermetically sealed DSC pans. Two scans were performed on each sample where the T_g's were taken as the inflection points on the second scans.

4.3.4.2 Thermal gravimetric analysis

Weight loss profiles were analyzed with a TA Instruments TGA Q0500 under N_2. The TGA was balanced against an empty reference pan prior to each run. The samples were heated at 10 °C min^{-1} to 700 °C.

4.4 Results and Discussion

There has been a great deal of research in an effort to passivate the surface of cobalt nanoparticles against oxidation.[5,7,129,130] The approach has been to utilize copolymer templates to form the nanoparticles in solution and further collapse the copolymer sheath into stable graphite or ceramic coatings upon elevated heat treatments. Investigations of silica shells around the cobalt nanoparticles suggested that the silica-coated cobalt nanoparticles were not sufficiently durable to protect against oxidation.[8] However, these silica shells did provide surfaces which could be easily re-functionalized following elevated heat treatments.[7] Research in our laboratories suggests, however, that a graphitic coating (derived from styrenic anchor blocks having pendent phthalonitrile groups) was more robust than silica, thus serving as an enhanced oxygen barrier.[5] Therefore, a cobalt nanoparticle stabilizer that combines both the phthalonitrile moieties with polysiloxanes was the motivation for this research. It was anticipated that this combined stabilizer would serve as a shell precursor that would harness the advantages of the phthalonitriles (graphitic precursor and oxygen barrier) and the siloxane (silica precursor and functionalizable surface precursor). Therefore, a polysiloxane stabilizer with pendent phthalonitrile groups was designed to provide a combined graphite and silica precursor for subsequent collapse onto the colloidal cobalt.

4.4.1 Synthesis of Poly(dimethyl-*co*-methylhydro)siloxane (PDMS-*co*-PMHS)

Polysiloxanes are widely investigated due to their unique properties and the vast numbers of functional groups that can be introduced in the backbone or chain ends. This class of materials is utilized in a variety of applications such as liquid crystals, photocrosslinking, ionic conductivity, and electroluminescence.[74,81,131] Copolysiloxanes consisting of methylhydrosiloxane and dimethylsiloxane units can serve as precursor polymers that can be chemically modified to introduce desired functional groups. The concentration of methylhydrosiloxane repeat units can be varied to tailor the resultant functional polymer with the desired properties. The properties of the copolymers depend on the side chain groups, their proportion to the main chain, as well as their distribution along the backbone.

It is well established that polysiloxanes can be synthesized via living anionic ring opening polymerization or cationic or anionic equilibration polymerizations.[3,132-136] The unstrained tetrasiloxane rings can be equilibrated to prescribed molecular weights by adjusting the ratio of the cyclic monomers to endcapping reagents, and the choice of acidic or basic equilibration catalyst is dictated by the nature of the siloxane repeat units. Since the Si-H bond is labile to base, the equilibration reactions in this research were conducted with triflic acid as the catalyst. Such procedures are well documented in the literature.[74,133] Redistribution reactions of polysiloxanes lead to a distribution of linear and cyclic species at equilibrium, then after neutralization of the catalyst, the low molecular weight cyclics can be removed via vacuum distillation. The molecular weight distributions of such polymers are approximately two.

In this research, the concentration of methylhydrosiloxane groups relative to dimethylsiloxane units in the copolymer backbones were systematically varied by copolymerizing two cyclic tetrasiloxane monomers, D_4 and D_4H (figure 1). Triflic acid served as a strong acid catalyst with hexamethyldisiloxane as the endcapping reagent. The sequences of these copolymer backbones were expected to be random due to the nature of the redistribution process. It is important to note that D_4H must be polymerized under acidic conditions to avoid abstraction of the hydrido moiety by base. A series of copolymers were synthesized utilizing this approach (table 4.1).

The cationic copolymerization of D_4 and D_4H leads to an equilibrium between linear chains and cyclics. The cyclics are extracted by vacuum distillation when equilibrium was achieved and represent approximately 10-13% of the siloxane content according to Canouet et al.[74]

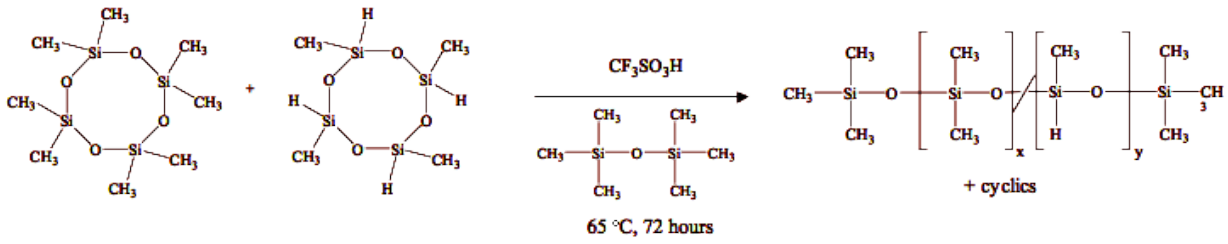

Figure 4.1. Acid catalyzed equilibration polymerization of D_4 and D_4H.

The progress of the copolymerization of D_4 and D_4H depends on the relative reactivities of the two monomers. It is desirable to obtain completely random placement of D^H and D units. However, Cancouet et al. reported that the initial stages of the polymerization contain copolymers that are noticeably richer in D^H suggesting that D_4H is incorporated into the copolymer at a much quicker rate that the dimethylsiloxane monomer.[74] In solutions containing triflic acid, Graczyk and Lasocki found that the

relative reactivity ratios of D_4 (r_1) to D_4H (r_2) were $r_1 = 0.82$ and $r_2 = 1.26$.[137] From these ratios, they deduced that the homopolymerization of D_4H occurs more readily than does the polymerization or cross-polymerization of D_4. The compositions reported were relative to the feed compositions after 60-70 % conversion. The chemical compositions obtained in this research were well controlled, as evidenced by the experimental compositions and molecular weights being close to targeted values in all cases.

Table 4.1 A series of PDMS-*co*-PMHS copolymers were synthesized via cationic equilibration polymerization.

Target Percent Composition		**Target M_n (g mol^{-1})**		**Repeat Unit Percent Composition from ^{29}Si NMR**		**M_n by ^{29}Si NMR (g mol^{-1})**	
PDMS	PMHS	PDMS	PMHS	PDMS	PMHS	PDMS	PMHS
0	100	0	2000	0	100	0	2000
20	80	1700	12000	20	80	1900	11500
25	75	518	1320	24	76	518	1320
50	50	1036	840	49	51	1400	1200
50	50	5400	4380	50	50	4400	3500
75	25	1550	420	74	26	1800	500
75	25	7800	2000	76	24	6400	1600
85	15	60000	9000	85	15	43000	6000
85	15	16000	2300	86	14	10500	1500

4.4.2 Characterization of PDMS-*co*-PMHS random copolymers

4.4.2.1 Molecular architectures

The copolymers were rigorously purified to remove any residual acid and cyclics. The relative compositions of each component in the copolymers after isolation were confirmed by ^{1}H and ^{29}Si NMR. In the ^{1}H NMR spectra, the methyl integrals from the $Si(\underline{CH_3})_2$ resonances at 0.11 ppm were resolved from the methyl resonances of the H-$Si(\underline{CH_3})$ at 0.19 ppm (figure 4.2). The insets in figure 4.2 depict magnifications of the H-$Si(\underline{CH_3})$ and $Si(\underline{CH_3})_2$ resonances. The splitting pattern results from the atomic connectivity/chemical environments of the repeat units. This pattern represents triad effects where each signal was assigned utilizing variations in intensities with

compositions. The H-Si($\underline{CH_3}$) repeat unit may be surrounded by two dimethylsiloxane units, one dimethylsiloxane and one methylhydrosiloxane, or two methylhydrosiloxane repeat units. The major composition is the H-Si($\underline{CH_3}$) surrounded by two H-Si($\underline{CH_3}$) as evidenced by integrations of the peak resonances. The same triad effect is observed for the dimethylsiloxane repeat unit methyl protons. The major composition is the Si($\underline{CH_3}$)$_2$ surrounded by one Si($\underline{CH_3}$)$_2$ and one H-Si(CH_3) repeat unit as evidenced by proton integrations.

This triad pattern is also true for the resonances due to the Si-$\underline{H}$ at 4.7 ppm. The signal is split into a triad sequence with the high field signal due to the $\underline{H}$-Si(CH_3) unit in between two Si(CH_3)$_2$ units. The middle signal at 4.7 ppm is due to a $\underline{H}$-Si(CH_3) unit surrounded by a $\underline{H}$-Si(CH_3) and Si(CH_3)$_2$ unit which represents the major contribution. The low field signal has a $\underline{H}$-Si(CH_3) unit with two neighboring $\underline{H}$-Si(CH_3). These are same compositions observed in the proton resonances for the methyls on the polymer backbone. There are approximately 50 % of these units in the overall Si-H sequence.

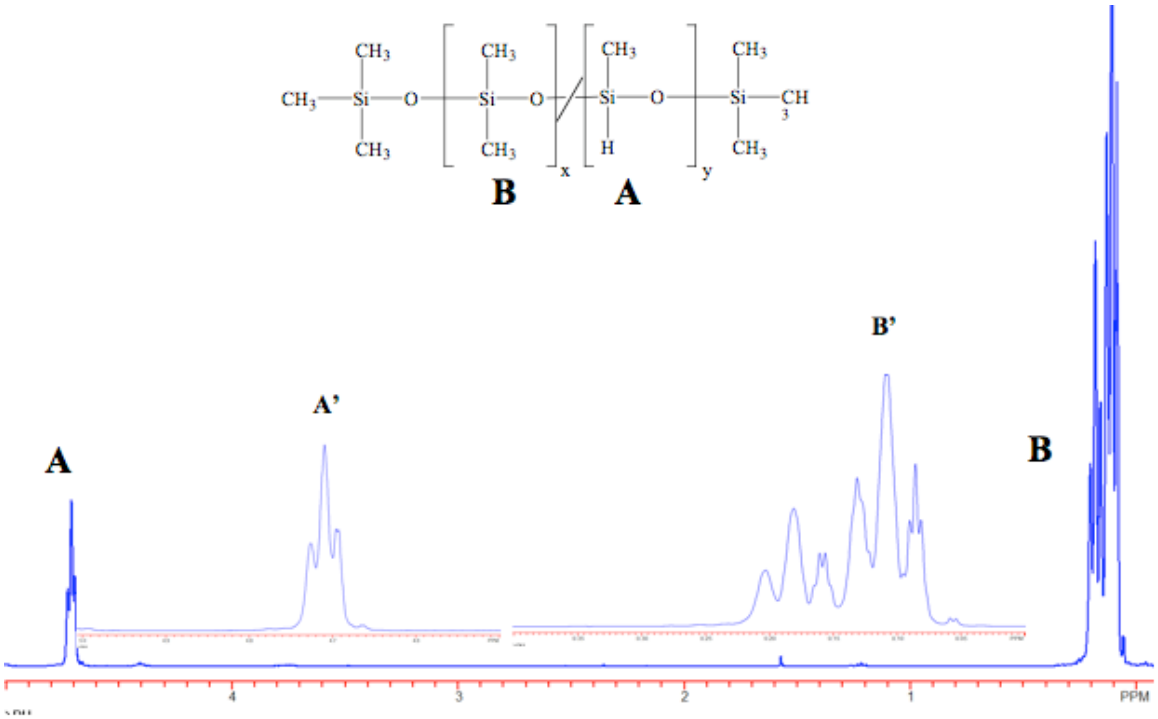

Figure 4.2 ^{1}H NMR of PDMS-*co*-PMHS indicating triad effects on the proton resonance. A' and B' represent magnifications of the resonances at 4.7 and 0 ppm respectively.

^{29}Si NMR was utilized to aid in determining the copolymer compositions, the number average molecular weights of each component, and copolymer molecular architecture. ^{29}Si NMR provides a valuable tool for characterizing polysiloxanes because of its wide frequency chemical shift range. The dimethylsiloxane silicons are well separated from the methylhydrosiloxane silicons in the ^{29}Si NMR. The D resonances were observed at -18 to -22 ppm while the D^{H} units were observed at -34.7 to -37.5 ppm. Resonances due to the end groups were observed at 8 and 10 ppm (figure 4.3). A similar triad sequence effect was observed in the ^{29}Si NMR as was observed in the ^{1}H NMR. The resonances resulting from both the silicons of the D and D^{H} units appeared as heptads superimposed onto triads. The slow relaxation time of the ^{29}Si NMR results in increased sensitivity therefore allowing the heptad sequence to be observed. The triad

pattern results from the different chemical environment of the silicon atoms, the thus, the chemical shift of a silicon atom is greatly influenced by the neighboring units. Therefore, the copolymer microstructure or repeat unit sequence may be deduced from the ^{29}Si NMR. ^{29}Si NMR is more sensitive than proton NMR and the splitting patterns are more complicated. The splitting patterns and chemical shifts are in good agreement with the literature.[74,138,139] Cancouet et al. observed heptads superimposed onto triads for several compositions of PDMS-*co*-PMHS random copolymers.

The copolymer compositions were obtained by ratioing the repeat unit integrals corresponding to each moiety relative to the end groups. In all cases, the M_n's and compositions derived from ^{29}Si NMR paralleled the targeted values.

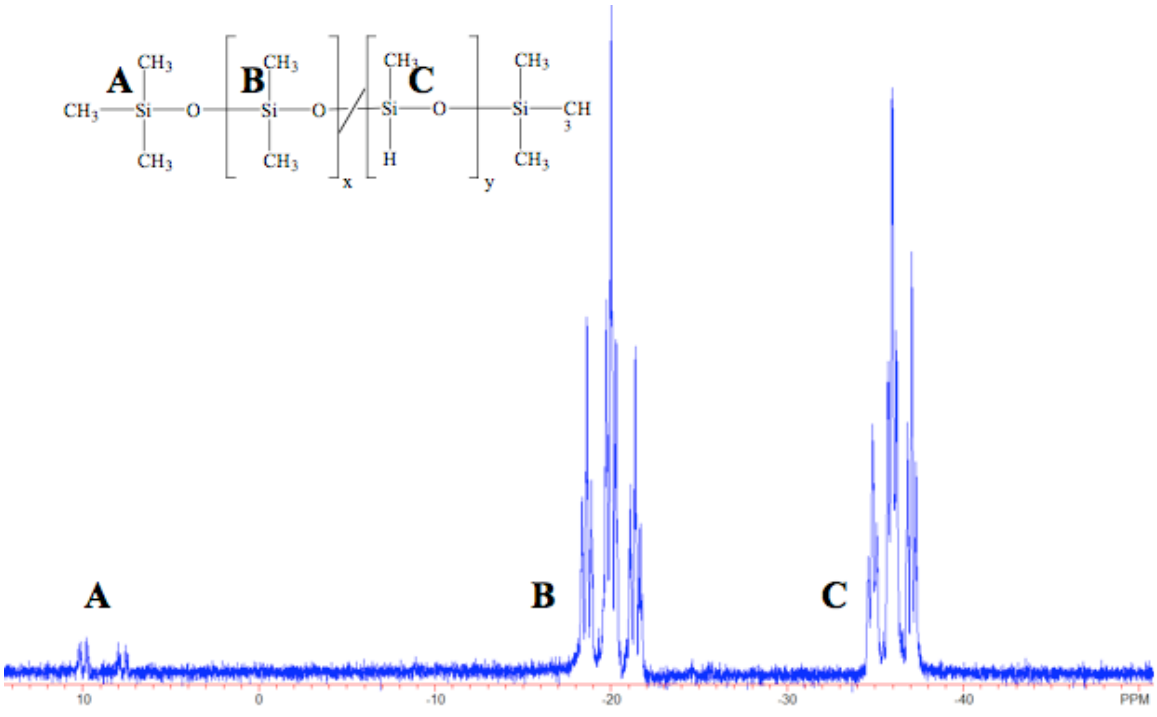

Figure 4.3 ^{29}Si NMR of PDMS-*co*-PMHS.

4.4.3 Chemical modification of PDMS-*co*-PMHS copolymers

Chemical modifications of polysiloxanes play a large role in both academic and industrial sectors. Hydrosilation of unsaturated moieties across Si-H bonds is utilized widely to chemically modify polysiloxanes.[80,88] These reactions are usually catalyzed by platinum catalysts or transition metal salts, but such reactions can also occur by thermal or photochemical processes.[81] Syntheses of hybrid materials can be conducted by the direct addition of unsaturated derivatives to PMHS. The resultant polymers have tailored properties, which can include mediated hydrophilicity, chirality, photo-curable compositions, or optical activity. Thermal stability has also been enhanced for polysiloxanes by hydrosilation of boron containing allyl derivatives. Large groups such as allyl-derivatized carbohydrates [85]can hinder reaction and result in incomplete hydrosilation. Other functional groups including allyl derivatives of nitriles[86] and ethers[87] have been hydrosilated with PMHS with complete conversion.

This research is focused upon introducing a phthalonitrile moiety into the backbone of PDMS-*co*-PMHS. Phthalonitriles are known for their oxidative and thermal stability.[140,141] These groups have been shown to serve as excellent precursors to graphitic shells around cobalt nanoparticles.[5]

PDMS-*co*-PMHS copolymers were hydrosilated with 4-allyl-phenoxyphthalonitrile using Karstedt's catalyst in anhydrous toluene to form copolymers of poly(dimethyl-*co*-2-propyl-2-phenoxyphthalonitrile) (PDMS-*co*-PHTH) (figure 4). Solutions of Karstedt's catalyst and excess 4-allyl-phenoxyphthalonitrile were prepared separately. This order of addition was important to achieve quantitative hydrosilation. It is believed that complexation of the platinum with the allyl moiety prior to introduction

of the Si-H resulted in decreased side reactions. PDMS-*co*-PMHS copolymers were added to the platinum/phthalonitrile solution and the reaction progress was monitored by ^{1}H NMR. The reactions were golden yellow and were complete within four hours.

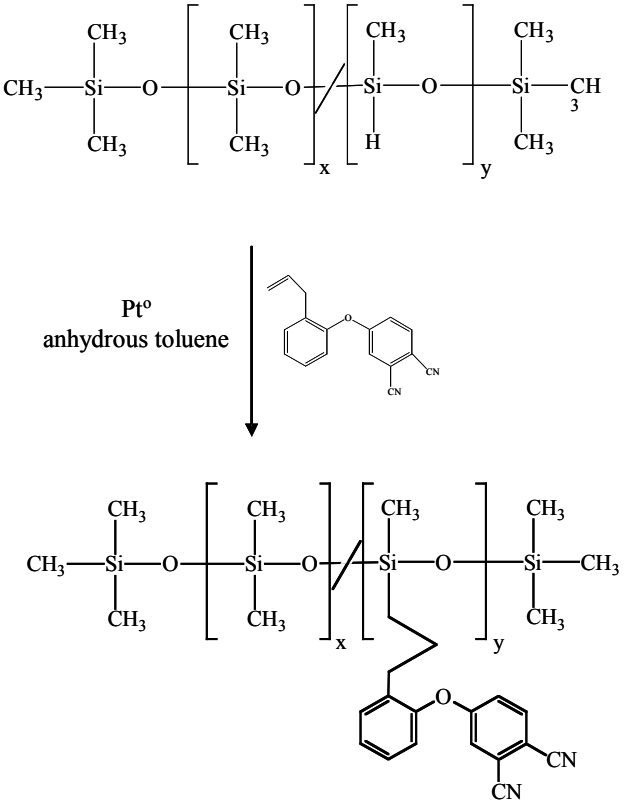

Figure 4.4 A reaction scheme depicting the hydrosilation of Si-H units on a PDMS-*co*-PMHS copolymer with 4-allyl-phenoxyphthalonitrile.

These reactions occurred quickly and with quantitative conversion for all compositions investigated. The exothermic reactions resulted in temperature increases to as high as 75 °C (figure 4.5). ^{1}H NMR of the rigorously purified PDMS-*co*-PHTH shows that the Si-H resonance at 4.5 ppm and the allyl protons from the phthalonitrile disappeared completely during the reaction. New resonances (b, c, and d in figure 4.5) appeared resulting from the addition of the Si-H across the phthalonitrile allyl bond.

Hydrosilation reactions yield both α and β addition products.[81] It is difficult to quantitatively discern the α and β addition products in this work, but these reactions typically yielded 90% or greater of the β addition products (figure 4.6). The phenyl resonances from the phthalonitrile moieties were observed above 7 ppm.

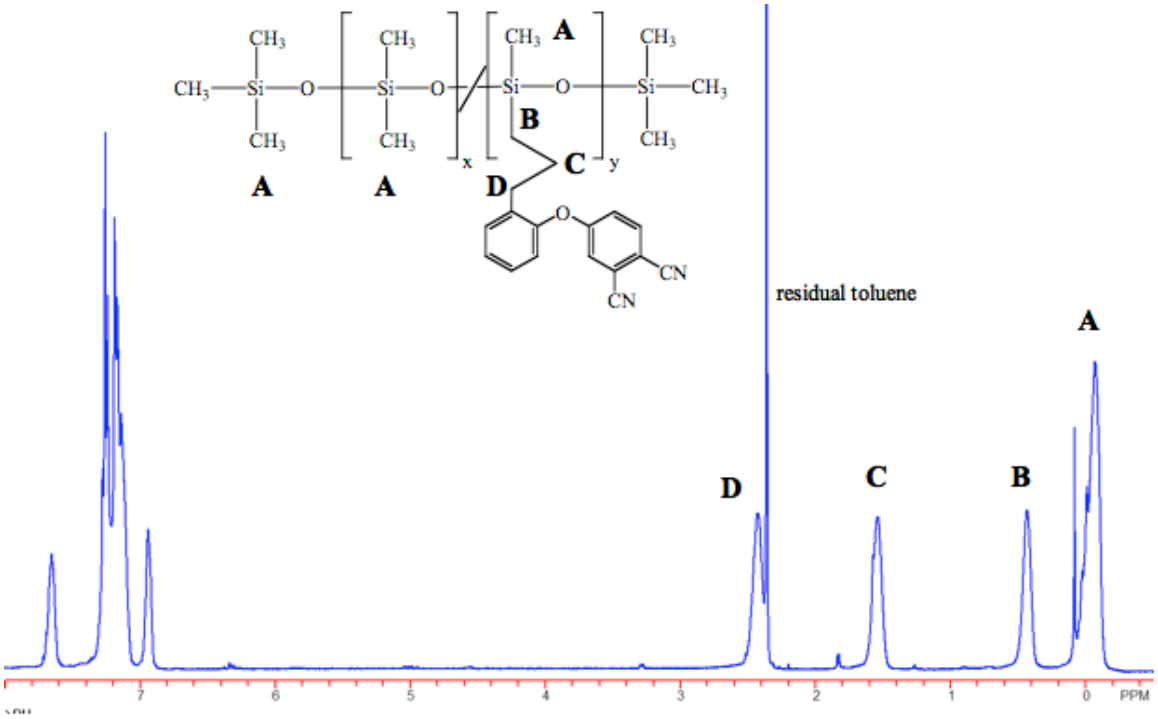

Figure 4.5 ^{1}H NMR reveals quantitative hydrosilation of 2-allylphenoxyphthalonitrile onto the backbone of a PDMS-*co*-PMHS copolymer to form PDMS-*co*-PHTH.

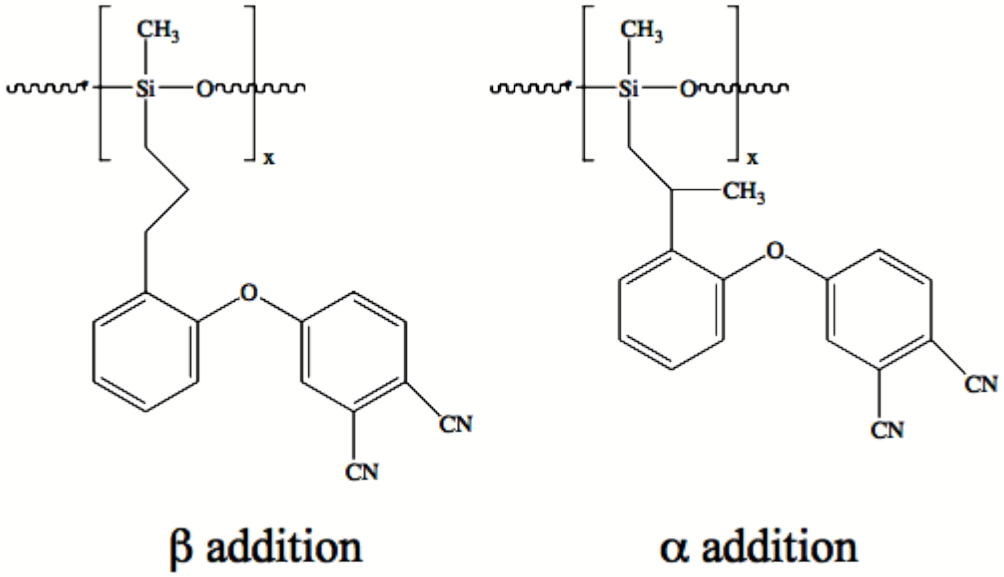

Figure 4.6 The β addition product is the major product of the hydrosilation reaction.

^{29}Si NMR was utilized in conjunction with ^{1}H NMR to confirm the extent of hydrosilation for these copolymers. The hydrosilations were quantitative for all copolymers as indicated by an absence of resonances due to Si-H at -35 ppm (figure 4.6). A new resonance appeared corresponding to siloxane repeat units containing the phthalonitrile groups at -24 ppm. The reaction mixtures were sensitive to the concentration of phthalonitrile. Higher phthalonitrile concentrations caused phase separation from the toluene solvent during reaction due to the increased polarity of the system as they were hydrosilated. Hydrosilation of the PMHS homopolymer with 2-allylphenoxyphthalonitrile resulted in precipitation of the polymer before quantitative hydrosilation occurred. This was likely due to the polar nature of the backbone causing incompatibility with the toluene solvent. Therefore, it was important that for all compositions above 25% phthalonitrile, the polymer was added slowly in several aliquots to the phthalonitrile/toluene solutions. Table 4.2 depicts the weight compositions obtained from these reactions for all copolymers. After hydrosilation, the overall weight

composition of the PDMS decreased as compared to the precursor PDMS-*co*-PMHS copolymers due to the high molecular weight of the pendent phthalonitrile units.

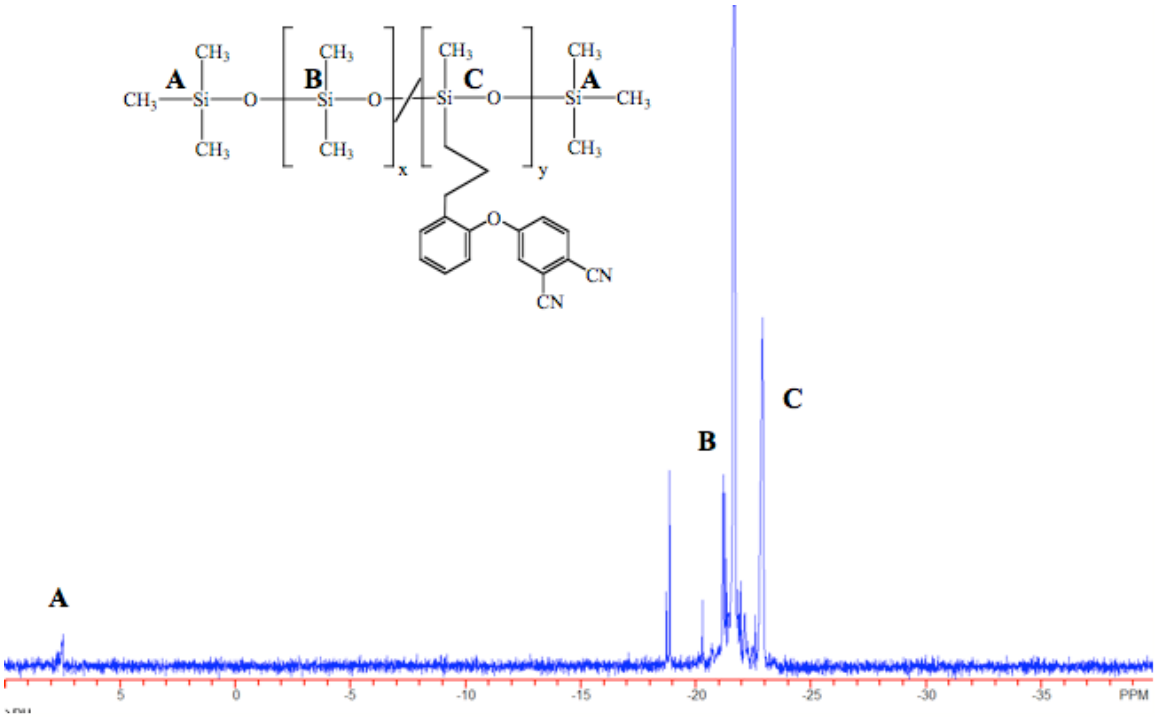

Figure 4.7 Quantitative hydrosilation shown by ^{29}Si NMR (note the absence of Si-H and the appearance of a new resonance corresponding to the phthalonitrile Si at –24 ppm).

Table 4.2 Weight compositions obtained after hydrosilation are determined via ^{29}Si NMR. The molecular weight of the phthalonitrile containing units increase substantially.

M_n by ^{29}Si NMR (g mol^{-1})		**Repeat Unit Percent Composition from ^{29}Si NMR**		**M_n by ^{29}Si NMR (g mol^{-1})**		**Weight Percent Composition from ^{29}Si NMR**	
PDMS	PMHS	PDMS	PMHS	PDMS	PHTH	PDMS	PHTH
0	2000	0	100	0	n/a	0	n/a
1900	11500	20	80	1900	61400	3	97
518	1320	24	76	518	7040	7	93
1400	1200	49	51	1400	6400	18	82
4400	3500	50	50	4400	18560	20	80
1800	500	74	26	1800	2560	41	59
6400	1600	76	24	6400	8640	43	57
43000	6000	85	15	43000	32000	57	43
10500	1500	86	14	10500	8000	57	43

4.4.4 Thermal Characterization of PDMS-*co*-PMHS and PDMS-*co*-PHTH

The thermal properties of these functionalized copolymers were investigated to probe their morphologies. Thermal transitions of polymers are based on molecular motion at a given kT. Increased rigidity of the polymer backbone increases the glass transition temperature. Microphase separation in copolymers depends on relative polarities of the units and molecular weights of the sequences. A 2000 g mol^{-1} PMHS homopolymer exhibits a glass transition temperature of -139 °C whereas PDMS homopolymers have T_g's of approximately -125 °C. Random PDMS-*co*-PMHS

copolymers have a single glass transition temperature from -130 to -135 °C depending on the weight fraction of the dimethylsiloxane, and this suggests that these copolymers form single phases. The T_g increases as the weight fraction of PDMS increases as dictated by the Flory-Fox equation. In addition, the typical crystallization exotherms and melting endotherms are not observed for these copolymers, which suggests that the PMHS units disrupt the ability of the PDMS to crystallize.

The PDMS-*co*-PHTH copolymers had glass transition temperatures ranging from -47-20 °C depending on the concentration of the pendent phthalonitrile units (table 4.3). This suggests that the phthalonitrile moiety along the backbone of the siloxane inhibits free rotation about the Si-O bond. The T_g's increased proportionally to the concentration of phthalonitrile.

Table 4.3 The glass transition temperatures of the PDMS-*co*-PHTH copolymers are a function of phthalonitrile concentration.

M_n by ^{29}Si NMR (g mol^{-1})		**Repeat Unit Percent Composition from ^{29}Si NMR**		**M_n by ^{29}Si NMR (g mol^{-1})**		**T_g (° C)**
PDMS	PMHS	PDMS	PMHS	PDMS	PHTH	PDMS-*co*-PHTH
0	2000	0	100	0	n/a	n/a
1900	11500	20	80	1900	61400	20
518	1320	24	76	518	7040	16
1400	1200	49	51	1400	6400	4
4400	3500	50	50	4400	18560	3
1800	500	74	26	1800	2560	-34
6400	1600	76	24	6400	8640	-35
43000	6000	85	15	43000	32000	-47
10500	1500	86	14	10500	8000	-47

Thermal gravimetric analysis was utilized to investigate the thermal stability and char residues of the PDMS-*co*-PMHS and PDMS-*co*-PHTH copolymers. It was reasoned that their char yields should relate closely to their propensity to form protective shells around cobalt nanoparticles upon pyrolysis. The materials were analyzed under nitrogen atmospheres utilizing conditions mimicking the high temperature annealing processes utilized for the copolymer-cobalt complexes. The polymers were ramped from room temperature to 700 °C at 10 °C min^{-1}. Table 4.4 depicts the results of these analyses. PDMS and PMHS homopolymers typically exhibit weight losses of 95-100%, and PDMS-*co*-PMHS copolymers lose approximately 95% of their weight. However,

PDMS-*co*-PHTH copolymers show increased weight retention with increased phthalonitrile content. This is likely due to the thermo-oxidative stability of the phthalonitrile unit suggesting that these copolymers might form enhanced oxygen barriers for the cobalt nanoparticles upon pyrolysis. The weight losses correlate well with the weight compositions of the PDMS (table 4.4).

Table 4.4 Weight loss profiles of PDMS-*co*-PHTH copolymers in nitrogen.

Weight Percent Composition from ^{29}Si NMR		**M_n by ^{29}Si NMR (g mol^{-1})**		**Weight Loss in Nitrogen (%)**
PDMS	PHTH	PDMS	PHTH	
0	100	0	n/a	n/a
20	80	1900	61400	58
24	76	518	7040	53
49	51	1400	6400	64
50	50	4400	18560	63
74	26	1800	2560	76
76	24	6400	8640	75
85	15	43000	32000	80
86	14	10500	8000	82

4.4.5 Synthesis and characterization of poly(siloxane-*g*-styrene) copolymers for use as cobalt nanoparticle stabilizers

The stabilization of dispersions of cobalt nanoparticles with various macromolecules has been investigated for many years.[126,142,143] The macromolecular stabilizers for cobalt nanoparticles in the present work involve a copolymer containing an

anchor block and a tail block. The anchor block adheres or coordinates with the metal surface while the tail block extends into the solvent providing steric stabilization of the dispersion. Two stabilizers have been the research focus: 1) polysiloxane copolymers wherein both the anchor block and tail block were siloxane-based, and 2) polystyrene copolymers wherein the tail block is polystyrene and the anchor block is derived from vinyl-4-phenoxyphthalonitrile (figure 4.7).[3,5] The goal of the current research is to combine attributes from both systems to harness the advantages of both the siliceous and the graphitic precursors.

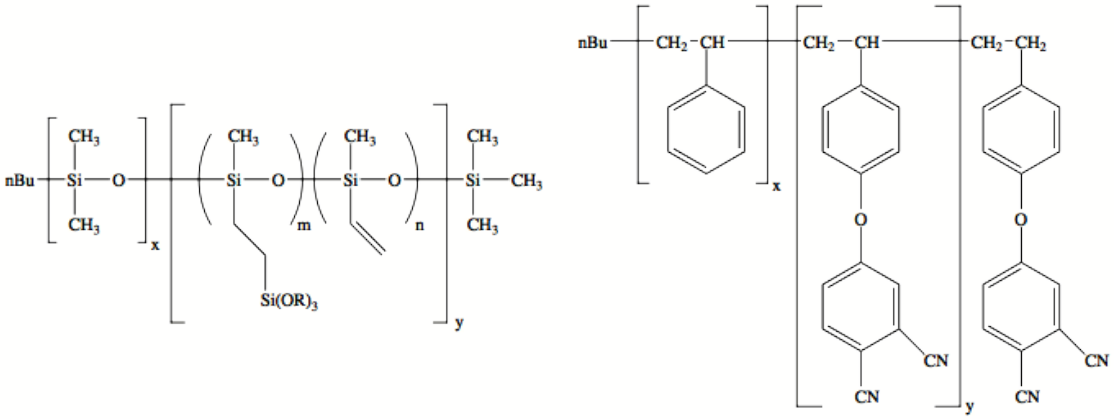

1.) poly(dimethylsiloxane)-*b*-[(methylvinylsiloxane)-*co*-(trimethoxysilyl-2-ethyl)siloxane]

2.) poly(styrene)-*b*-(4-vinylphenoxyphthalonitrile)

Figure 4.8 Previously investigated macromolecular cobalt nanoparticle stabilizers[3,5]

4.4.5.1 Preparation of a monovinyl-functional polystyrene to form the copolymer grafts of a macromolecular dispersion stabilizer for cobalt nanoparticles

These copolymer dispersion stabilizers were designed such that the backbone was a polysiloxane with pendent phthalonitrile groups and this was the intended anchor block. A polystyrene grafted to the backbone served as the tail dispersant block. The synthetic scheme required a monovinyl-functional polystyrene as the oligomeric graft.

The anionic polymerization of polystyrene has been widely studied and is known to produce polymers with low polydispersity and excellent control over the molecular weights (figure 4.8).[144] The polystyrene grafts were synthesized via living anionic polymerization utilizing n-butyllithium as the initiator. The reaction was terminated with dimethylvinylchlorosilane.

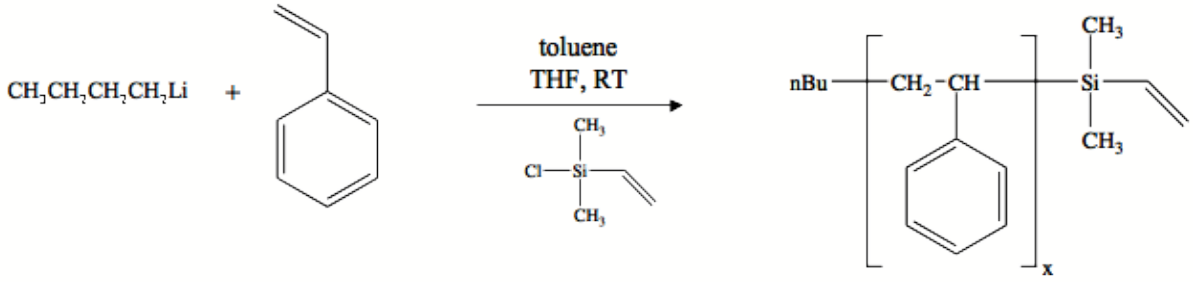

Figure 4.9 The living anionic polymerization of monovinyl terminated polystyrene.

Living polystyrene polymerizations in toluene have been reported previously.[145] The termination reactions were conducted at -78 °C to prevent any attack of the propagating anion on the vinylsilyl group.

4.4.5.1.1 Molecular weights, molecular weight distributions, of monovinyl-functional polystyrene oligomers

The oligomeric polystyrene grafts were analyzed via ^{1}H NMR. It is important that the ratio of butyl to vinyldimethylsilyl end groups is 1:1 indicating that no reaction on the vinylsilyl group occurred during termination and that the termination reaction was quantitative. Figure 4.9 shows the ^{1}H NMR of a purified 6900 g mol^{-1} vinyl functional polystyrene. The targeted M_n was 7000 g mol^{-1}. The theoretical peak integral for the phenyl protons of a 7000 g mol^{-1} polystyrene backbone should be 336 and the actual peak integral was 334 closely matching the targeted value. In addition, there should be 3 vinyl protons for every 336 phenyl protons, and this was observed on the ^{1}H NMR spectrum. The M_n for both polymers agreed well with targeted values via ^{1}H NMR.

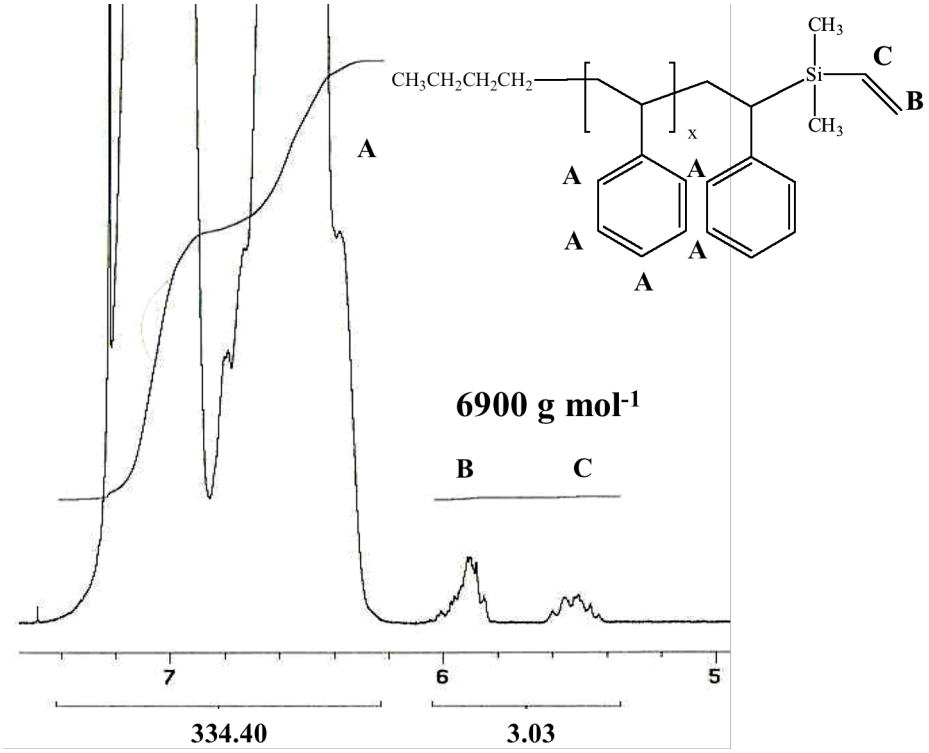

Figure 4.10 ^{1}H NMR spectrum depicting the ratio of end groups to the repeat unit resonances.

Gel Permeation Chromatography (GPC) was utilized to analyze the molecular weights and molecular weight distributions of the polystyrene grafts. Living anionic polymerizations are characterized by their low polydispersity and control over molecular weight. GPC showed polydispersities close to 1 for both polymers (table 4.5), thus suggesting that the polymerizations had proceeded in a living manner. The molecular weights obtained by GPC were in agreement with those obtained by ^{1}H NMR and also with the targeted values.

Table 4.5 Characterization of molecular weights, molecular weight distributions and thermal properties of monovinyl functional polystyrene

Target M_n (g mol^{-1})	M_n by ^1H NMR (g mol^{-1})	M_n by GPC (g mol^{-1})	PDI	T_g (° C)	Weight Loss (%)
7000	6900	6000	1.10	88	99
20, 000	20, 000	21, 000	1.07	95	98

4.4.5.1.2 Thermal analysis of the monovinyl polystyrene

Thermal analysis was performed on the polymers described in table 4.5. DSC was utilized to probe the thermal transitions of the polystyrene. The thermograms revealed that the glass transition temperatures were close to the literature values for similar molecular weights. Thermal gravimetric analysis revealed quantitative weight loss under nitrogen for these materials. The major weight losses occurred at approximately 400 °C. It was important to probe the weight loss profiles in order to correlate the data with their behavior during high temperature annealing processes. It was desirable to have no polystyrene remaining in the formation of the nanoparticle shells, since non-magnetic styrene would dilute the maximum possible magnetizations of the coated cobalt nanoparticles.

4.4.5.2 Chemical modifications of PMHS and PDMS-*co*-PMHS to form polystyrene and phthalonitrile containing nanoparticle stabilizers

The final nanoparticle stabilizer composition was prepared by a sequential series of hydrosilation reactions onto the backbone of either PDMS-*co*-PMHS or PMHS homopolymers. The effect of the PDMS interdispersed in the backbone on the cobalt nanoparticle shell will be the subject of the next chapter.

A 6400-1600 g mol^{-1} PDMS-*co*-PMHS copolymer was hydrosilated with a 6900 g mol^{-1} monovinyl-functional polystyrene in toluene containing catalytic concentrations of

Karstedt's catalyst (figure 4.10 a). One graft per PDMS-*co*-PMHS chain was targeted for these reactions. The siloxane copolymer was added in several aliquots to the catalyst solution and stirred for four hours to ensure complete hydrosilation. An exotherm which raised the reaction temperature to 65 °C was observed.

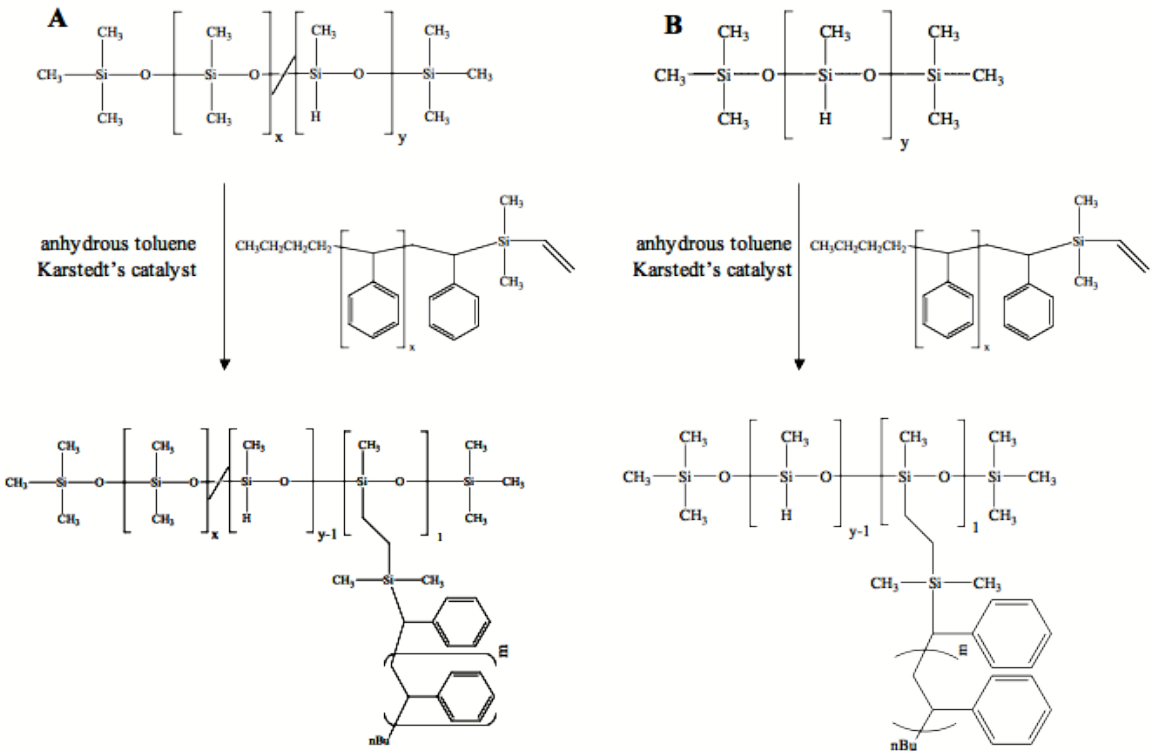

Figure 4.11 Hydrosilation of monovinyl-polystyrene onto the backbone of both a.) PDMS-*co*-PMHS and b.) PMHS

In addition, a 2000 g mol^{-1} homopolymer of PMHS was hydrosilated with a 6900 g mol^{-1} graft, such that an average of one polystyrene chain was grafted onto the PMHS backbone (leaving ~59 repeat units of Si-H available for further chemical modification). The final stabilizer structures were prepared from quantitative hydrosilations of 2-allylphenoxphthalonitrile onto the PDMS-*co*-PMHS-*g*-PS and PMHS-*g*-PS precursor copolymers to form PDMS-*co*-PHTH-*g*-PS and PHTH-*g*-PS copolymers, respectively (figure 4.11, table 4.6).

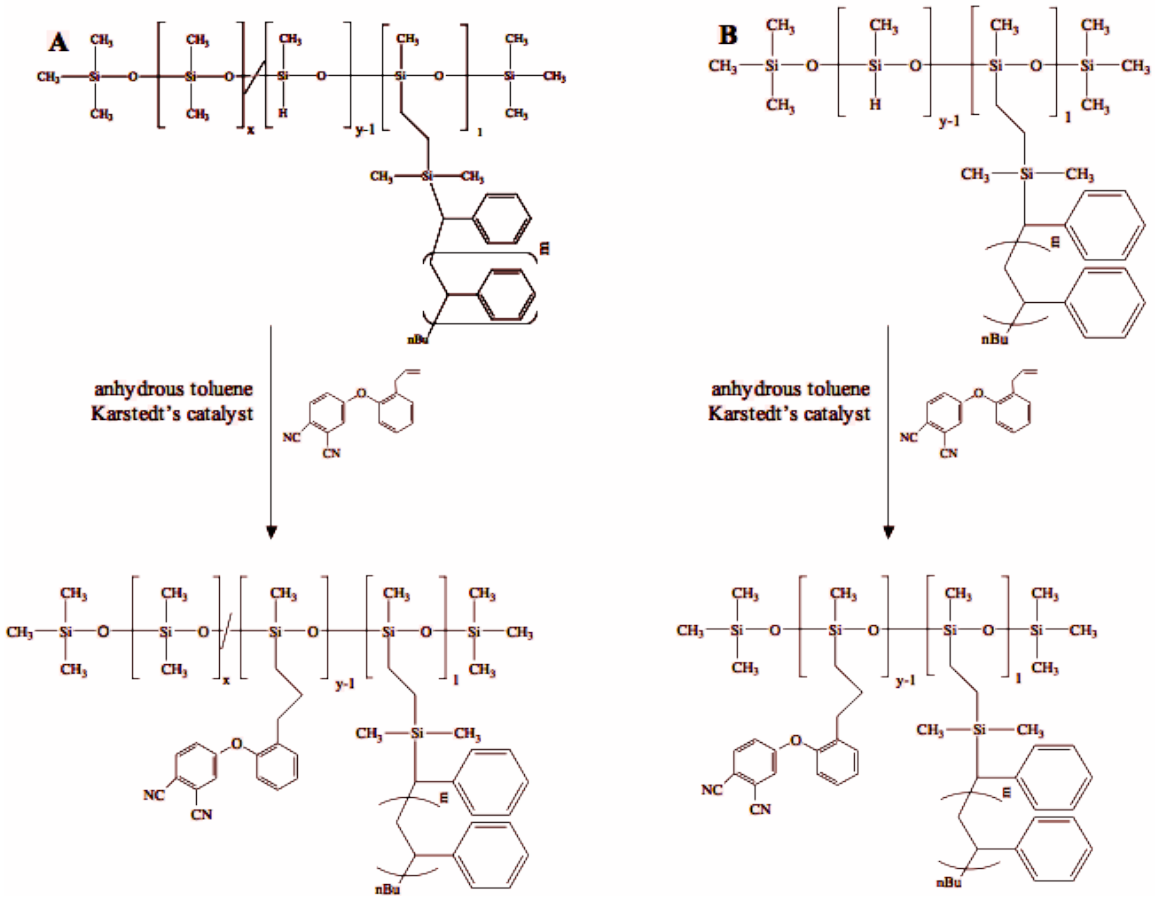

Figure 4.12 Hydrosilation of 2-allylphenoxyphthalonitrile onto the backbones of both a.) PDMS-*co*-(PMHS-*g*-PS) and b.) PMHS-*g*-PS resulting in the final nanoparticle stabilizer structure.

Table 4.6 Final stabilizer molecular weights

Copolymer	M_n by ^1H NMR (g mol^{-1})
[PDMS-*co*-PHTH]-*g*-PS	6400 – 8400 – 6900
PHTH-*g*-PS	10, 240 – 6900
PHTH-*g*-PS	10, 240 – 20, 000

The reaction products were characterized via ^1H NMR to confirm their compositions. Figure 4.12 depicts a representative spectrum after rigorous purification for a PHTH-*g*-PS copolymer with a backbone molecular weight of 10, 240 g mol^{-1} with a

polystyrene graft of 6900 g mol^{-1}. Quantitative hydrosilation of phthalonitrile onto the PMHS is possible with a pendent polystyrene graft. No phase separation was observed during the reaction suggesting that the polystyrene graft aided in dispersing the resultant copolymer in hydrophobic media. It is important to note the absence of resonances due to Si-H and the appearance of the phthalonitrile moieties in addition to the polystyrene.

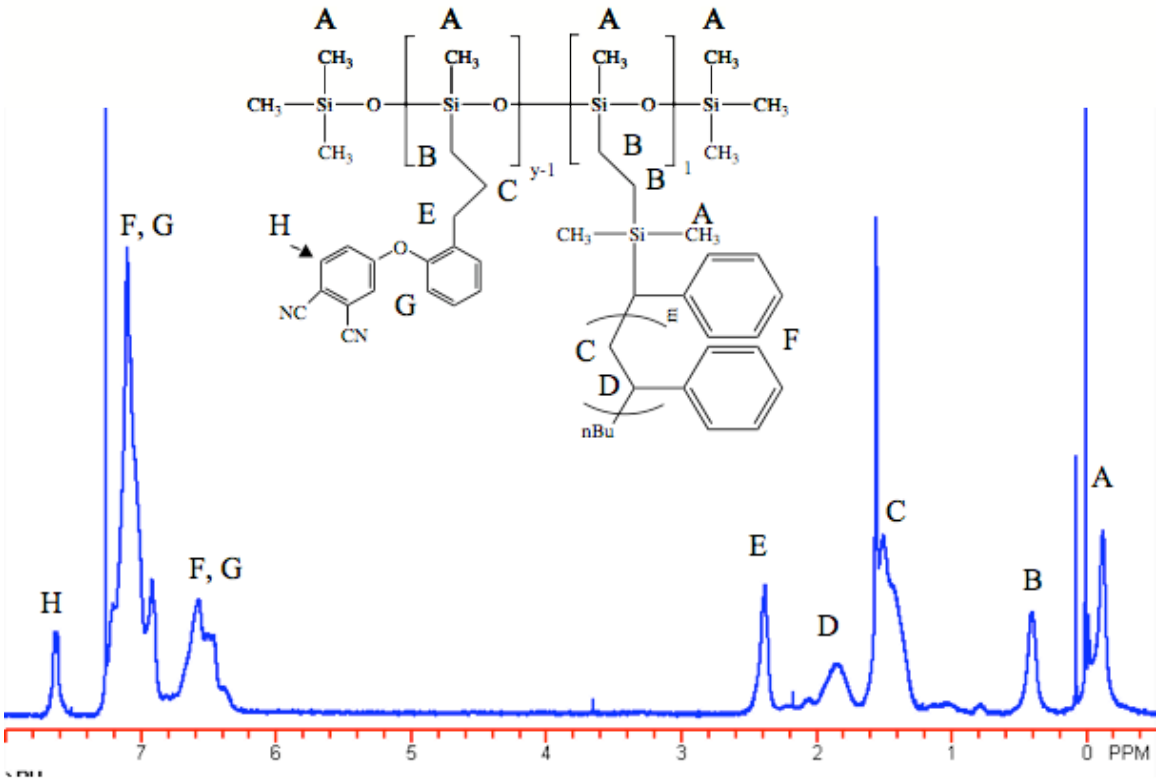

Figure 4.13 ^{1}H NMR depicting the complete chemical modification of a PHTH-*g*-PS copolymer nanoparticles stabilizer.

4.4.5.2.1 Thermal analysis of the polysiloxane graft copolymer stabilizers

The thermal properties of these copolymer stabilizers were characterized by DSC (to probe morphology) and TGA (to probe thermal stability). The DSC thermograms for each copolymer showed two glass transitions corresponding to the components in the overall copolymer composition (table 4.7). This suggests that microsphase separation had occurred between the polysiloxane backbone (which

contained the phthalonitrile pendent groups) and the polystyrene grafts. We believe that such a morphology may be important for a stabilizer in that a phase separated solution structure is desired to form the cobalt nanoparticles within micellar cores.

Table 4.7 Glass transition temperatures for PHTH-*g*-PS and [PDMS-*co*-PHTH]-*g*-PS copolymers

Copolymer	**T_g^1 (° C)**	**T_g^2 (° C)**
[PDMS-*co*-PHTH]-*g*-PS ([6400 – 8400] – 6900 g mol^{-1})	-35	88
PHTH-*g*-PS 10, 240 – 6900 g mol^{-1}	27	88
PHTH-*g*-PS 10, 240 – 20, 000 g mol^{-1}	27	95

The weight loss profiles of the graft copolymers were investigated by heating the materials at 10 °C min^{-1} up to 700 ^{o}C (figure 4.13). The PDMS based graft copolymer had a single major weight loss at approximately 450 °C and approximately 9 % char yield. This suggests that most, if not all, of the polystyrene decomposes and that the phthalonitrile component serves as the major char contributor. It has been shown previously in this chapter that the PDMS component has nearly quantitative weight loss when serving as a component in PDMS-*co*-PHTH copolymers. The weight loss for the PHTH-*g*-PS is more than expected which suggests that all of the PS decomposes in addition to some of the siloxane backbone. These results suggest that the formation of protective shells around the cobalt nanoparticles will consist solely of phthalonitrile-based networks and silica. This shell formation will be further described in the following chapter.

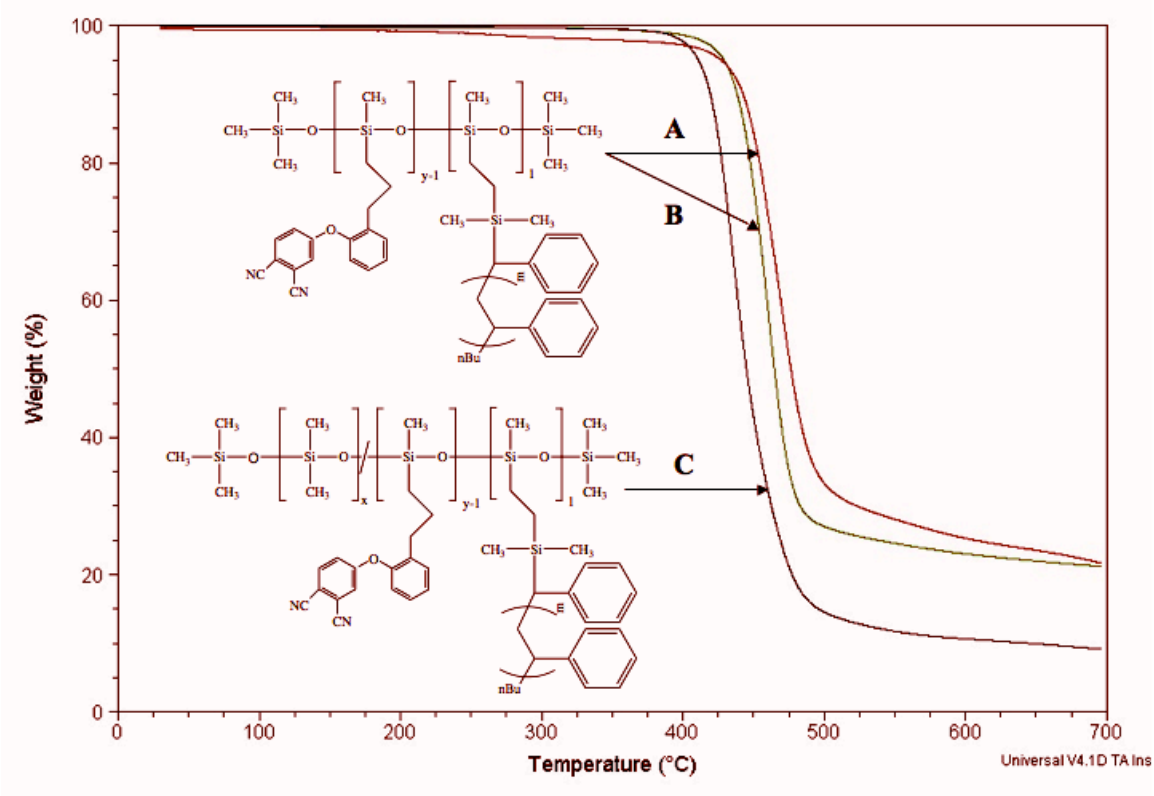

Figure 4.14 Thermal gravimetric analysis of a.) 10, 240 – 6900 g mol^{-1} PHTH-PS, b.) 10, 240 – 20, 000 g mol^{-1} PHTH-PS, and c.) 6400 – 8400 – 6900 g mol^{-1} [PDMS-*co*-PHTH]-*g*-PS

CHAPTER 5 Synthesis and Characterization of Cobalt Nanoparticles with Graphitic-Siliceous Coatings

5.1 Synopsis

This chapter focuses on the synthesis and characterization of cobalt nanoparticle complexes with graphitic-siliceous coatings. The primary objective of this phase of the research was to determine whether copolymers containing both polysiloxanes and phthalonitrile moieties could form robust coatings on cobalt that could protect the cobalt surfaces from oxidation. Complexes of the copolymers and cobalt nanoparticles were synthesized by thermolyzing dicobalt octacarbonyl in the presence of PDMS-*co*-PHTH-*g*-PS or PHTH-*g*-PS in toluene or dichlorobenzene. Thermolysis reactions in the presence of select copolymer compositions produced stable dispersions of cobalt nanoparticles with significant saturation magnetizations. The complexes were further subjected to high temperature treatments, which resulted in increased saturation magnetization and the formation of graphitic-siliceous shells. Aging studies are currently underway on these complexes to investigate whether they can prevent oxidation of the cobalt nanoparticle surfaces. Early results show this to be promising.

5.2 Experimental

5.2.1 Materials

Toluene (MW 92.14 g mol^{-1}, d 0.865 g mL^{-1}, MP -63 °C, BP 110 °C, Burdick and Jackson, 99.9 %) was washed twice with conc. H_2SO_4 and neutralized with water. It was dried over $MgSO_4$ for 1 h, then over CaH_2 overnight and distilled just before use. 1,2-Dichlorobenzene (MW 147.00 g mol^{-1}, d 1.306 g mL^{-1}, MP -17 °C, BP 180 °C, 99 %, Aldrich) was dried over CaH_2 overnight and vacuum distilled prior to use. $Co_2(CO)_8$ with 1-5% hexane (MW 341.95 g mol^{-1}, d 1.73 g mL^{-1}, MP 51 °C, Alfa Aesar) was stored under argon in the freezer without any further purification. This compound is a bright orange solid at room temperature.

5.2.2 Synthesis of cobalt nanoparticles in the presence of a PHTH-*g*-PS graft copolymer at 110 °C in toluene (T1)

A representative reaction is described utilizing an 8400 g mol^{-1} PHTH-*g*-6900 g mol^{-1} PS (PHTH-*g*-PS) copolymer. The graft copolymer had an average of one polystyrene graft per chain and the remaining repeat units had pendent phthalonitrile moieties. Dispersions of cobalt in toluene or dichlorobenzene in the presence of other copolymers were prepared in an analogous manner. A 500-mL, three-neck, round bottom flask equipped with a condenser, mechanical stirrer with a vacuum ready adapter, and argon purge was flame-dried under argon. The apparatus was placed in a temperature controlled silicone oil bath over a hot plate (without a magnetic stirrer). The PHTH-*g*-PS copolymer (1.0 g, 0.0019 eq phthalonitrile) was transferred to the reaction vessel. Anhydrous toluene (30 mL) was added via syringe to the reaction flask. Dicobalt octacarbonyl (1.0 g, ≈0.0035 mol) was weighed into the reaction vessel and dissolved under argon. A greenish-brown gas filled the flask immediately upon adding the dicobalt

octacarbonyl. The reaction temperature was raised to approximately 110 °C (toluene reflux) and that temperature was maintained for approximately three h while being monitored by FT-IR. A separate reaction was conducted for 5 h for purposes of an FT-IR study. After cooling, a stable magnetic dispersion of cobalt nanoparticles coated with the copolymer resulted.

5.2.3 Synthesis of cobalt nanoparticles in the presence of a [PDMS-*co*-PHTH]-*g*-PS graft copolymer at 110 °C in toluene

An exemplary reaction is described utilizing a graft copolymer [PDMS-*co*-PHTH]-*g*-PS wherein the backbone is 14,800 g mol^{-1} and was comprised of 24 % of the repeat units containing phthalonitrile and 76 % dimethylsiloxane repeat units. The PS graft was 6900 g mol^{-1}. (T2) A separate reaction was performed utilizing a [PDMS-*co*-PHTH]-*g*-PS copolymer wherein the backbone was 14,800 g mol^{-1} and was comprised of 24 % of the repeat units containing phthalonitrile and 76 % dimethylsiloxane repeat units. The PS graft was 20,000 g mol^{-1}. (T3) A 500-mL, three-neck, round bottom flask equipped with a condenser, mechanical stirrer with a vacuum ready adapter, and argon purge was flame dried under argon. The apparatus was placed in a temperature controlled silicone oil bath over a hot plate without a magnetic stirrer. The procedure follows that described in 5.2.2. After cooling, a stable magnetic dispersion of cobalt particles resulted.

5.2.4 Synthesis of cobalt nanoparticles in the presence of a PHTH-*g*-PS graft copolymer at 180 °C in dichlorobenzene

An exemplary reaction is described utilizing a PHTH-*g*-PS copolymer where the polymer backbone was 8400 g mol^{-1} (D1). It had an average of one polystyrene graft that was 6900 g mol^{-1}. A separate reaction was also conducted utilizing a PHTH-*g*-PS

copolymer where the polymer backbone was 8400 g mol^{-1} and the PS graft was 20,000 g mol^{-1} (D2). A 500-mL, three-neck, round bottom flask equipped with a condenser, mechanical stirrer with a vacuum ready adapter, and argon purge was flame dried under argon. The apparatus was placed in a temperature controlled silicone oil bath over a hot plate without a magnetic stirrer. The procedure follows that described in 5.2.2 except that the solvent was dichlorobenzene, and the reaction was conducted at 180 °C for three h. The decomposition of the dicobalt octacarbonyl was monitored via FT-IR for the disappearance of the $Co_4(CO)_{12}$ intermediate. After cooling, a stable magnetic dispersion of cobalt particles resulted.

5.2.5 Preparation of cobalt nanoparticles with surfaces containing silica and graphite

Cobalt nanoparticles coated with the copolymers described in sections 5.2.2-5.2.4 were dried under vacuum at 120 °C overnight. The dry powders were heated under nitrogen for 2 h at 700 °C in a quartz tube furnace. The siliceous-graphitic-cobalt powders were stored in septum-sealed glass vials under argon.

5.2.6 Characterization of magnetic fluids

FTIR spectra were obtained using a Bruker Tensor 27 FT-IR spectrometer with two drops of the samples run neat between salt plates. Transmission electron micrographs were acquired using a Philips 420T TEM run at 100kV. TEM samples containing cobalt stabilized with copolymers were prepared by diluting toluene or dichlorobenzene dispersions with additional toluene until they had the appearance of "weak tea". A drop was syringed onto a carbon-coated copper grid and the toluene was evaporated. A Standard 7300 Series Lakeshore vibrating sample magnetometer (VSM) was used to determine the magnetic properties of the cobalt samples including saturation

magnetization and any hysteresis. The magnetic moment of each dried sample was measured over a range of applied fields from -8000 to +8000 Oe with a sensitivity of 0.1 emu. A Quantum Design magnetic properties measurement system (MPMS-7) equipped with a superconducting quantum interference device (SQUID) sensor was used to make cobalt specific magnetization measurements (σ) at varying applied fields (H) from –70,000 to +70,000 Oe at 300 K and 5 K, with 100 Oe spacings between –1000 and +1000 Oe. Low-temperature measurements were conducted both after cooling the sample in zero applied field and in an applied field of 70,000 Oe. The purpose of the different measurements was to study: 1) the saturation magnetization at 300 K, 2) the hysteretic behavior at 300 K, 3) the presence of an exchange bias owing to a cobalt oxide layer on the surface of the cobalt nanoparticles, and 4) the presence of paramagnetic species owing to any residual cobalt carbonyl species in the sample. Weight loss profiles were analyzed with a TA Instruments TGA Q0500 under N_2. XPS was performed with a Perkin-Elmer 5400 with a Mg X-ray source at 1253.6 eV.

5.2.7 Characterization of graphite-silica-cobalt complexes

5.2.7.1 Thermal gravimetric analysis

Weight loss profiles were analyzed with a TA Instruments TGA Q0500 under N_2. Weight loss profiles were analyzed with a TA Instruments TGA Q0500 under N_2. The TGA was balanced against an empty reference pan prior to each run. The samples were heated at 10 °C min^{-1}.

5.2.7.2 X-ray photoelectron spectroscopy

XPS was performed with a Perkin-Elmer 5400 with a Mg X-ray source at 1253.6 eV.

5.3 Results and discussion

Investigations into protecting the surfaces of cobalt against oxidation have been conducted by several groups.[5,7,129,146] There have been efforts to coat the surfaces with silica during the cobalt nanoparticle synthesis.[130] These methodologies lead to nanoparticle systems with relatively low magnetization, which subtracts from the overall appeal of the cobalt nanoparticle: high saturation magnetization per gram material. There have also been investigations into forming polymeric networks around the particles.[147] These systems have included copolymers with pendent anchor units that, after formation of the nanoparticle, can be cured thermally or with catalysts.[147] All of the polymer-coated cobalt materials oxidized over time.

In an effort to combine both systems, this work describes PDMS-*co*-PHTH-*g*-PS and PHTH-*g*-PS copolymers and their utility as steric dispersion stabilizers and shell precursors to prevent oxidation of cobalt nanoparticles (figure 5.1).

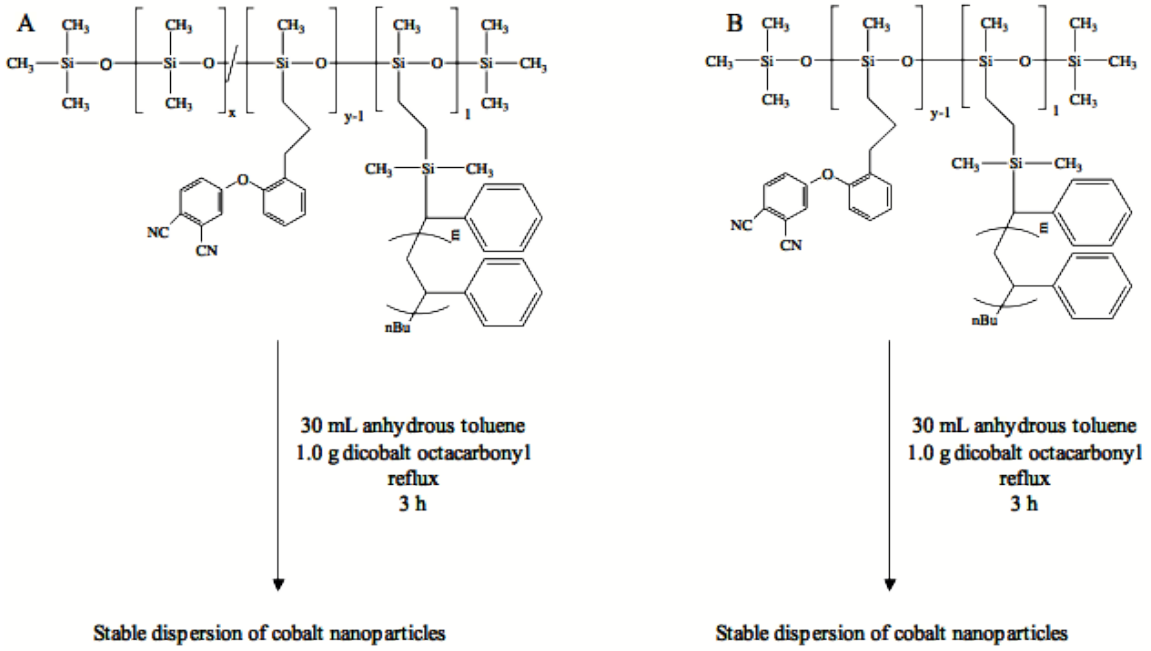

Figure 5.1 Dispersions of copolymer-cobalt nanoparticles were prepared by thermolysis of dicobalt octacarbonyl in the presence of a) [PDMS-*co*-PHTH]-*g*-PS and b) PHTH-*g*-PS.

5.3.1 Synthesis and characterization of copolymer-cobalt nanoparticle dispersions

The synthesis and characterization of cobalt nanoparticle dispersions are discussed herein. They were formed in thermolysis reactions of dicobalt carbonyl in the presence of graft copolymer micellar templates wherein the pendent phthalonitrile units complexed with cobalt nanoparticles and the polystyrene grafts functioned as tails protruding into the toluene or dichlorobenzene reaction solvent.

Thermolysis reactions of dicobalt octacarbonyl to form cobalt nanoparticles have been well studied in our laboratories utilizing toluene as the solvent.[1-3,5,120] Separate thermolysis reactions of dicobalt octacarbonyl and the copolymer were performed in either toluene or dichlorobenzene and the reaction mixtures were refluxed at 110 °C (for reactions in toluene) and 180 °C (for reactions in dichlorobenzene) to displace and evolve

the carbon monoxide and form sterically stabilized cobalt nanoparticle dispersions. Dispersions prepared in toluene with the PHTH-*g*-PS (T1) and [PDMS-*co*-PHTH]-*g*-PS (T2, T3) copolymers were dark purple homogeneous fluids without any visible precipitates. The magnetizations were qualitatively examined by placing a strong magnet on the side of the reaction vessel and moving the fluid. These fluids did not exhibit a significant response to the external magnet. In addition, VSM was utilized to further probe their magnetic properties. Table 5.1 shows the saturation magnetization values for these dispersions. These values did not correlate well with previous research suggesting that the thermolysis reactions were not complete. Our laboratories had previously reported magnetization values for similar systems on the order of 20 emu g^{-1}.[1-3,5,120]

Table 5.1 Specific saturation magnetizations for copolymer-cobalt dispersions after 3 h thermolysis under toluene reflux.

Copolymer (M_n in g mol^{-1})	**Reaction Temperature (° C)**	**M_s (emu g^{-1} sample)**
T1	110	0.8
T2	110	1.2
T3	110	0.95

The dispersions prepared in toluene and those prepared in dichlorobenzene were examined by transmission electron microscopy (TEM) to probe any morphology/property relationships that would contribute to understanding the differences between the reaction temperatures. Samples for microscopy were prepared by casting dilute suspensions of copolymer-cobalt complexes from toluene or dichlorobenzene onto carbon-coated copper grids. TEM micrographs of cast samples

from the T1 and T2 copolymer-cobalt dispersions showed dark, ≈70-100 nm diameter cobalt nanoparticles (figure 5.2). Stevenson et al., Rutnakorpituk et al., and Vadala et al. prepared copolymer stabilized dispersions of cobalt nanoparticles wherein the sizes ranged from approximately 8-15 nm in diameter.[1-3] In addition, Baranauskas et al. demonstrated the reaction progress of these cobalt nanoparticle syntheses utilizing TEM.[5,147] The initial stages of the reactions were characterized by larger diameter particles that were ~50-70 nm in diameter. As the reactions proceeded, the particle sizes decreased to 8-10 nm in diameter.

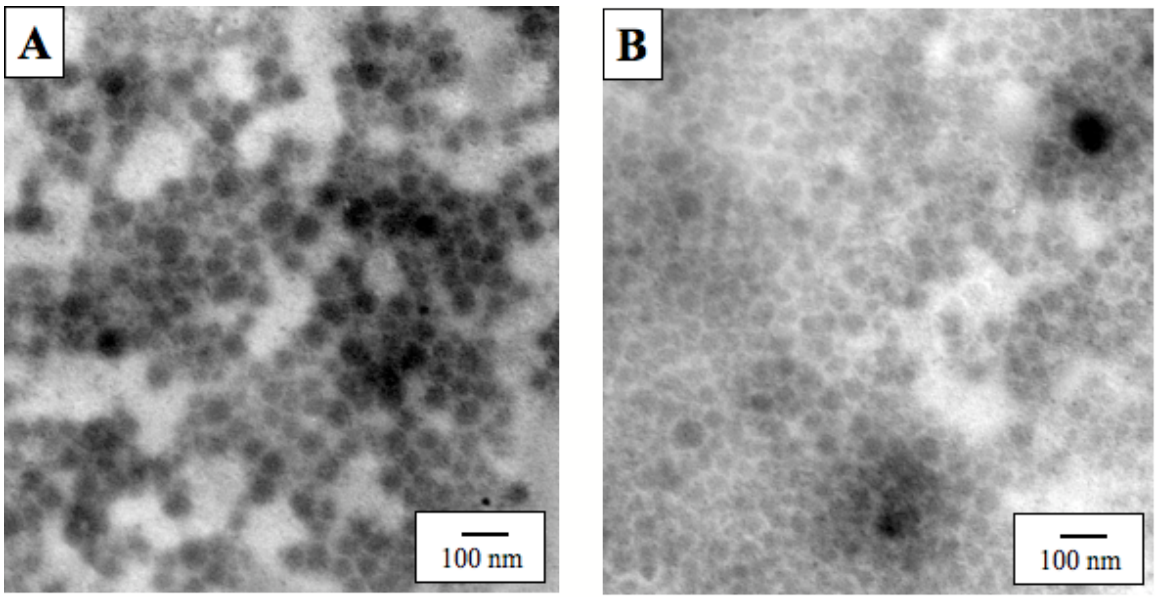

Figure 5.2 TEM micrographs depicting copolymer-cobalt nanoparticle complexes prepared with A) T1 and B) T2 showed diffuse nanoparticles suggesting these thermolyses were incomplete.

The particles prepared in dichlorobenzene were also examined by TEM to observe any differences between the cobalt nanoparticles that had been formed at 110 (T1-T3) vs. 180 ºC (D1 and D2). The micrographs showed the expected dark (electron dense) cobalt nanoparticles with ~10-15 nm in diameter, and the sizes were comparable

to previously reported values for cobalt nanoparticles prepared in the presence of other copolymer templates (figure 5.3).[1-3]

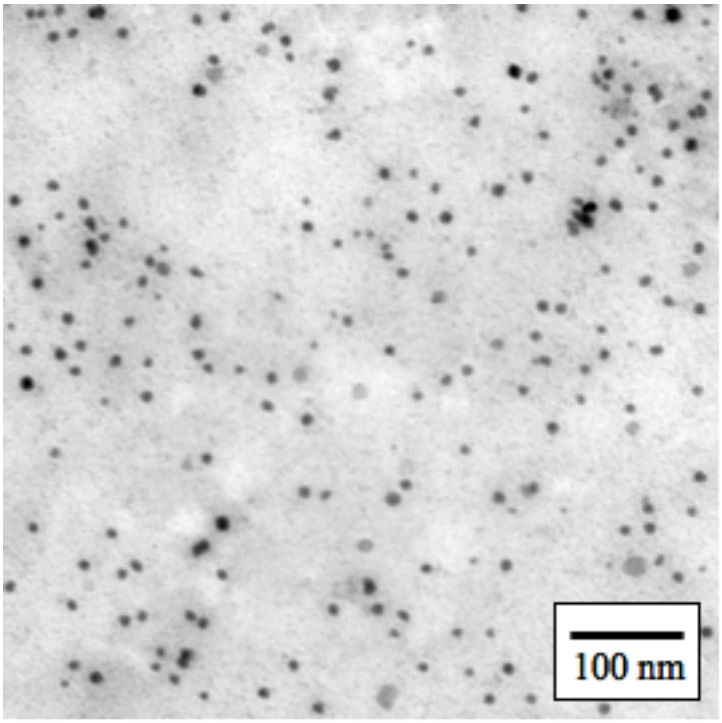

Figure 5.3 TEM micrograph depicting the smaller (relative to figure 5.2) particle sizes obtained from thermolysis of the D2 copolymer-cobalt complexes at 180 °C.

The nanoparticles formed from the two reaction conditions were further probed by FTIR by observing changes in structure and the decrease of the carbonyl peaks. For T1 and T2, the carbon monoxide region around 2000 cm^{-1} initially showed three absorbance bands at 2020, 2050, and 2070 cm^{-1} attributed to terminal CO, and a peak at 1860 cm^{-1} due to the bridging carbonyls (figure 5.4).[148] Two new peaks at 2055 and 2065 cm^{-1} appeared in the IR spectra as the reactions proceeded. These peaks were attributed to a $Co_4(CO)_{12}$ intermediate based on previous assignments.[1,3] The reactions were conducted at approximately 110 °C for three hours. It is important to note that there was

residual carbonyl remaining after three hours, and that even for reactions conducted for longer periods, the carbonyl absorption remained in the FT-IR (figure 5.4 (d)).

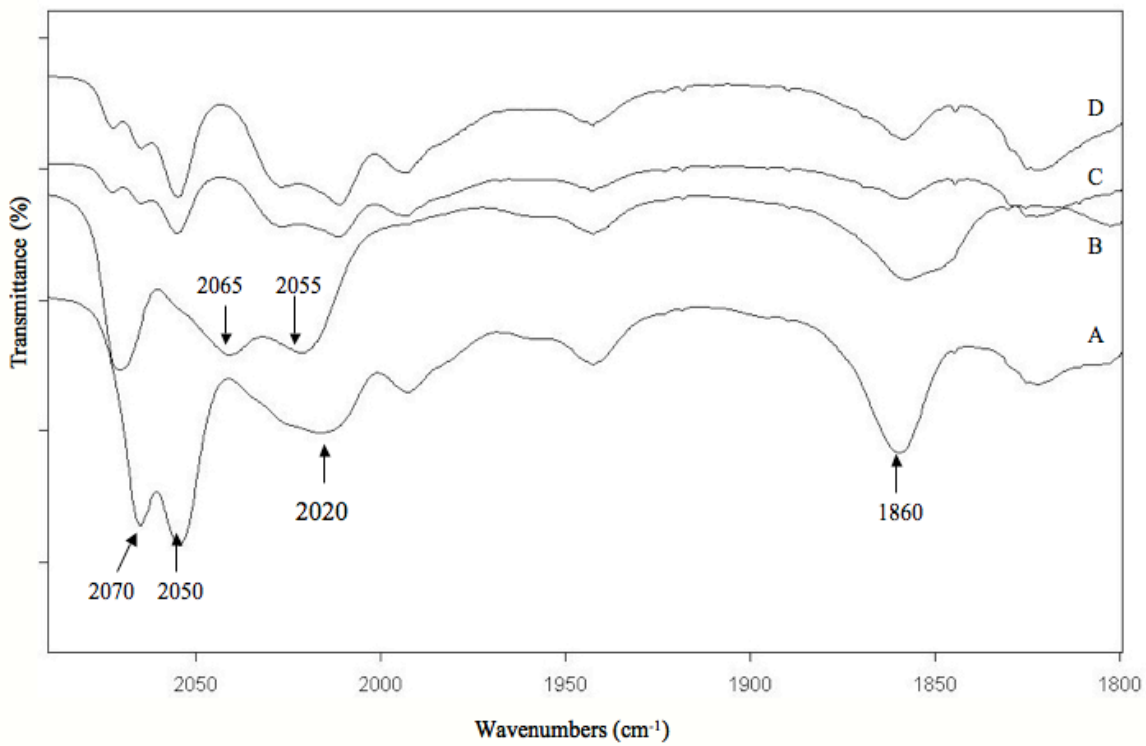

Figure 5.4 The thermolysis of T1: A) initial reaction mixture showing peaks at 2020, 2050, and 2070 cm^{-1} corresponding to terminal CO and 1860 cm^{-1} attributed to bridging CO; B) a spectrum representing the intermediate reaction stage showing new peaks at 2065 and 2055 cm^{-1} attributed to $Co_4(CO)_{12}$; C) reaction mixture after two hours showing a decrease in intensity of the peaks at 2065 and 2055 cm^{-1}; and D) reaction after five hours depicting the presence of residual carbonyl species in the mixture.

The FT-IR for D1 showed a substantial decrease in the peaks associated with the $Co_4(CO)_{12}$ intermediate after one and a half hours, and the carbonyl peaks completely disappeared after three hours reaction time (figure 5.5).

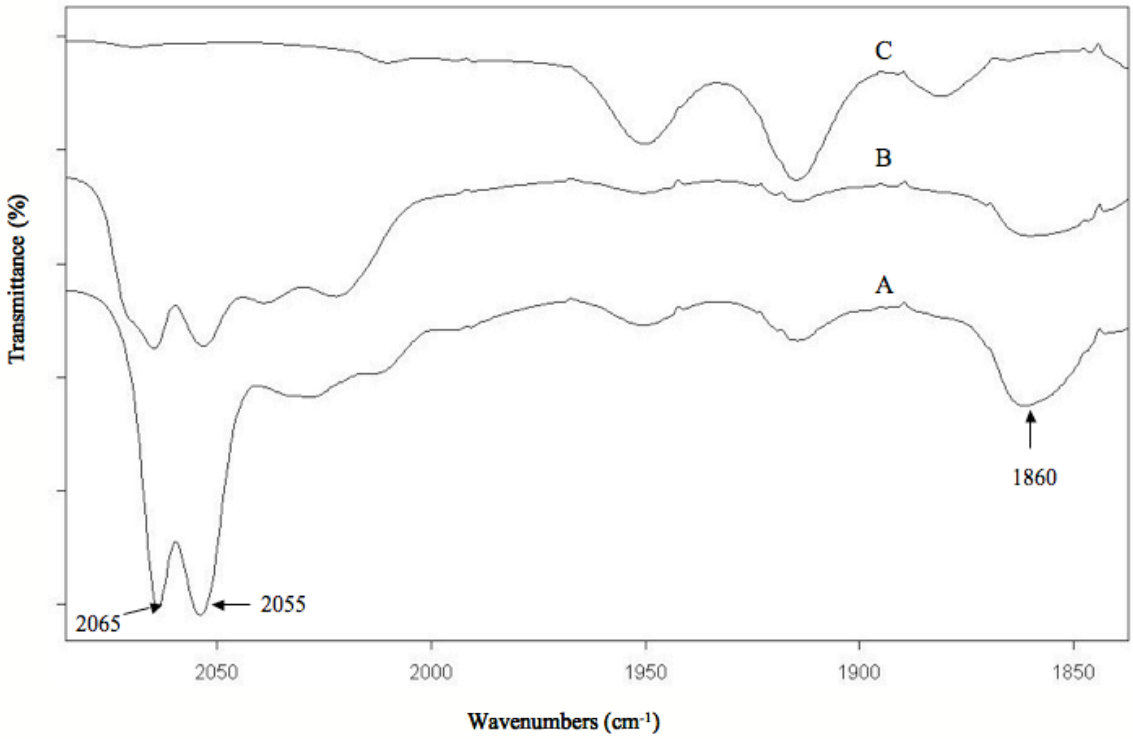

Figure 5.5 Thermolysis of dicobalt octacarbonyl in the presence of a PHTH-*g*-PS copolymer in dichlorobenzene at 180 °C (D1): A) a spectrum showing the $Co_4(CO)_{12}$ intermediate already forming in the initial stages of reaction; B) reaction after one hour showing a decrease in the carbonyl intensities; C) a spectrum depicting the reaction after three hours showing no residual carbonyl.

Thermal gravimetric analysis was utilized to quantify the amount of carbonyl remaining after thermolysis in toluene. A dried copolymer-cobalt powder prepared from the T1 complex was ramped from room temperature to 250 °C at 10 °C min^{-1} and held isothermally for two hours (figure 5.6). Approximately 20 % weight loss was observed at 180 °C, and it was reasoned that this weight loss was due to residual carbonyl being evolved. The original reaction composition was comprised of 1.0 g of copolymer and 1.0 g of dicobalt octacarbonyl. The carbonyl ligands accounted for 33 wt % of this original composition. Therefore, it was hypothesized that the nanoparticles were swollen with

residual carbonyl species and that this was responsible for the larger-than-expected size that had been observed in the TEM micrographs.

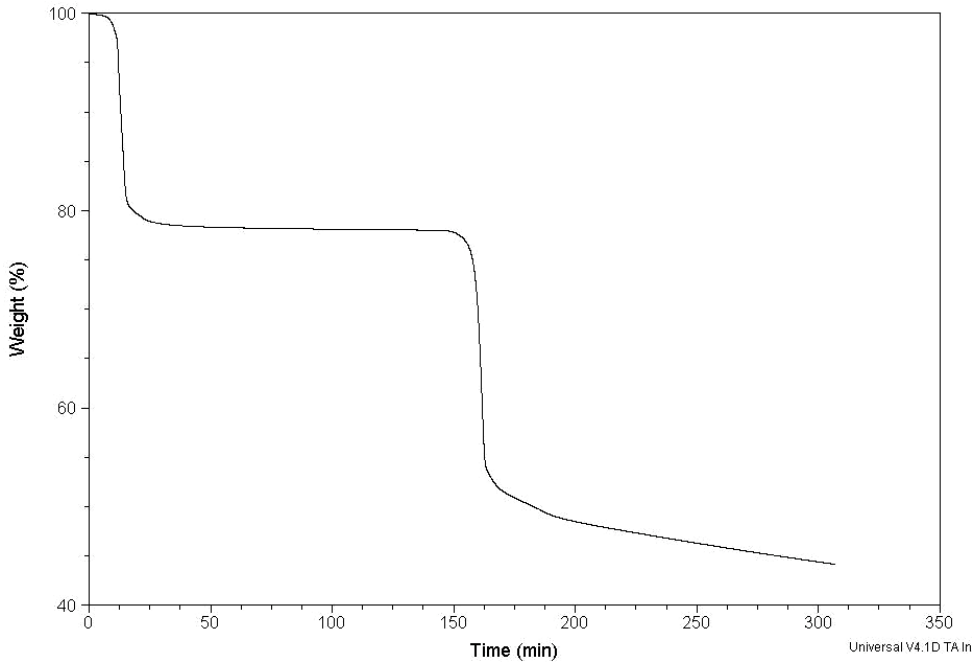

Figure 5.6 A weight loss profile shows the amount of residual carbon monoxide in the nanoparticles after thermolysis in toluene.

The FT-IR, TEM and TGA data all suggested that the higher temperature of 180 ^{o}C was necessary to completely displace and evolve the carbonyl species when the reactions were conducted in the presence of these particular copolymer dispersants. Interestingly, we had previously observed that thermolysis at toluene reflux temperatures of dicobalt carbonyl in the presence of some other copolymers containing polysiloxane blocks also retained residual carbonyl species[3,8], but the effect was not as pronounced as in this case. It is becoming clear that copolymer dispersants with some chemical structures can displace carbonyls in thermolysis reactions from dicobalt octacarbonyl at

lower temperatures than others. This strongly suggests that the chemical structure of the copolymer binding groups can participate in the displacement reactions. This has also been suggested previously by others.[126,142,143]

5.3.2 Synthesis and characterization of siliceous-graphitic-cobalt complexes

Elevated heat treatments are often utilized to form ceramics and graphite to form oxygen-impermeable networks. Previous work by Baranauskas et al. demonstrated that graphitic surfaces could be formed from phthalonitrile units pendent on a polystyrene backbone, and that this protected the underlying cobalt nanoparticles from oxidation.[5] In addition, Vadala et al. provided methods to prepare cobalt nanoparticles encased in thin silica coatings.[7] These provided a means for functionalization of the thermally treated surfaces through post-modifications with functional silanes. Unfortunately, those coatings did not rigorously prevent oxidation.[8]

Elevated heat treatments were performed on the T1, T2, and D1 complexes. Heretofore, T1 after pyrolysis is P1; T2 after pyrolysis is P2; and T3 after pyrolysis is P3. In addition, D1 and D2 will be named Z1 and Z2, respectively. The samples were dried for 24 hours *in vacuo* and placed into a tube furnace wherein the temperature was ramped to 700 °C and held isothermally for two hours under a nitrogen atmosphere. The resultant powders were examined by XPS to probe the elemental compositions of the surfaces. Table 5.2 shows the atomic ratios on the surfaces for P1, P2 and P3. The ratios of Si:O did not resemble those of a silica surfaces in all samples. However, the binding energy of all the samples was 103.7-103.9 eV, which is the reported binding energy for silica. This suggests that the surfaces were siliceous. In addition, the P1 particles retained less silicon after pyrolysis than those prepared from PDMS due to the lower

concentration of Si in the PHTH-*g*-PS composition. In contrast, the percent carbon was elevated in the PHTH-*g*-PS samples as expected.

Table 5.2 X-ray Photoelectron Spectroscopy was utilized to examine the surfaces of the pyrolyzed copolymer-cobalt complexes prepared from toluene solutions.

Copolymer Shell Precursor (M_n in g mol^{-1})	**Silicon (%)**	**Oxygen (%)**	**Carbon (%)**	**Nitrogen (%)**	**Cobalt (%)**
P1	8	19	68	0	5
P2	10	26	59	0	5
P3	9	24	61	0	6

The surface compositions for the cobalt complexes formed from solutions of PHTH-*g*-PS in dichlorobenzene, Z1 and Z2, were also examined by XPS (table 5.3). The surfaces of these complexes prior to pyrolysis had surface compositions relative to the copolymers anchored onto the cobalt nanoparticles wherein the Si:O ratio was expected to be 1:1. The surface analysis after elevated heat treatments revealed an atomic ratio of Si:O of approximately 1:2 suggesting that these copolymers also formed a silica-like layer. In addition, nitrogen appears in the XPS spectra post-pyrolysis resulting from the phthalonitrile groups. The percent cobalt is also much less than the previous systems formed in toluene solutions suggesting that these coatings might be thicker and have larger contributions of phthalonitrile to the overall compositions.

Table 5.3 X-ray Photoelectron Spectroscopy was utilized to examine the surfaces of the pyrolyzed copolymer-cobalt complexes prepared from dichlorobenzene solutions.

Element	Sample		Sample	
	D1	**Z1**	**D2**	**Z2**
Silicon (%)	21	14	23	11
Oxygen (%)	24	32	21	27
Carbon (%)	55	52	66	59
Nitrogen (%)	0	1	0	1
Cobalt (%)	0	1	0	2

Thermal gravimetric analysis was utilized to examine the weight loss profile for D1. D1 was dried thoroughly and was ramped at 10 °C min^{-1} to 700 °C and held isothermally for two hours (figure 5.8). The major weight loss for this material occurred at 450 °C and then the curve began to plateau. The weight retained (60 %) was greater than the theoretical amount of cobalt present in the material if all of the copolymer decomposed (42 %). This suggested that a thermally stable coating had formed around the cobalt nanoparticles. The effect of this coating on magnetic properties will be discussed in the next section.

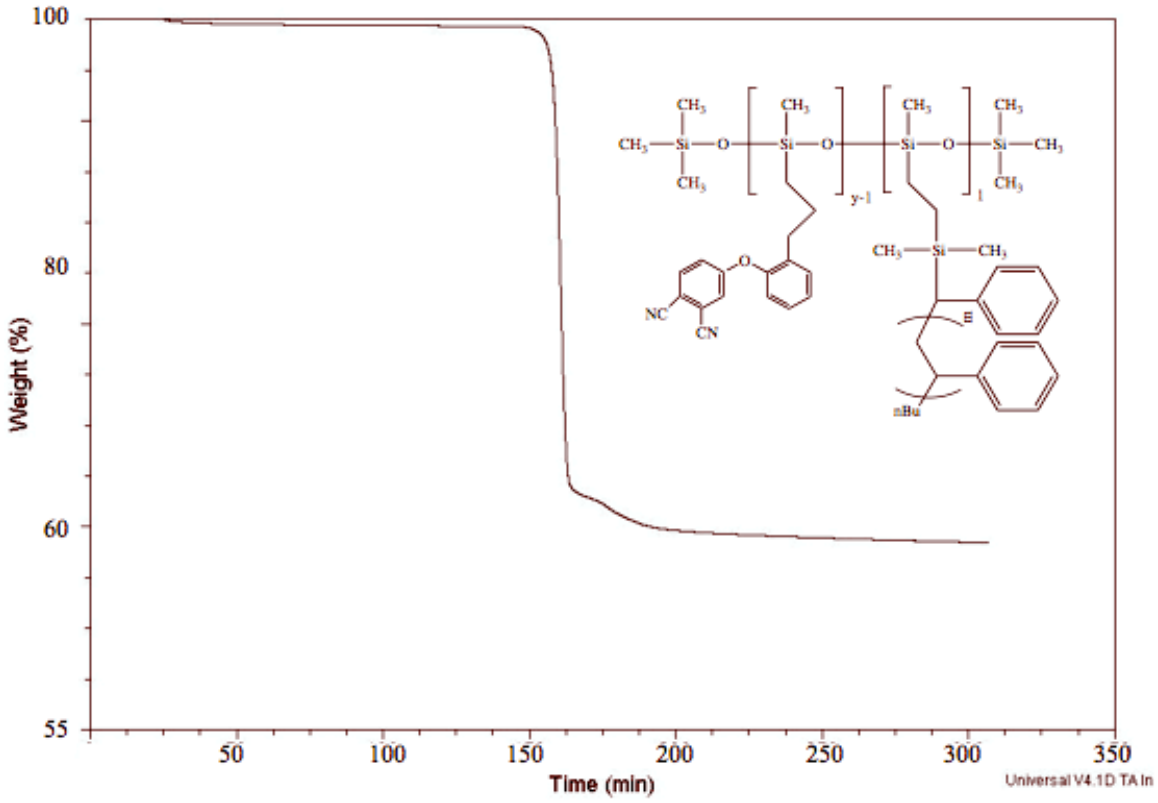

Figure 5.8 Weight loss profile for D1.

5.3.3 Magnetic properties of the siliceous-graphitic-cobalt complexes

The magnetic properties of these materials which had been thermolyzed at 110 ° or 180 °C, then pyrolyzed at 700 ºC, were examined by SQUID magnetometry. Figure 5.7 depicts the hysteresis loops obtained from these measurements for P1 and P2 after heating at 700 °C. The saturation magnetization for the materials depicted in figure 5.7A (P2) is 22 emu g^{-1}sample whereas 5.7B (P1) is 48 emu g^{-1} sample. These values are lower than previously reported values for similar systems. This may be due to the presence of carbonyls prior to pyrolysis. The samples were then mechanically ground and aged in air. The saturation magnetization for the graphite-silica-cobalt complex derived from the PDMS-*co*-PHTH-*g*-PS as a shell precursor decreased substantially over time. However, the cobalt complexes derived from the PHTH-*g*-PS copolymer did not oxidize in air but

the reasons underlying the low initial saturation magnetization needed to be investigated. It was hypothesized that completing the carbon monoxide displacement reaction *in situ* prior to elevated heat treatments may have an effect on the final saturation magnetization.

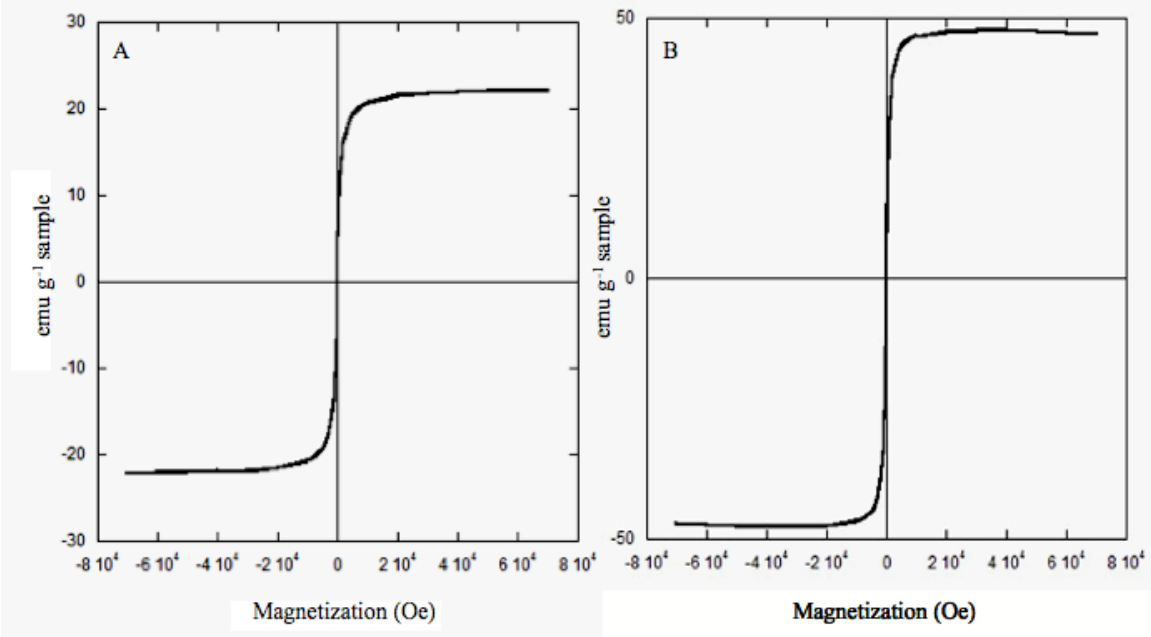

Figure 5.7 Magnetic hysteresis curves depicting the saturation magnetization for both A) P1; and B) P2

The saturation magnetizations of Z1 and Z2 at room temperature were substantially higher than those achieved from the systems originally thermolyzed in toluene solutions. Figure 5.9 shows the magnetization vs. field graphs obtained from the SQUID measurements for two heat-treated samples wherein the molecular weight of the polystyrene graft of the shell precursor was varied from 6900 to 20,000 g mol^{-1}. The saturation magnetization for Z1 was 84 emu g^{-1} sample (figure 5.8 A) whereas the saturation magnetization for Z2 was 61 emu g^{-1} sample (figure 5.8 B).

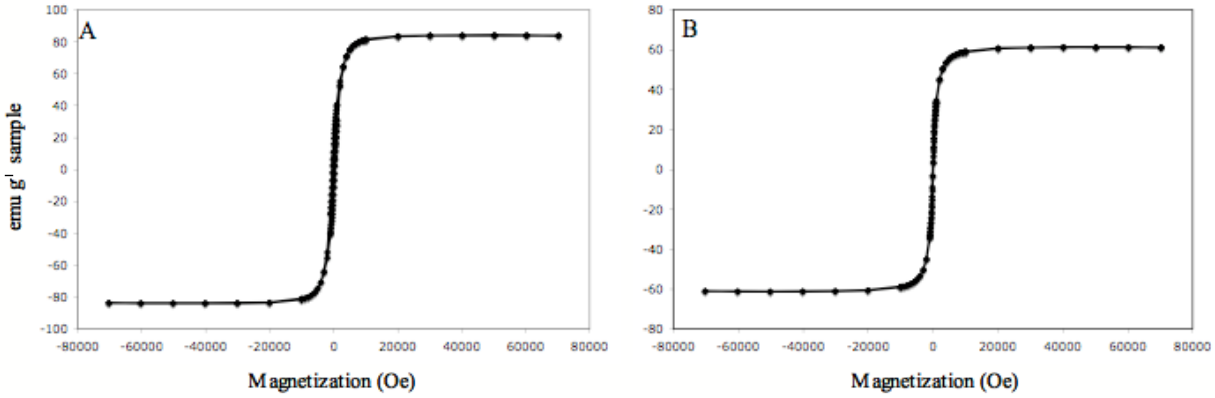

Figure 5.8 SQUID measurements demonstrating A) the magnetic susceptibility of Z1, and B) the magnetic susceptibility of Z2

The oxidative durability was further examined by SQUID magnetometry (figure 5.9 and 5.10). These siliceous-graphitic-cobalt complexes were mechanically ground and exposed to air. Previous systems begin to show oxidation immediately when ground and exposed to air.[7,8] This has been shown by a drastic decrease in saturation magnetization. However, the measurements of these materials after 14 days indicated that Z1 and Z2, the cobalt nanoparticle systems derived from PHTH-*g*-PS copolymer shell precursors, had not changed. This strongly suggests that they have been protected against oxidation under ambient conditions.

Further aging experiments are currently underway to analyze the durability of such materials after longer periods. Future studies will also include attempts to better control particle size of the pyrolyzed materials and to develop methods for re-functionalization of their surfaces after the heat treatments.

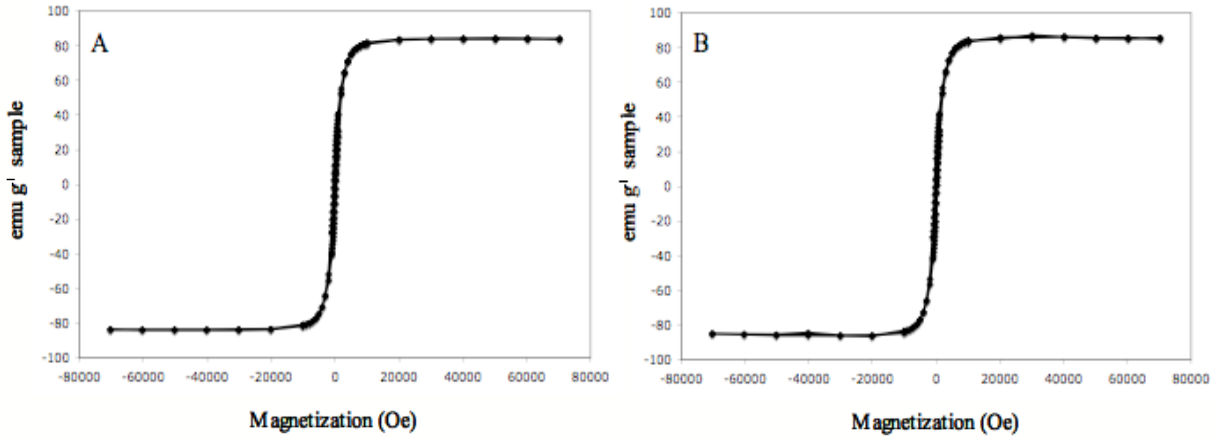

Figure 5.9 SQUID measurements demonstrating A) the magnetic susceptibility of Z1 at 0 days, and B) the same complex after 14 days after mechanically grinding and exposure to air.

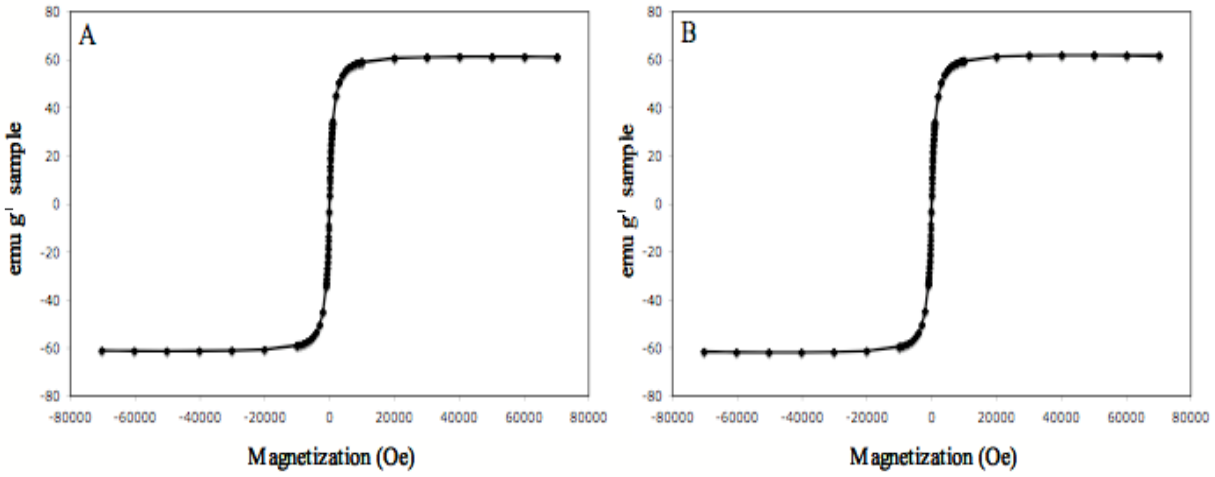

Figure 5.10 SQUID measurements demonstrating A) the magnetic susceptibility of Z2 at 0 days, and B) the same complex after 14 days of exposure to air.

CHAPTER 6 Synthesis and Characterization of Heterobifunctional Poly(ethylene oxide)

6.1 Synopsis

This chapter discusses the synthesis and characterization of hydroxypropylvinylsilane initiators for poly(ethylene oxide) polymerizations. Poly(ethylene oxide) oligomers were prepared with one, two and three vinyl groups at one end, then the vinylsilane endgroups were reacted with mercaptoacetic acid to produce carboxylic acid functional poly(ethylene oxide)s. It is anticipated that these carboxylic acid functional oligomers will complex to magnetite nanoparticles, and that these complexes will be dispersible in aqueous media.

The initiators were prepared via a series of chemical modifications, and characterized by ^{1}H NMR. Hydroxypropylvinylsilanes were utilized to initiate the polymerization of ethylene oxide. End group analysis by ^{1}H NMR showed a ratio of end groups as 1:1. Molecular weights determined from both ^{1}H NMR and GPC were close to targeted values indicating good control over the molecular weight. These systems were almost monodisperse in their molecular weight distributions as determined by GPC. The carboxylic acid functional poly(ethylene oxide) oligomers were prepared from ene-thiol addition reactions of mercaptoacetic acid across the vinyl functional termini. ^{1}H NMR was utilized to demonstrate reaction completion.

6.2 Experimental
6.2.1 Materials

Tetrahydrofuran (THF, EM Science 99.5%) was dried over calcium hydride and refluxed over sodium with benzophenone until the solution was deep purple. It was fractionally distilled into a flame-dried, round bottom flask prior to each reaction. Vinylmagnesium chloride (Aldrich, 1.6M in THF) was used as received. 3-Chloropropyltrichlorosilane (MW 211.98 g mol^{-1}, d 1.3590 g mL^{-1}, BP 181 °C), 3-chloropropyldichloromethylsilane (MW 191.56 g mol^{-1}, d 1.204 g mL^{-1}, BP 180 °C), and 3-chloropropylchlorodimethylsilane (MW 171.14 g mol^{-1}, d 1.043 g mL^{-1}, BP 179 °C) (all from Gelest, Inc.) were fractionally distilled prior to use. NaI (MW 149.895 g mol^{-1}, Aldrich) was dried under vacuum at 110 °C overnight. Hexamethylphosporamide (HMPA, MW 179.20 g mol^{-1}, d 1.030 g mL^{-1}, MP 7 °C, BP 230-232 °C/740 mm Hg, Aldrich) was used as received. Sodium bicarbonate (MW 85 g mol^{-1}, Aldrich, 99 %) was used as received. Potassium metal (MW 39.098 g mol^{-1}, Aldrich, 98 %) was stored in mineral oil and used as needed. Naphthalene (MW 128.17 g mol^{-1}, Aldrich) was used as received. Ethylene oxide (MW 44.05 g mol^{-1}, d 0.882 g mL^{-1}, MP -111 °C, BP 10.7 °C, Aldrich, 99.5 %), in pressurized 227 g stainless steel lecture bottles, was utilized as received. Diethyl ether (MW 74.12 g mol^{-1}, d 0.706 g mL^{-1}, MP -116 °C, BP 34.6 °C, EMD Chemicals) was used as received. Toluene (MW 92.14 g mol^{-1}, d 0.865 g mL^{-1}, MP -63 °C, BP 110 °C, Burdick and Jackson, 99.9 %) was stirred over calcium hydride, distilled, and deoxygenated by sparging with nitrogen through the solution prior to use for 2 h. Mercaptoacetic acid (MW 92.12 g mol^{-1}, d 1.325 g mL^{-1}, MP -16 °C, BP 96 °C/5 mm Hg, Aldrich, 97 %) and 2,2'-azobisisobutyronitrile (AIBN, MW 164.21 g mol^{-1}, MP 103-105 °C, Aldrich, 98 %) were used as received. Dichloromethane (MW 86.93 g mol^{-}

[1], d 1.325 g mL^{-1}, MP -97 °C, BP 39.8 – 40 °C, Aldrich, 99.6 %), acetone (MW 58.08 g mol^{-1}, d 0.791 g mL^{-1}, MP -94 °C, BP 56 °C, Aldrich, 99.6%), chloroform (MW 119.38 g mol^{-1}, d 1.492 g mL^{-1}, MP -63 °C, BP 60.5 – 61.5 °C, Aldrich, 99.5 %), and acetic acid (MW 60.05 g mol^{-1}, d 1.049 g mL^{-1}, MP 16.2 °C, BP 117 – 118 °C, Aldrich, 99.99%) were used as received.

6.2.2 Synthesis of 3-chloropropyltrivinylsilane (CPTVS)

A procedure to prepare a 3-chloropropyltrivinylsilane (MW 186 g mol^{-1}) is provided. Vinylmagnesium chloride (0.14 mol, 88.47 mL of 1.6 M vinylmagnesium chloride in THF) was transferred via cannula to a flame-dried, septum-sealed round bottom flask equipped with a condenser and magnetic stir bar. 3-Chloropropyltrichlorosilane (0.047 mol, 0.14 eq chlorosilane, 7.36 mL, 10 g) was added via glass syringe in two equal aliquots to the reaction vessel. The reaction was conducted at 60 ºC for 24 h. The product was concentrated by removing the THF via conventional distillation. The remaining reaction mixture was dissolved in dichloromethane (150 mL). The salt by-products were removed by vacuum filtration. The product was vacuum distilled 100 °C at 0.8 Torr and analyzed via ^{1}H NMR. The reaction had approximately 50 % yield and the final product was a clear, colorless. ^{1}H NMR ($CDCl_3$): δ 0.83 ppm (2 H), δ 1.82 ppm (2 H), δ 3.5 (2 H), and δ 5.8-6.2 ppm (9 H).

6.2.3 Synthesis of 3-chloropropyldivinylmethylsilane (CPDVS)

The preparation of 3-chloropropyldivinylmethylsilane (MW 174 g mol^{-1}) follows the same procedure as 6.2.2. Vinylmagnesium chloride (0.104 mol, 65.25 mL of 1.6 M vinylmagnesium chloride in THF) and 3-chloropropyldichloromethylsilane (0.0522 mol, 0.104 eq chlorosilane, 10g, 8.31 mL) were reacted 60 ^{o}C for 24 h. The product was

vacuum distilled 93 °C at 0.8 Torr and analyzed via ^{1}H NMR. The reaction had approximately a 50 % yield and the final product was a clear, colorless liquid. ^{1}H NMR ($CDCl_3$): δ 0.77 ppm (2 H), δ 1.8 ppm (2 H), δ 3.48 (2 H), and δ 5.7-6.2 ppm (6 H).

6.2.4 Synthesis of 3-chloropropylvinyldimethylsilane (CPVS)

The preparation of 3-chloropropylvinyldimethylsilane (MW 162 g mol^{-1}) follows the same procedure as 6.2.2. Vinylmagnesium chloride (0.058 mol, 36.52 mL of 1.6 M vinylmagnesium chloride in THF), and 3-chloropropylchlorodimethylsilane (0.058 mol, 0.058 eq chlorosilane, 10 g, 9.59 mL) were reacted at 60 °C for 24 h. The product was vacuum distilled 86 °C at 0.8 Torr and analyzed via ^{1}H NMR. The reaction had approximately a 50 % yield and the final product was a clear, colorless liquid. ^{1}H NMR ($CDCl_3$): δ 0.65 ppm (2 H), δ 1.78 ppm (2 H), δ 3.45 (2 H), and δ 5.6-6.2 ppm (3 H).

6.2.5 Synthesis of 3-iodopropyltrivinylsilane (IPTVS)

The preparation of a 3-iodopropyltrivinylsilane (MW 277.905 g mol^{-1}) is provided. A two-fold excess of NaI (0.054 mol, 8.1 g) was charged to a round bottom flask equipped with a magnetic stir bar. The reaction vessel was sealed with a septum and flame-dried. Acetone (25 mL) was added via syringe to the flask. 3-Chloropropyltrivinylsilane (0.027 mol, 5 g) was charged to the reaction vessel via syringe. The reaction was stirred at 60 °C for 48 h until 95% conversion was achieved as determined by ^{1}H NMR. The acetone was removed by rotary evaporation and the reaction mixture was dissolved in chloroform (150 mL). The excess NaI and the NaCl salt by-product were removed by vacuum filtration. The product was vacuum distilled at 70 °C at 0.8 Torr. The reaction had a yield of 95 % and the final product was a clear,

colorless liquid. ^{1}H NMR ($CDCl_3$): δ 0.8 ppm (2 H), δ 1.85 ppm (2 H), δ 3.2 (2 H), and δ 5.7-6.2 ppm (9 H).

6.2.6 Synthesis of 3-iodopropyldivinylmethylsilane (IPDVS)

The preparation of a 3-iodopropyldivinylmethylsilane (MW 265.905 g mol^{-1}) follows the same procedure as described in 6.2.5. A two-fold excess of NaI (0.058 mol, 8.7 g) and 3-chloropropyldivinylmethylsilane (0.029 mol, 5 g) were utilized. The reaction was stirred at 60 °C for 48 h until at least 95% conversion was achieved as determined by ^{1}H NMR. The acetone was removed by rotary evaporation and the reaction mixture was dissolved in chloroform. The excess NaI and the NaCl by-product were removed by vacuum filtration. The product was vacuum distilled at 63 °C at 0.8 Torr. The reaction had a yield of 95 % and the final product was a clear, colorless liquid. ^{1}H NMR ($CDCl_3$): δ 0.65 ppm (2 H), δ 1.72 ppm (2 H), δ 3.21 (2 H), and δ 5.65-6.2 ppm (6 H).

6.2.7 Synthesis of 3-iodopropylvinyldimethylsilane (IPVS)

The preparation of 3-iodopropylvinyldimethylsilane (MW 253.905 g mol^{-1}) follows the same procedure as described in 6.2.5. A two-fold excess of NaI (0.062 mol, 9.29 g) and 3-chloropropylvinyldimethylsilane (0.031 mol, 5 g) was utilized. The reaction was stirred at 60 °C for 48 h until at least 95% conversion was achieved as determined by ^{1}H NMR. The acetone was removed by rotary evaporation and the reaction mixture was dissolved in chloroform. The excess NaI as well as the NaCl salt by-product were removed by vacuum filtration. The product was vacuum distilled at 56 °C at 0.8 Torr. The reaction had a yield of 95 % and the final product was a clear,

colorless liquid. ^{1}H NMR ($CDCl_3$): δ 0.60 ppm (2 H), δ 1.72 ppm (2 H), δ 3.21 (2 H), and δ 5.6-6.2 ppm (3 H).

6.2.8 Synthesis of 3-hydroxypropyltrivinylsilane (HPTVS)

A method for synthesizing 3-hydroxypropyltrivinylsilane (MW 168 g mol^{-1}) is provided. HMPA (10 mL) was added to a round bottom flask equipped with a condenser and magnetic stir bar. Sodium bicarbonate (0.018 mol, 1.53 g) was added to the HMPA solution. One should note that the majority of the sodium bicarbonate remains undissolved. 3-Iodopropyltrivinylsilane (0.018 mol, 5 g) was added to the reaction vessel via syringe. De-ionized water (0.17 mol, 3 mL) was added via syringe. The reaction was stirred at 100 °C for 24 h. The product was extracted twice with chloroform in a separatory funnel. The chloroform was removed by rotary evaporation and the product was vacuum distilled at 90 °C at 0.8 Torr. The reaction had a yield of 95 % and the final product was a clear, colorless liquid. ^{1}H NMR ($CDCl_3$): δ 0.75 ppm (2 H), δ 1.62 ppm (2 H), δ 3.60 (2 H), and δ 5.7-6.2 ppm (9 H).

6.2.9 Synthesis of 3-hydroxypropyldivinylmethylsilane (HPDVS)

The preparation of 3-hydroxypropyldivinylmethylsilane (MW 156 g mol^{-1}) follows the same procedure as described in 6.2.8. 3-Iodopropyldivinylmethylsilane (0.019 mol, 5 g), sodium bicarbonate (0.019 mol, 1.62 g), and de-ionized water (0.17 mol, 3 mL) were reacted at 100 °C for 24 h. The product was extracted twice with chloroform in a separatory funnel. The chloroform was removed by rotary evaporation and the product was vacuum distilled 82 °C at 0.8 Torr. The reaction had a yield of 95 % and the final product was a clear, colorless liquid. ^{1}H NMR ($CDCl_3$): δ 0.65 ppm (2 H), δ 1.60 ppm (2 H), δ 3.6 (2 H), and δ 5.65-6.2 ppm (6 H).

6.2.10 Synthesis of 3-hydroxypropylvinyldimethylsilane (HPVS)

The preparation of 3-hydroxypropylvinyldimethylsilane (144 g mol^{-1}) follows the same procedure that was described in 6.2.8. 3-Iodopropylvinylmethylsilane (0.020 mol, 5g), sodium bicarbonate (0.020 mol, 1.7 g), and de-ionized water (0.17 mol, 3 mL) were reacted at 100 °C for 24 h. The product was extracted twice with chloroform in a separatory funnel. The chloroform was removed by rotary evaporation and the product was vacuum distilled at 76 °C at 0.8 Torr. The reaction had a yield of 95 % and the final product was a clear, colorless liquid. ^{1}H NMR ($CDCl_3$): δ 0.55 ppm (2 H), δ 1.58 ppm (2 H), δ 3.60 (2 H), and δ 5.6-6.2 ppm (3 H).

6.2.11 Preparation of a potassium naphthalate standard base solution in THF

An exemplary procedure to prepare a 0.95 M solution of potassium naphthalene in THF is provided. Naphthalene (0.095 mol, 12.16 g) was weighed into the flame-dried flask, sealed with a septum and flushed heavily with nitrogen. THF (100 mL) was added to the flask via a glass syringe. Potassium (0.095 mol, 3.7 g) was cut, the oil was removed by blotting on a Kimwipe and added to the flask very quickly. The flask was resealed and flushed heavily with nitrogen. The flask was again flushed with nitrogen. The reaction flask was covered with aluminum foil and stirred for 24 h. The final solution was a green liquid. It was titrated against a standardized HCl solution to obtain exact concentrations.

6.2.12 Synthesis of poly(ethylene oxide) with a trivinylsilylpropoxy group at one end and a hydroxyl group at the other end (TVSP-PEO)

The synthesis of a trivinylsilylpropoxy terminated poly(ethylene oxide) is provided. A 300-mL Parr pressure reactor equipped with a mechanical stirrer, thermocouple, and valve controlled gas inlets and outlets was cooled to -50 °C utilizing

an isopropanol dry ice bath. Ethylene oxide (0.341 mol, 15 g) was weighed before addition on an analytical balance and added to a Parr pressure reactor. Addition was driven by a pressure gradient. 3-Hydroxypropyltrivinylsilane initiator (0.0075 mol, 1.26 g) was added to a flame-dried, septum-sealed round bottom flask via syringe. THF (10 mL) was added to the vessel containing the initiator. Potassium naphthalate (0.0071 mol base, 1 mol initiator : 0.95 mol base, 7.5 mL of a 0.95 M solution of potassium naphthalene in THF) in THF was added to the flask containing the initiator to form the required alkoxide initiator. The color changed from dark green to golden yellow. The initiator solution was added to the Parr pressure reactor (while the reactor was stirring) via syringe. THF (10 mL) was deoxygenated under a nitrogen purge through the solution for 1 h was added to the Parr reactor via syringe. The reactor was allowed to warm to room temperature and the reaction was stirred at room temperature for 24 h. The reaction was monitored by noting a drop in pressure from 30 to 20 psi. The reaction was quenched with acetic acid (0.0075 mol, 3 mL of a 2.5 M solution of acetic acid in THF) under nitrogen. The poly(ethylene oxide) was precipitated into cold diethyl ether. It was dried under vacuum and dissolved in dichloromethane (250 mL). The PEO/dichloromethane solution was washed twice with water and ~75% of the dichloromethane was removed via rotary evaporator. The PEO was precipitated into cold diethyl ether and dried under vacuum at 40 °C overnight. The reaction, after purification, yielded 90 % by weight and had a M_n of 2800 g mol^{-1} with a PDI of 1.13.

6.2.13 Synthesis of poly(ethylene oxide) with a divinylsilylpropoxy group at one end and a hydroxyl group at the other end (DVSP-PEO)

The synthesis of a divinylmethylsilylpropyl terminated poly(ethylene oxide) follows the same procedure as described in 6.2.13. 3-Hydroxypropyldivinylmethylsilane

(0.0075 mol, 1.17 g) was utilized as the initiator. Potassium naphthalene (0.0071 mol, 1 mol initiator : 0.95 mol base, 7.47 mL of a 0.95M potassium naphthalene solution in THF) in THF was utilized to prepare the alkoxide. The reaction was quenched with acetic acid (0.0075 mol, 3 mL of a 2.5 M solution of acetic acid in THF). The poly(ethylene oxide) was precipitated into cold diethyl ether, dried under vacuum, and dissolved in dichloromethane (250 mL). The PEO/dichloromethane solution was washed twice with water and ~75% of the dichloromethane was removed via rotary evaporator. The PEO was re-precipitated into cold diethyl ether and dried under vacuum at 40 °C overnight. The reaction, after purification, yielded 88 % by weight and had a M_n of 2900 g mol^{-1} with a PDI of 1.08.

6.2.14 Synthesis of poly(ethylene oxide) with a monovinylsilylpropoxy group at one end and a hydroxyl group at the other end (VSP-PEO)

The synthesis of a vinyldimethylsilylpropyl terminated poly(ethylene oxide) follows the same procedure that was described in 6.2.13. 3-Hydroxypropylvinyldimethylsilane (0.0075 mol, 1.08 g) was utilized as the initiator. Potassium naphthalate (0.0071 mol, 1 mol initiator : 0.95 mol base, 7.47 mL of a 0.95 M potassium naphthalene solution in THF) in THF was utilized to prepare the alkoxide. The reaction was quenched with acetic acid (0.0075 mol, 3 mL of a 2.5 M solution of acetic acid in THF). The poly(ethylene oxide) was precipitated into cold diethyl ether, dried under vacuum, and dissolved in dichloromethane (250 mL). The PEO/dichloromethane solution was washed twice with water and ~75% of the dichloromethane was removed via rotary evaporator. The PEO was precipitated into cold diethyl ether and dried under vacuum at 40 °C overnight. The reaction, after purification, yielded 90 % by weight and had a M_n of 2800 g mol^{-1} with a PDI of 1.13.

6.2.15 Synthesis of a poly(ethylene oxide) with three carboxylic acids at one end and a hydroxyl group at the other end

A 2500 g mol^{-1} poly(ethylene oxide) oligomer with three vinyl groups at one end (2 g, 0.0024 eq vinyl) was added to a clean, flame-dried, septum-sealed, argon-purged flask equipped with a magnetic stir bar. Deoxygenated toluene (10 mL) was injected into the flask via glass syringe. AIBN (0.0059 g, 3.6 x 10^{-5} mol, 0.0015 mol AIBN per 1 eq vinyl) was added to the reaction vessel. Mercaptoacetic acid (0.0072 mol, 3 mol % excess based on eq vinyl, 0.50 mL, 0.66 g) was added to the flask via a syringe. The reaction was placed in an oil bath at 80 ºC, sparged with argon for 15 min, and stirred for two h. The reaction was concentrated by removing toluene. The concentrated PEO was precipitated into cold ethyl ether. It was vacuum filtered and allowed to dry under vacuum at 40 °C for 6 h.

6.2.16 Synthesis of a poly(ethylene oxide) with two carboxylic acids at one end and a hydroxyl group at the other end

A 2800 g mol^{-1} poly(ethylene oxide) oligomer with two vinyl groups at one end (2 g, 0.0014 eq vinyl) was added to a clean, septum-sealed, flame-dried, argon-purged flask equipped with a magnetic stir bar. Deoxygenated toluene (10 mL) was injected into the flask via glass syringe. AIBN (0.003 g, 2.1 x 10^{-5}, 0.0015 mol AIBN per 1 eq vinyl) was added to the reaction vessel. Mercaptoacetic acid (0.0042 mol, 3 mol % excess based on eq of vinyl, 0.29 mL, 0.39 g) was added to the flask via a syringe. The reaction was placed in an oil bath at 80 ºC, sparged with argon 15 min, and stirred for two h. The reaction was concentrated by removing toluene. The concentrated PEO was precipitated into cold ethyl ether. It was vacuum filtered and allowed to dry under vacuum at 40 °C for 6 h.

6.2.17 Synthesis of a poly(ethylene oxide) with one carboxylic acid at one end and a hydroxyl group at the other end

A 2500 g mol^{-1} poly(ethylene oxide) oligomer with one vinylsilyl group at one end (2 g, 8 x 10^{-4} eq vinyl) was added to a clean, septum-sealed, flame-dried, argon-purged flask equipped with a magnetic stir bar. Deoxygenated toluene (10 mL) was injected into the flask via glass syringe. AIBN (0.002 g, 1.2 x 10^{-5}, 0.0015 mol AIBN per eq vinyl) was added to the reaction vessel. Mercaptoacetic acid (0.0024 mol, 3 mol % excess based on eq of vinyl, 0.17 mL, 0.22 g) was added to the flask via a syringe. The reaction was placed in an oil bath at 80 ºC, sparged with argon 15 min, and stirred for two h. The reaction was concentrated by removing toluene. The concentrated PEO was precipitated into cold ethyl ether. It was vacuum filtered and allowed to dry under vacuum at 40 °C for 6 h.

6.3 Characterization

6.3.1 ^{1}H Nuclear Magnetic Resonance Spectroscopy

All ^{1}H NMR spectra were obtained on a Varian Unity 400 MHz NMR spectrometer operating at 400 MHz. The NMR parameters included a pulse width of 28.6° and a relaxation delay of 1.000 sec at ambient temperature. The samples were all dissolved in *d*-$CHCl_3$ or d_6-DMSO for obtaining the spectra.

6.3.2 Gel permeation chromatography

Gel permeation chromatograms were obtained in HPLC grade THF at 30 °C on a Waters Alliance Model 2690 chromatograph equipped with a Waters HR 0.5 + HR 2 + HR 3 + HR 4 styragel column set. A Viscotek viscosity detector and a refractive index detector were utilized with polystyrene calibration standards to generate a universal molecular weight calibration curve for absolute molecular weight analyses. Samples were prepared by dissolving 30-35 mg in 10 mL HPLC grade tetrahydrofuran.

6.4 Results and Discussion

Poly(ethylene glycol) (PEG) or poly(ethylene oxide) (PEO) is a linear or branched polyether typically terminated with hydroxyl groups. PEO is a hydrophilic and biocompatible polymer.[99,100,149] The polyether has other unique properties including weak immunogenicity, rapid renal clearance *in vivo*, and resistance to biodegredation. PEO is soluble in both aqueous and organic media creating a suitable substrate for derivatization and chemical modification/conjugation. The water solubility is largely due to the binding of 2-3 water molecules to each ethylene oxide unit of the backbone.[99]

Poly(ethylene oxide)'s low immunogenicity and water solubility make it a prime candidate for utilization in medicine. There are applications in drug delivery, bio-separations, protein modification, and implants (for non-fouling surfaces). In order to functionalize a surface or protein, the PEO must be derivatized at one or both ends of the molecule. The functional group is tailored to the molecule (surface structure or protein amino acid residue) that will be coupled to the PEO. PEO can be derivatized to contain binding moieties that will interact with metal surfaces such as terminal carboxylic acid groups via a variety of synthetic methodologies.[6,108,113]

Carboxylic acids have been widely utilized as the anchoring unit of a macromolecule to the surface of magnetite nanoparticles. Previous investigations have included the use of oleic acid, tricarboxylic acid terminated polydimethylsiloxane, and various other systems.[4,109] However, these are all hydrophobic systems that do not yield magnetite complexes dispersible in aqueous media. There are a few reports of carboxylic acid containing water soluble polyethers used as stabilizers for metal nanoparticles.

Tamaura et al. investigated α,ω-poly(ethylene oxide) dicarboxylic acid as a possible steric stabilizer for magnetite. It was proposed that one terminus of the PEO would complex to the magnetite surface while the free carboxylic acid serves to couple lipase.[113] In addition, Harris et al. developed a series of triblock copolymers containing PEO tail blocks with carboxylic acid functional polyurethane central anchor blocks. The research focused on developing magnetite complexes coated with hydrophilic stablizers for dispersion in aqueous media.[6]

The research presented in this chapter focused on preparing novel carboxylic acid functional poly(ethylene oxides), which might be utilized as magnetite stabilizers to form complexes dispersible in aqueous media. The premise for the research is derived from analogous hydrophobic siloxane stabilizers, which possess one terminal trivinylsilyl group per chain. This trivinylsilyl group is chemically converted into carboxylic acids via known ene-thiol addition reactions. It was desirable to prepare poly(ethylene oxide) initiators that resulted in a terminal propylvinylsilyl group on the PEO chains wherein the number of vinyl groups varies from one to three. These vinyl groups can be modified with carboxylic acids to prepare water soluble poly(ethylene oxide) stabilizers for magnetite.

6.4.1 Preparation of propylvinylsilane initiators for poly(ethylene oxide)

6.4.1.1 Synthesis and characterization of 3-chloropropylvinylsilanes

Functional organosilanes may be prepared via a variety of synthetic methodologies. The chemistry of these molecules parallels that of organic compounds; however, the silicon atom leads some distinct differences. In particular, the silicon atom is more electropositive than carbon therefore nucleophilic substitution at the silicon is often more facile. Chlorosilanes often serve as intermediates for the preparation of organosilanes. They can be reacted with Grignard reagents or other organometallics yielding organic substitution at the silicon atom.[22,71]

The poly(ethylene oxide) initiators were prepared utilizing standard Grignard reactions. A series of commercially available 3-chloropropylchlorosilanes served as the precursors containing one to three chlorine groups directly bonded the silicon atom. Vinylmagnesium chloride was utilized as the Grignard reagent and the reactions proceeded through nucleophilic substitution of the chlorines on the silicon (figure 6.1).

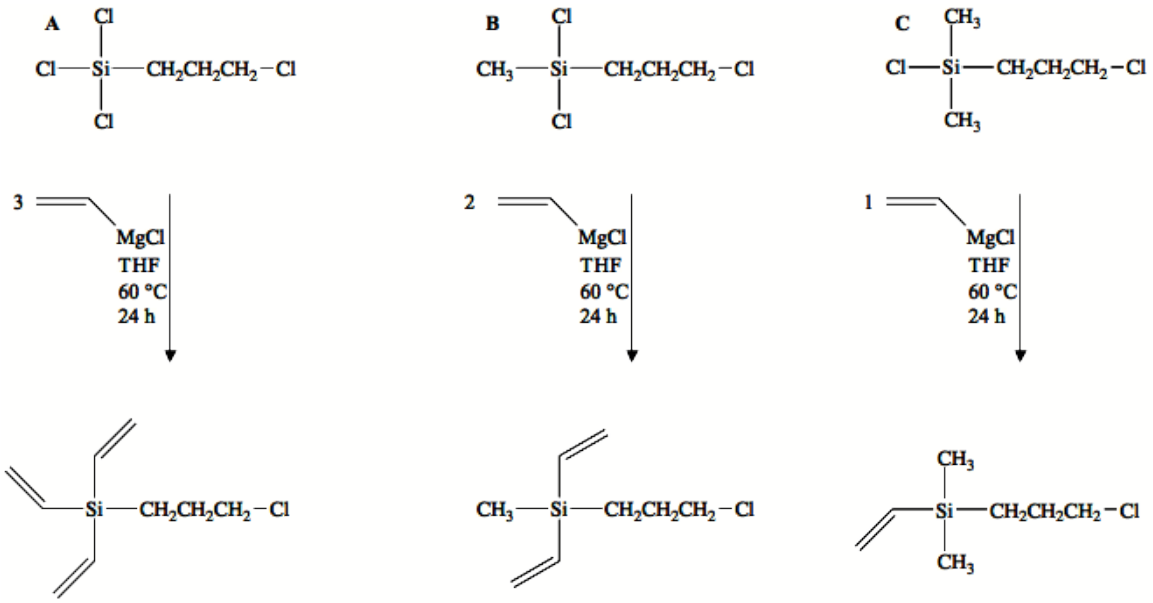

Figure 6.1 Synthetic reaction schemes depicting the preparation of a.) 3-chloropropyltrivinylsilane, b.) 3-chloropropylmethyldivinylsilane, and c.) 3-chloropropyldimethylvinylsilane

The Grignard reactions had a latent exotherm to 60 °C as the vinylmagnesium chloride was charged. The amount of vinylmagnesium chloride was chosen such that there was one vinylmagnesium chloride per silylchloride. Reactions with excess Grignard reagents lead to unwanted substitution at the 3-chloropropyl position. The reactions proceeded with immediate precipitation of $MgCl_2$ and were allowed to continue for 24 h to ensure complete substitution of the silylchlorides.

It was important to quantitatively remove all THF and to completely decompose any remaining Grignard reagent after the reaction was completed. The THF was removed by distillation after which the reaction mixture was exposed to air to decompose the Gignard reagent. Otherwise, it was observed that the THF polymerized and substantially decreased product yields.

The molecular structures of the final products were examined by ^{1}H NMR. Figure 6.2 shows a representative ^{1}H NMR spectrum of the chlorosilane starting reagent. The methylene directly adjacent to the silicon atom (protons A) was observed at 1.58 ppm, the methylene labeled protons B were observed at 2.0 ppm. However, the methylene directly attached to the chlorine substituent resonated at 3.5 ppm. These proton assignments were utilized in comparison to the final products and were useful in defining the final products' molecular structures.

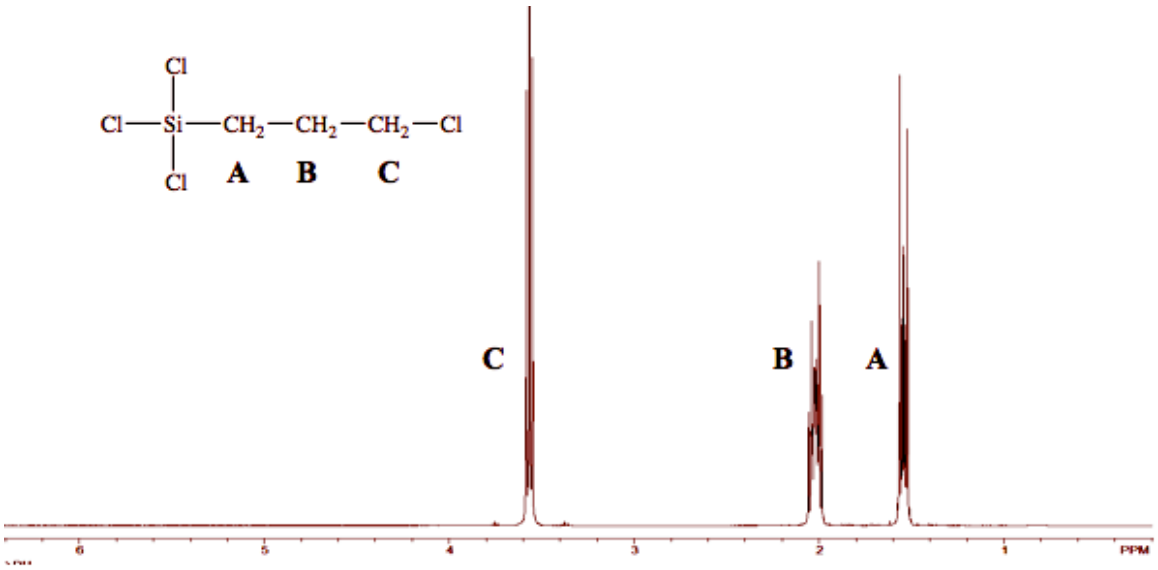

Figure 6.2 The molecular structure of 3-chloropropyltrichlorosilane as examined by ^{1}H NMR

Figure 6.3 depicts ^{1}H NMR spectra of the three final products obtained from reactions shown in figure 6.1. The molecular structures are characterized both by the peak shifts in the propyl methylenes and the resonance integrals. The CPTVS has proton resonance integral ratios of 9:2:2:2 for protons labeled A - D respectively. The proton integral ratios for the CPDVS and CPVS are 6:2:2:2 and 3:2:2:2, respectively. For all products, the methylene proximal to the silicon atom shifts to ~0.8 ppm after substitution of the vinyl group occurs.

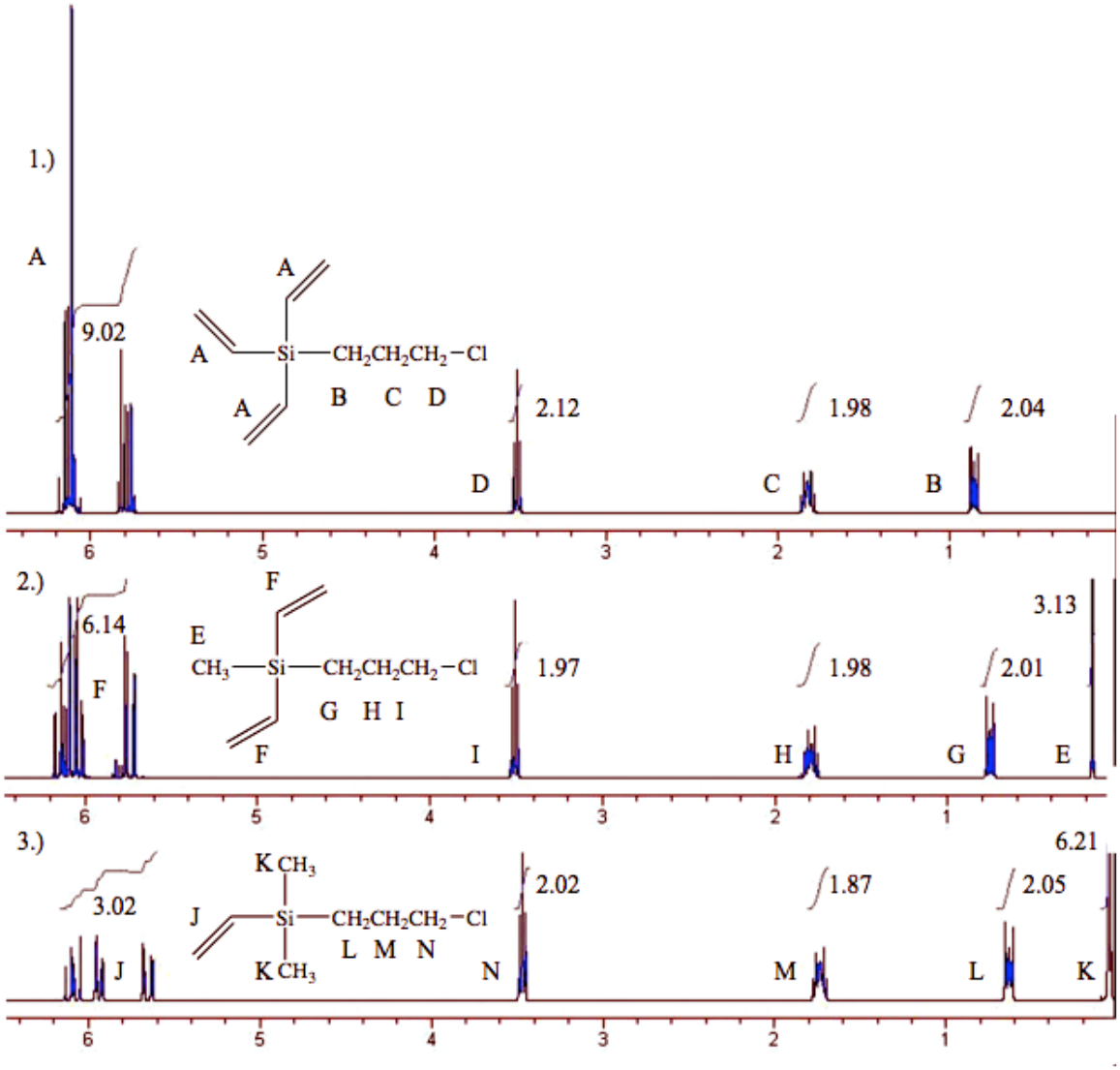

Figure 6.3 3-Chloropropyltrivinylsilane (1), 3-chloropropylmethyldivinylsilane (2), and 3-chloropropyldimethylvinylsilane (3) were examined by ^{1}H NMR to verify their molecular structures.

6.4.1.2 Synthesis of 3-iodopropylvinylsilanes

The transformation of an alkyl chloride to an alkyl iodide is a well known reaction in organic chemistry.[150] This reaction occurs via S_N2 nucleophilic substitution on primary alkyl chlorides where iodine functions as the nucleophile. This reaction is hindered by the nucleophilic strength of the leaving group: chloride anion. Nucleophilic strength can be

compared to basicity where chloride anion has a pK_b of 6.3×10^{-17} and iodide anion has a pK_b of 6.3×10^{-20}. In other words, chlorine is a stronger nucleophile than iodine. In addition, the C-I bond (bond strength – 53 kcal mol^{-1}) is much weaker than that of a C-Cl bond (bond strength – 80 kcal mol^{-1}) making the iodine atom a better leaving group.[150,151]

This S_N2 equilibrium, however, may be shifted to the iodine substitution by choosing a reaction medium in which the by-product is insoluble such as acetone. The counter ion is also of great importance in this reaction. Lithium halides are all soluble in acetone whereas sodium halides decrease in solubility from NaI > NaBr > NaCl where sodium chloride is virtually insoluble. The precipitation of the sodium chloride results in an equilibrium shift towards complete conversion of primary alkyl chlorides to primary alkyl iodides.[150]

Figure 6.4 depicts the reaction conditions utilized in the conversion of CPTVS, CPDVS, and CPVS to their corresponding iodine containing compounds. A two-fold excess of NaI was utilized in their preparation to ensure the presence of iodide anions. These reactions were conducted at 60 °C for 48 h where precipitation of NaCl was apparent within 1 h for all reactions.

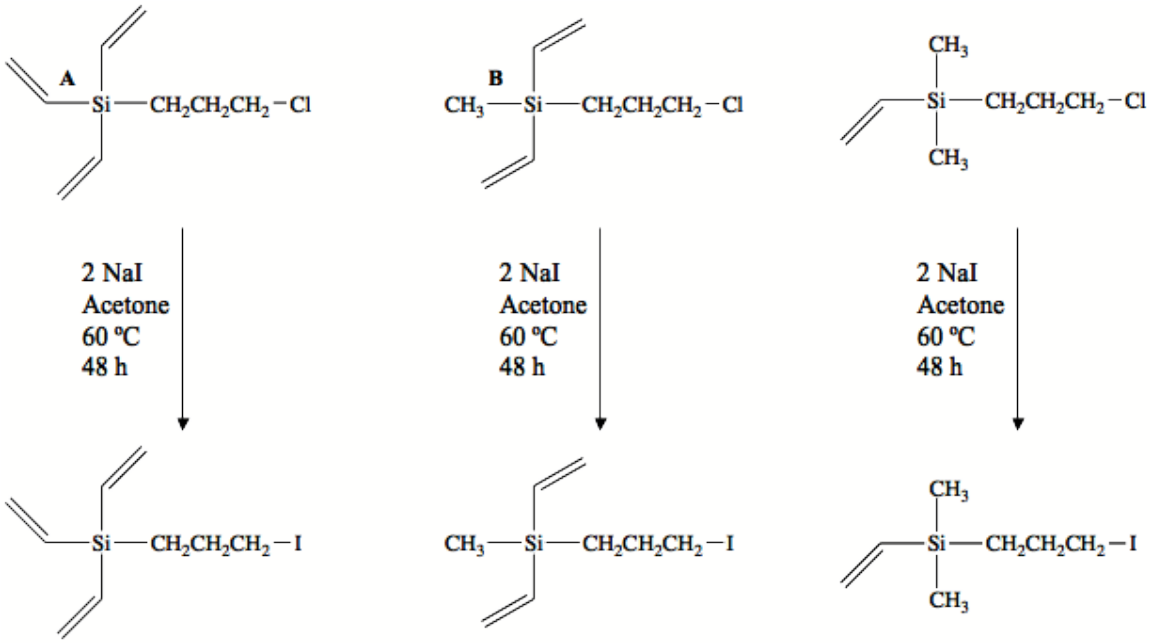

Figure 6.4 Synthetic reaction schemes depicting the preparation of a.) 3-iodopropyltrivinylsilane, b.) 3-iodopropylmethyldivinylsilane, and c.) 3-iodopropyldimethylvinylsilane

The substitution reaction was monitored by ^{1}H NMR. A representative ^{1}H NMR of a CPDVS/IPDVS conversion is shown in figure 6.6 where there is a concurrent increase in the peak at 3.2 ppm corresponding to the methylene directly attached to the iodine and a decrease in the peak at 3.6 ppm corresponding to the peak directly attached to the chlorine.

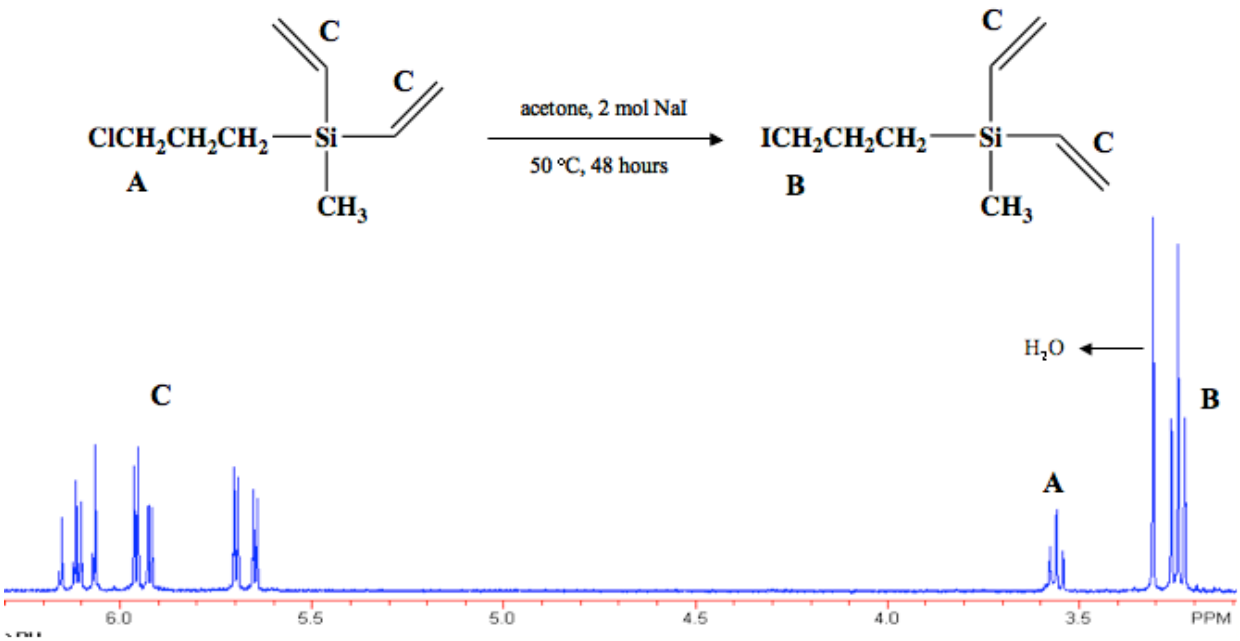

Figure 6.5 A representative ^{1}H NMR spectrum depicting the conversion of the 3-chloropropyldivinylmethylsilane to 3-iodopropyldivinylmethylsilane as indicated by the appearance of protons B at 3.2 ppm and the disappearance of protons A at 3.6 ppm.

The resulting products from the iodine substitution reactions include IPTVS, IPDVS, and IPVS. These 3-iodopropylvinylsilanes were examined via ^{1}H NMR to confirm their molecular structure (figure 6.6). The molecular structure was analyzed by comparing the resonance integrals of each proton set (number of vinyls : number of methylenes). Each compound synthesized possessed the theoretical ratio of protons: for IPTVS the ratio is 9:2:2:2, for IPDVS the ratio is 6:2:2:2, and for IPVS the ratio is 3:2:2:2. It is important to note that the proton resonance for the methylene proximal to the iodine appear at approximately 3.1 ppm which is expected for these electronic environments.

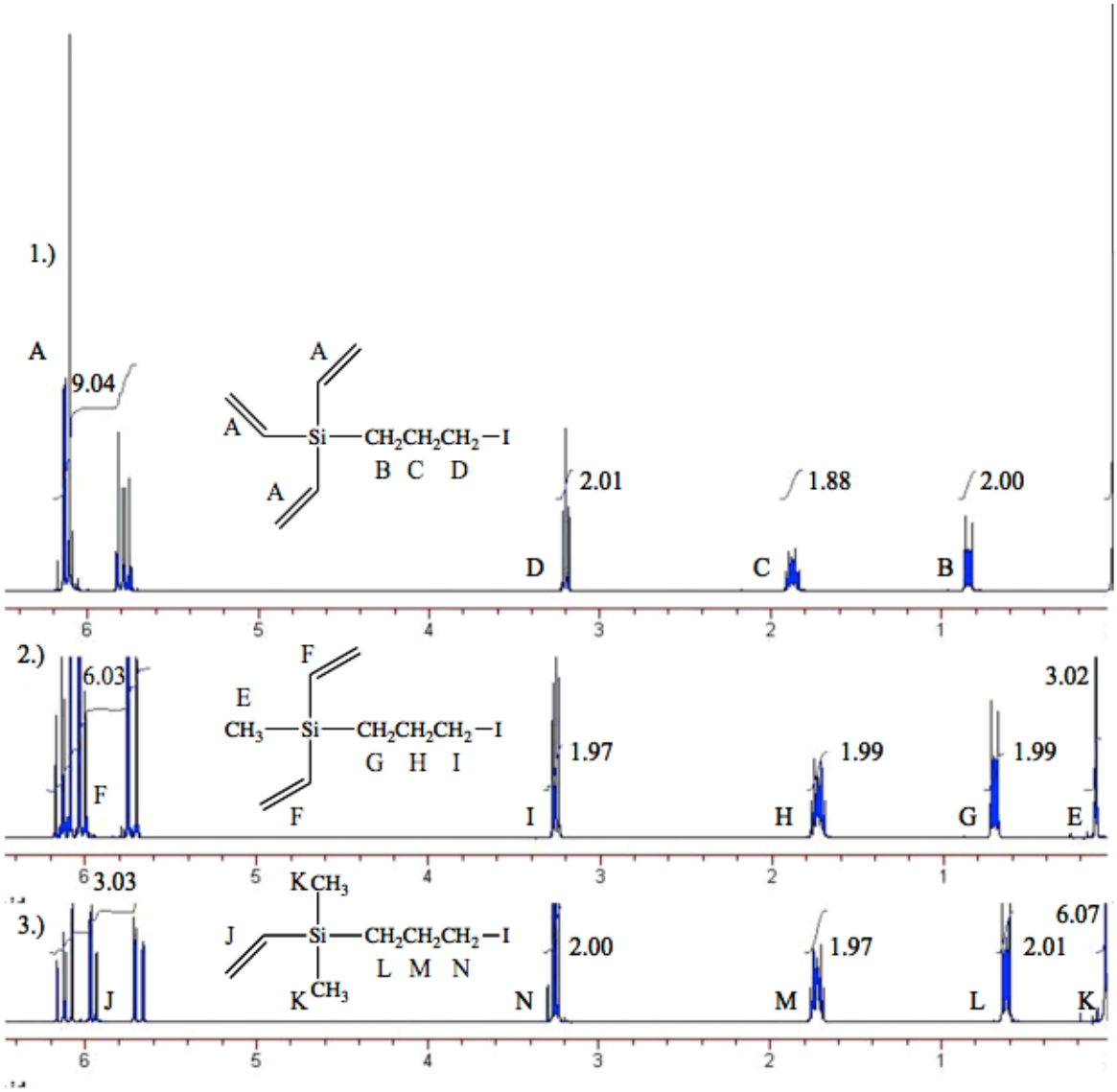

Figure 6.6 3-Iodopropyltrivinylsilane (1), 3-Iodopropylmethyldivinylsilane (2), and 3-Iodopropyldimethylvinylsilane (3) were examined by ^{1}H NMR spectra to verify their molecular structures.

6.4.1.3 Synthesis of 3-hydroxypropylvinylsilanes

The 3-iodopropylvinylsilanes were all subsequently converted to their corresponding alcohols via S_N2 reaction conditions. There have been several approaches to converting functional groups to oxygen species.[152-154] These approaches involve

increasing the nucleophilicity of the poor displacing anions by phase-transfer techniques or introducing rate enhancing polar aprotic solvents. Hutchins et al. probed the synthesis of alcohols from alkyl halides, specifically alkyl chlorides and alkyl iodides. They discovered that a combination of a polar aprotic solvent such as NMP or HMPA served as a good source of nucleophilic oxygen. They observed successful conversions of alkyl chlorides and iodides to their corresponding alcohols. The research showed that primary 1-iodooctane were converted to alcohols with high yield (> 90 %) in HMPA whereas the 1-chlorooctane did not reach these conversions (< 50 %) (below 30 % was converted in NMP).[151]

Therefore, it is necessary to convert the original 3-chloropropylvinylsilanes into their iodine counterparts before transformation into the alcohol species. Figure 6.7 shows the synthetic schemes for the reaction of water with the 3-iodopropylvinylsilanes. These reactions were conducted in HMPA at 100 °C. The sodium bicarbonate was added in a ratio of 1 mol iodine : 1 mol sodium bicarbonate. The sodium bicarbonate acted as an acid scavenger to neutralize HI by products. An excess of water (10 mol %) was added to these reactions and they were conducted at 100 °C. It is important to note that the sodium bicarbonate in these concentrations is not soluble in the reaction medium. However, the sodium bicarbonate solubilizes as the reaction proceeds which is likely due to the production of HI *in situ*. The reaction is complete within 24 h.

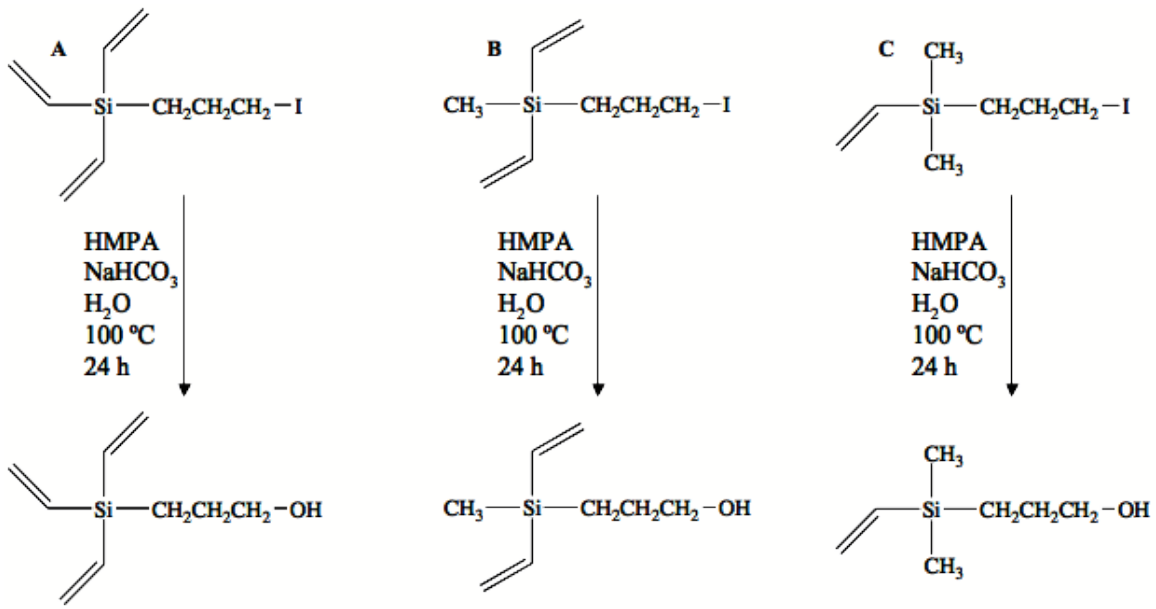

Figure 6.7 Synthetic reaction schemes depicting the preparation of a.) 3-hydroxypropyltrivinylsilane, b.) 3-hydroxypropylmethyldivinylsilane, and c.) 3-hydroxypropyldimethylvinylsilane

The final 3-hydroxypropylvinylsilanes were analyzed by ^{1}H NMR to probe their molecular structures. A comparison between the starting material protons and the final purified product is utilized to determine molecular structure. There is a shift of the methylene proximal to the OH from 3.2 ppm (corresponding to the methylene proximal to an iodine) to 3.6 ppm after substitution. The splitting pattern of this methylene resonance is a triplet. As in the cases with the 3-chloro- and 3-iodopropylvinylsilanes, the ratio of protons was determined. These values matched theoretical proton ratios of 9:2:2:2 for HPTVS, 6:2:2:2 for HPDVS, and 3:2:2:2 for HPVS.

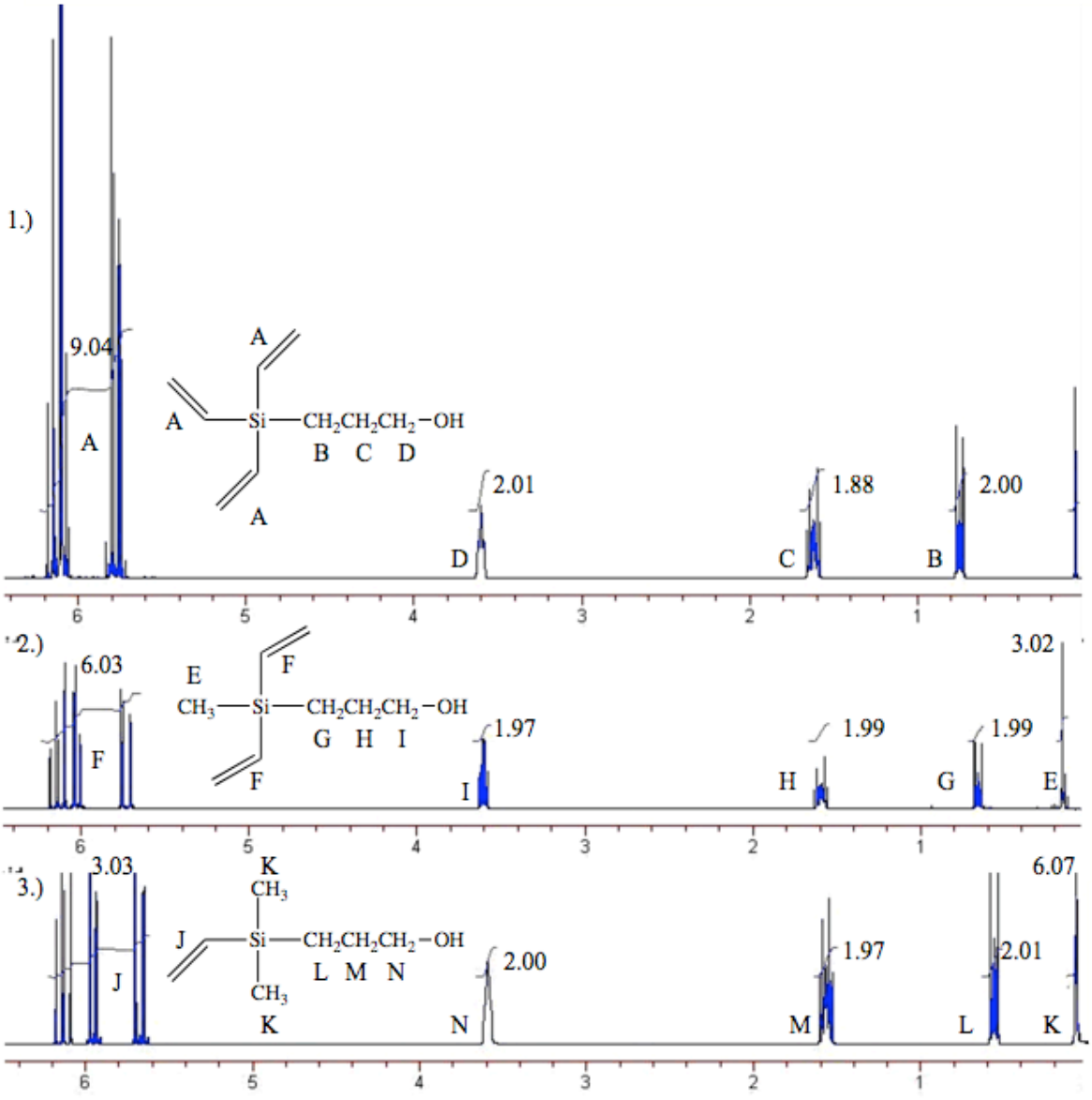

Figure 6.8 3-Hydroxypropyltrivinylsilane (1), 3-hydroxypropylmethyldivinylsilane (2), and 3-hydroxypropyldimethylvinylsilane (3) were examined by ^{1}H NMR spectra to verify their molecular structures.

6.3.2 Synthesis of Vinylsilylpropoxy-poly(ethylene oxide) oligomers

PEO is typically polymerized via anionic ring opening polymerization techniques. These reactions proceed by nucleophilic attack of the anionic initiator on the ethylene oxide methylenes. Initiators include hydroxides, alkoxides, oxides, and metal alkyls/aryls

such as potassium naphthalene.[102,103] These reactions are considered living polymerizations, which are characterized by great control over the molecular weight and molecular weight distributions. These polymerizations have the ability to impart functionality such as vinyl moieties on one chain end. In this particular case, the PEO will be difunctional with a vinyl terminus and a hydroxyl terminus. Figure 6.9 shows the reaction conditions utilized to synthesize vinyl functional poly(ethylene oxide)s.

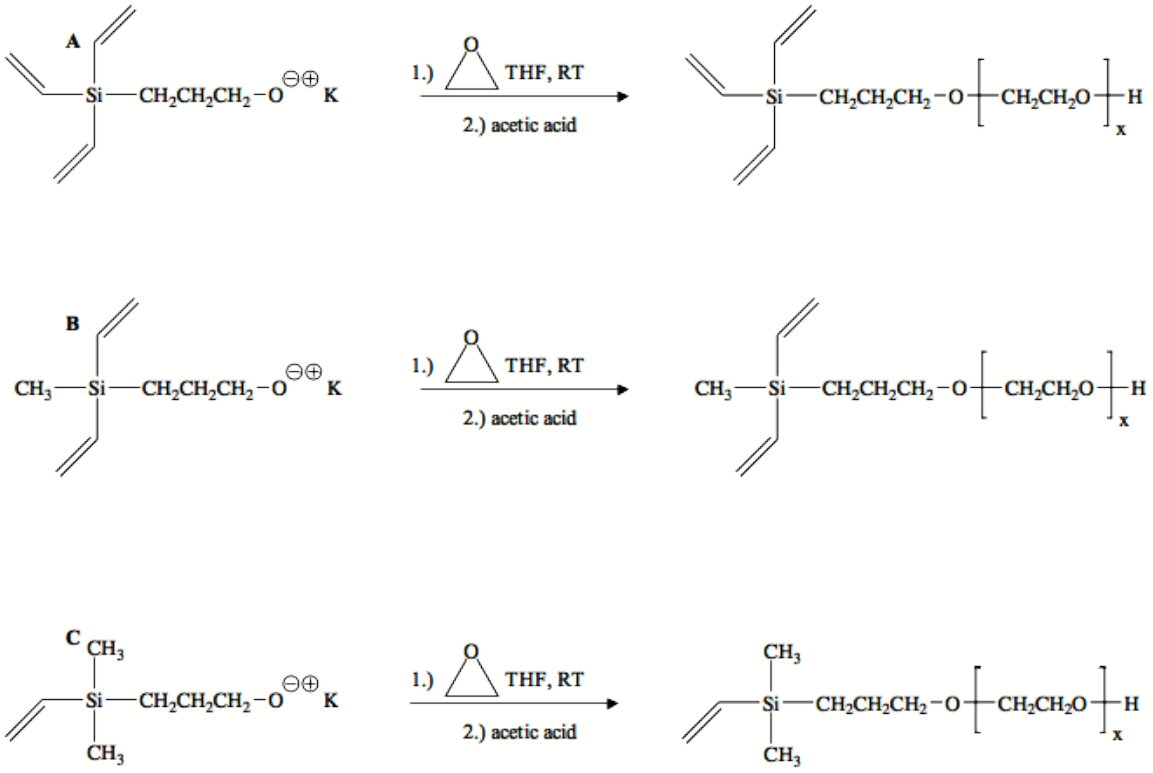

Figure 6.9 The ring opening polymerization of ethylene oxide utilizing the following initiators a.) 3-hydroxypropyltrivinylsilane,
b.) 3-hydroxypropylmethyldivinylsilane, and
c.) 3-hydroxypropyldimethylvinylsilane.

These reactions are performed under 30 psi at room temperature. As the reaction proceeds, the pressure drops to approximately 20 psi indicating that nearly all of the EO has been consumed or polymerized. The PEO is quenched with acetic acid and washed twice with water to neutralize the resulting potassium acetate. In addition, these

polymerizations were conducted utilizing a slight deficiency of base in preparing the initiator solution. This ratio served to preserve the vinyl groups during the initiator alkoxide formation and during the polymerization. It was observed that 1 mol initiator : 0.95 mol base functioned well in preserving the vinyl moieties.

End group analysis was performed via ^{1}H NMR to ensure that the end groups remained intact during the polymerization and that proper molecular weight could be targeted and controlled. Figure 6.10 depicts the ^{1}H NMR spectra obtained from the three PEO's synthesized. For each spectrum, the ratio of end group protons matched the theoretical values where the TVSP-PEO had ratios of 9:2:2:2; the DVSP-PEO had ratios of 6:2:2:2; and the VSP-PEO had ratios of 3:2:2:2.

Utilizing the end group resonances, number average molecular weight was also calculated. These values correspond well with the targeted molecular weights (table 6.1). In addition, GPC was utilized to examine the molecular weights and molecular weight distributions of these PEO's. The data presented in table 6.1 indicates that the M_n's achieved were close to their targeted values. The polydispersity indices (PDI) for these polymers were also narrow and monomodal with values approaching 1. This distribution suggests that these polymerizations were well-controlled and living in nature.

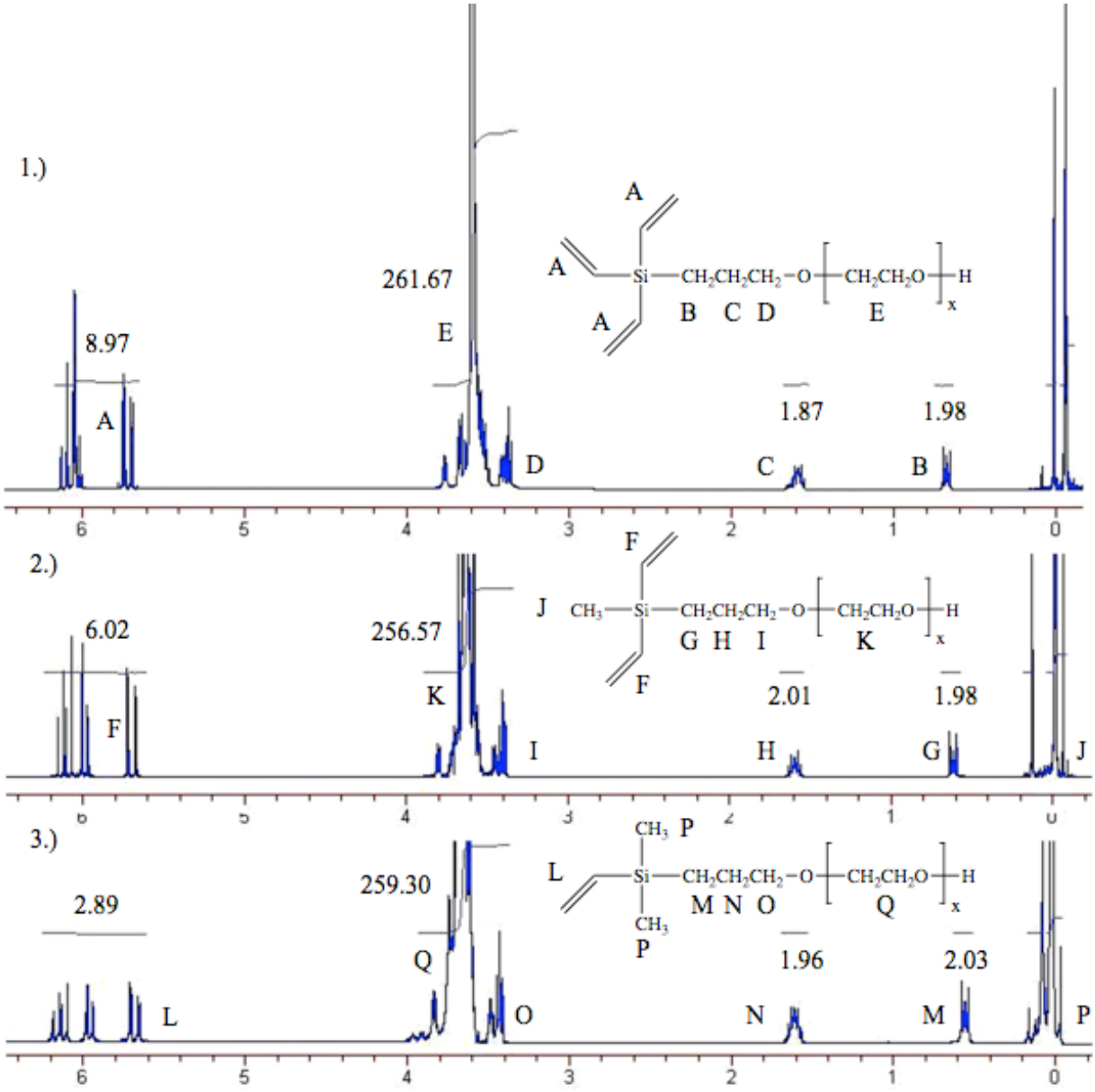

Figure 6.10 End group analysis was performed via ^{1}H NMR to obtain molecular weights and analyze molecular structure for a.) Trivinylsilylpropyl-PEO, b.) divinylmethylsilyl-PEO, and c.) vinyldimethylsilylpropyl-PEO.

Table 6.1 A summary of molecular weights and molecular weight distributions for the vinylsilylpropyl-PEO series.

End Group	Target M_n (g mol^{-1})	M_n via ^1H NMR (g mol^{-1})	M_n via GPC (g mol^{-1})	PDI
Trivinylsilylpropyl	2500	2800	2800	1.13
Divinylmethylpropyl	2500	2900	3000	1.08
Vinyldimethylpropyl	2500	2800	2600	1.07

6.4.3 Synthesis and characterization of poly(ethylene oxide) oligomers with carboxylic acids at one end and one hydroxy group at the other end

The series of poly(ethylene oxide)s were chemically converted to carboxylic acids utilizing the ene-thiol addition of mercaptoacetic acid across the vinyl groups under free radical conditions. The ene-thiol reaction has been utilized previously by Chojnowski et al. to convert pendent vinyl moieties on a PDMS-*b*-poly(methylvinylsiloxane) copolymer to carboxylic acid groups.[131] In addition, Wilson et al. showed that terminal trivinylsilyl groups on PDMS may be converted in a similar manner with good control over the chemistry.[4] The major product is the Markovnikov product in these aforementioned reactions. To our knowledge, the addition of mercaptoacetic acid to vinyl terminated PEO's has not been reported.

In the research presented here, carboxylic acids were introduced at one chain end utilizing AIBN as the free radical initiator (figure 6.11). These reactions were conducted at 80 °C in toluene. It is important that the reaction system is heavily deoxygenated prior to proceeding. This procedure ensures that oxygen does not inhibit the free radical processes.

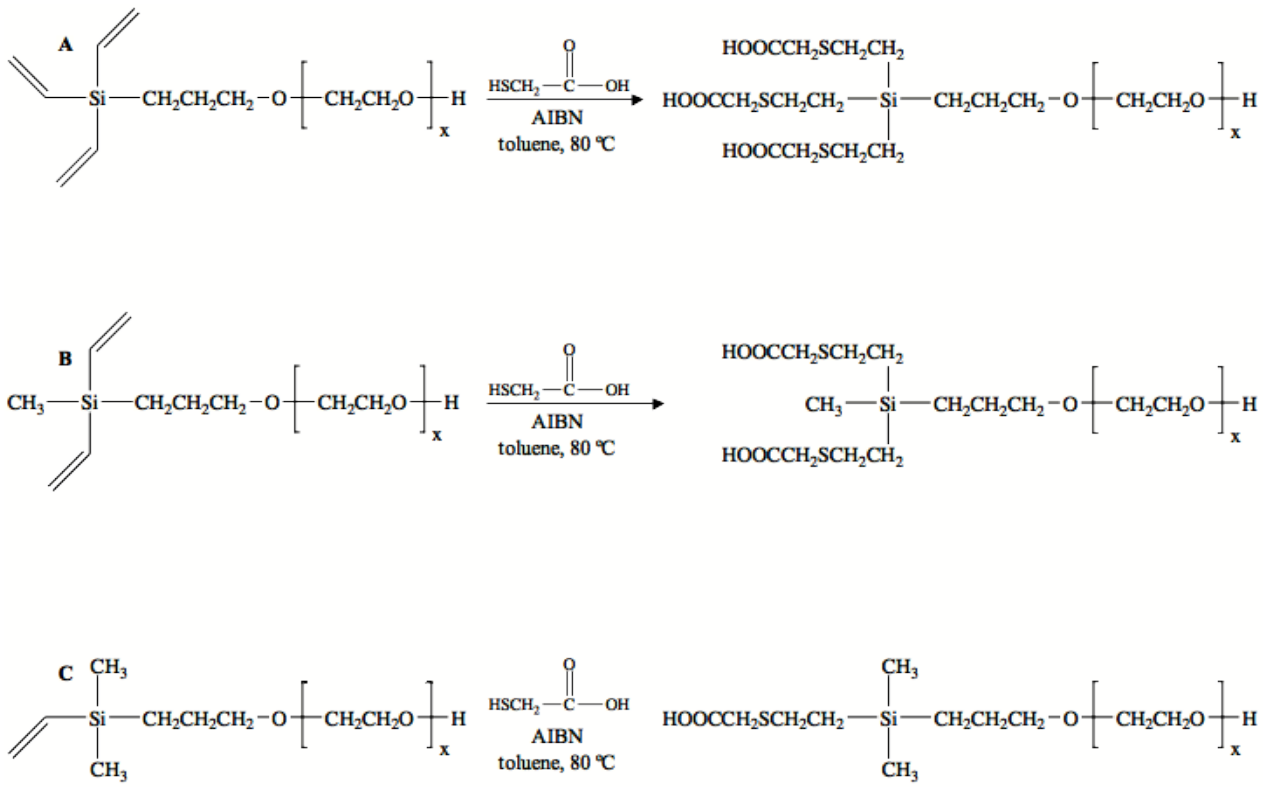

Figure 6.11 A reaction scheme depicting the functionalization of the terminal vinylsilyl groups utilizing the ene-thiol addition reaction.

The ene-thiol reactions were monitored via ^{1}H NMR by following the disappearance of vinyl proton resonances at approximately 6.0 ppm. The reactions are complete within 2 h. Figure 6.12 shows a representative ^{1}H NMR of a purified dicarboxylic acid functional PEO. There is an absence of vinyl peaks at 6.0 ppm and an appearance of new peaks corresponding to the Markovnikov addition products. These resonances correspond with previously reported values by Wilson et al. for tricarboxylic acid terminated PDMS.

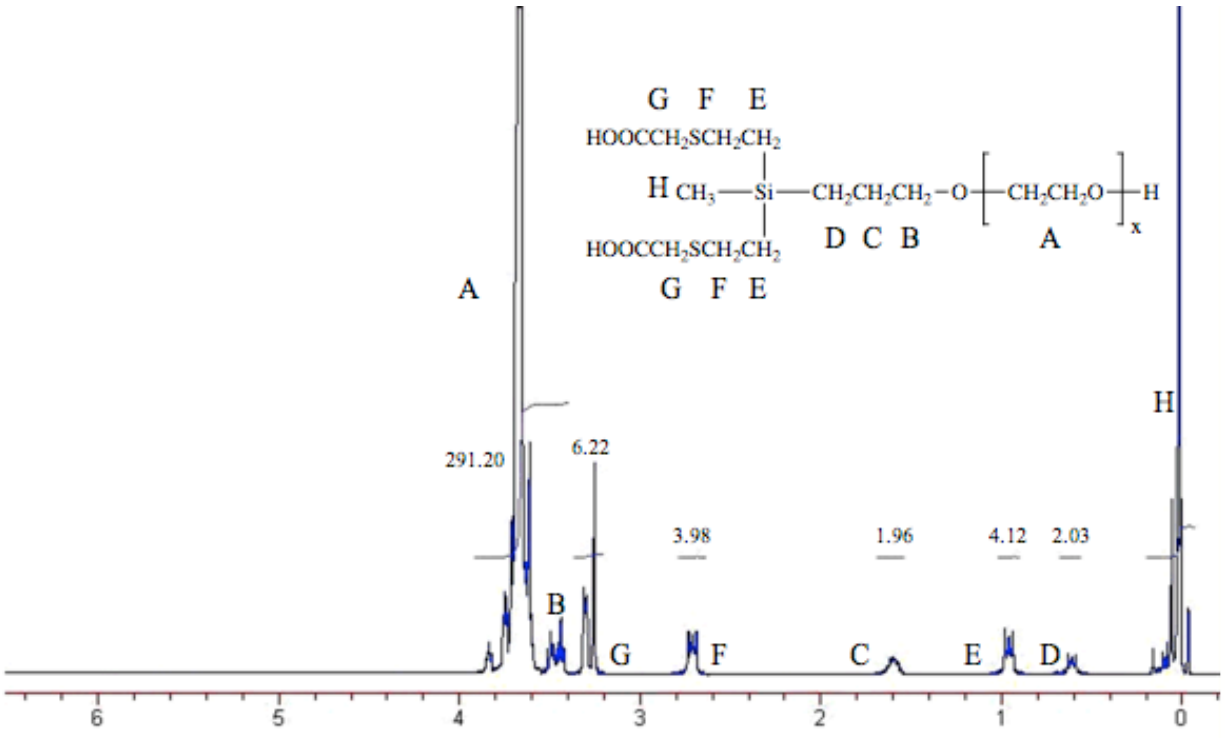

Figure 6.12 ^{1}H NMR reveals quantitative functionalization as evidenced by the disappearance of the vinyl resonances at 6.0 ppm and the appearance of peaks at 2.8 and 0.98 ppm.

CHAPTER 7 Conclusions

Cobalt nanoparticles encased in polysiloxane block copolymers can be heated at 600-700 ^{o}C to coat the particles with shells containing silica, and the heat-treatments also increase the saturation magnetization of the cobalt.[7] Specific saturation magnetizations of these materials are ~140 emu g^{-1} of cobalt, and the cobalt surfaces are protected against oxidation by the coatings. However, if the complexes are mechanically ground, the surfaces of the cobalt are exposed, and this exposure results in oxidation of the complexes and loss of magnetization.[8] Cobalt nanoparticles with surfaces containing silica can be functionalized by condensing organofunctional alkoxysilane reagents onto the surfaces, then the organofunctional groups can be further reacted with a variety of materials.[7] Methods have been demonstrated for modifying silica-coated cobalt nanoparticle surfaces with amines, isocyanates, poly(ethylene oxide-*co*-propylene oxide), PDMS and with poly(L-lactide).[7]

Copolymers of PDMS-*co*-PMHS and homopolymers of PMHS were synthesized via acid catalyzed equilibration polymerization with good control over the molecular weight and target compositions. Further reactions yielded graft copolymers comprised of a poly(methyl-2-propyl-2-phenoxyphthalonitrile) backbone with approximately one polystyrene graft (PHTH-*g*-PS), and these graft copolymers function well as dispersion stabilizers for cobalt nanoparticles in toluene or dichlorobenzene. Dichlorobenzene allowed for forming the cobalt nanoparticles at 180 ^{o}C, whereas toluene as the solvent restricted the reaction temperatures to 110 ^{o}C under ambient pressure. The higher temperature thermolyses produced complexes with less residual carbon monoxide and higher magnetizations immediately after the cobalt thermolysis step.

Cobalt nanoparticles encased in the PHTH-*g*-PS copolymers were subjected to elevated heat treatments at 700 °C to form a graphitic-siliceous coating as well as to anneal the cobalt (thus improving the magnetic properties). These graphitic-siliceous-cobalt complexes had high specific saturation magnetizations of approximately 80 emu g^{-1}. Early aging data suggest that these coatings provide an enhanced oxygen barrier for the complexes even after mechanical grinding, however, the long term oxidative stability of these complexes must be investigated. In addition, methods to functionalize the surfaces of the siliceous-graphitic-cobalt complexes will need to be developed.

A series of hydroxypropylvinylsilane initiators for poly(ethylene oxide) polymerizations were synthesized. Poly(ethylene oxide) oligomers were prepared with one, two and three vinyl groups at one end, then the vinylsilane endgroups were reacted with mercaptoacetic acid to produce carboxylic acid functional poly(ethylene oxide)s. It is anticipated that these carboxylic acid functional oligomers will complex to magnetite nanoparticles, and that these complexes will be dispersible in aqueous media. The complexation of the oligomers will be studied as a function of varying the number of terminal carboxylic acid groups. The properties in aqueous solution, such as dispersibility, will be examined. In addition, conjugating bioactive molecules to the free hydroxyl group after complexation to the magnetite surface will have to be probed.

Bibliography

(1) Rutnakornpituk M; Thompson MS; Harris LA; Farmer KE; Esker AR; Riffle JS; Connolly J; St Pierre TG *Polymer* **2002**, *43*, 2337-2348.

(2) Stevenson JP; Rutnakornpituk M; Vadala ML; Esker AR; Charles SW; Wells S; Dailey JP; RIffle JS; *Journal of Magnetism and Magnetic Materials* **2001**, *225*, 47-58.

(3) Vadala ML; Rutnakornpituk M; Zalich MA; ST Pierre TG; Riffle JS; *Polymer* **2004**, *45*, 7449-7461.

(4) Wilson KS; Rutnakornpituk M; Harris LA; Hoyt JK; Riffle JS; *224th ACS National Meeting*; The American Chemical Society: Boston, 2002.

(5) Baranauskas VV; Zalich MA; Saunders M; St Pierre TG; Riffle JS; *Chemistry of Materials* **2005**, *17*, 5246-5254.

(6) Harris LA; Goff JD; Carmichael AY; Riffle JS; Harburn JJ; St Pierre TG; Saunders M; *Chemistry of Materials* **2003**, *15*, 1367-1377.

(7) Vadala ML; Zalich MA; Fulks DB; St Pierre TG; Dailey JP; Riffle JS; *Journal of Magnetism and Magnetic Materials* **2005**, *293*, 162-170.

(8) Zalich MA; Vadala ML; Riffle JS; Saunders M; St Pierre TG; *Chemistry of Materials* **2006**.

(9) Zalich MA; Baranauskas VV; Riffle JS; Saunders M; St Pierre TG; *Chemistry of Materials* **2006**, *in press*.

(10) Vansant EF; Van Der Voort P; Vracken KC; In *Characterization and Chemical Modification of the Silica Surface*; Elsevier: New York, 1995; Vol. 93.

(11) Pope E; Sumio S; Klein L; In *Sol-Gel Science and Technology*; The American Chemical Society: Ohio, 1995.

(12) Brinker CJ; Scherer G; In *Sol-Gel Science: The Physics and Chemistry of Sol-Gel Processing*; Academic Press: Boston, NYC, Londong, 1990.

(13) Ebelmen; *Annales de Chimie et de Physique* **1846**, *57*, 319.

(14) Geffcken W; Berger E; German Patent 736,411, 1939.

(15) Schroeder H; *Physics of Thin Films* **1969**, *5*, 87-141.

(16) Levene L; Thomas IM; United States Patent 3,640,093, 1972.

(17) Dislich H; *Angewandt Chemie* **1971**, *10*, 363-370.

(18) Stober W; Fink A; Bohm E; *Journal of Colloid and Interface Science* **1968**, *26*, 62.

(19) Keefer KD; In *Better Ceramics Through Chemistry*; Wiley and Sons Inc.: New York, 1986.

(20) Iler RK; In *The Chemistry of Silica: Solubility, Polymerization, Colloid and Surface Properties, and Biochemistry*; Wiley and Sons Inc: New York, 1979.

(21) McGrath JE; Pullockraken JP; Riffle JS; Kilic S; Elsbernd CS; In *Ultrastructure Processing of Advanced Ceramics*; Wiley and Sons Inc.: New York, 1988.

(22) Plueddemann EP; In *Silane Coupling Agents*; Plenum: New York, 1982.

(23) McNeil KJ; DiCaprio JA; Walsh OA; Pratt RJ; *Journal of the American Chemical Society* **1980**, *102*, 1859.

(24) Pohl ER; Osterholtz FD; In *Kinetics and Mechanisms of Aqueous Hydrolysis*; Plenum Press: New York, 1985.
(25) Michael G; Ferch H; *Degussa* **1991**.
(26) Hurd AJ; *Materials Research Society Symposium Proceedings* **1990**, *172*.
(27) Hurd AJ; Flower WL; *Journal of Colloid and Interface Science* **1988**, *122*, 178.
(28) Babonneau F; Thorne K; Mackenzie JD; *Chemistry of Materials* **1989**, *1*, 554-558.
(29) Soraru GD; Jonschker S; Goedicke S; Menning M; *Journal of Non-Crystalling Solids* **1998**, *224*, 173.
(30) Yajima S; Hasegawa Y; Hayashi J; Iimura M; *Journal of Materials Science* **1979**, *13*, 2569.
(31) Wei GC; Kennedy CR; Harris LA; *American Ceramics Society Bulletin* **1984**, *63*, 1054.
(32) Pena-Alonso R; Rubio J; Rubio F; Oteo JL; *Journal of Sol-Gel Science and Technology* **2003**, *26*, 195-199.
(33) Bourget L; Leclerq D; Vioux A; *Journal of Sol-Gel Science and Technology* **1999**, *14*, 137-147.
(34) Cerofolini G; Meda L; Re N; In *Adsorption on silica surfaces*; Marcel Dekker Inc: New York, 2000.
(35) Keefer KD; In *Silicon-based polymer science: a comprehensive resource*; American Chemical Society: Washington DC, 1990; Vol. 224.
(36) Pacchioni G; Ierano G; *Physical Review B: Condensed Matter* **1997**, *56*, 304.
(37) McKinnis CL; Sutton JW *Journal of the American Chemical Society* **1959**, *42*, 194.
(38) Shafei GMS; In *Silica Surface Chemical Properties*; Marcel Dekker: New York, 2000.
(39) Brunauer S; Kantro DL; Weise CH; *Journal of Chemistry* **1956**, *34*, 1483.
(40) Iler RK; In *The Chemistry of Silica*; Cornell University Press: Ithaca NY, 1955.
(41) Zhuravlev LT; *Langmuir* **1987**, *3*, 316-318.
(42) Yates DE; Healy TW; *Journal of Colloid and Interface Science* **1976**, *55*, 9.
(43) Tadros TF; Lyklema J; *Journal of Electroanalytical Chemistry* **1968**, *17*, 267.
(44) Hiemstra T; Van Riemsdijk WH; Bolt GH; *Journal of Colloid and Interface Science* **1989**, *133*, 91.
(45) Hair ML; Hertl W; *Journal of Physical Chemistry* **1970**, *74*, 91.
(46) Yates DJC; Dembinski GW; Krell WR; Elliot JJ; *Journal of Physical Chemistry* **1969**, *3*, 911.
(47) Azrak RJ; Angell CL; *Journal of Physical Chemistry* **1973**, *77*, 3048.
(48) Vrancken KC; Van Der Voort P; Possemiers K; Grobet P; Vansant EF; In *The physisorption and condensation of aminosilanes on silica gel*; The Royal Society of Chemistry: Cambridge, 1993.
(49) Vracken KC; Possemiers K; Van Der Voort P; Vansant EF; In *Colloids*

and Surfaces A: Physiochemical and Engineering Aspects **1995**, *98*, 235-241.
(50) Roth CA; Ryan JW; Speier J; *Journal of Organic Chemistry* **1971**, *36*, 3120-3126.
(51) Saam J; Speier J; *Journal of Organic Chemistry* **1959**, *24*, 119-120.
(52) Kallury KMR; MacDonald PM; Thompson M; *Langmuir* **1994**, *10*, 492.
(53) Caravajal GS; Leyden DE; Maciel GE; In *Silanes, Surfaces, and Interfaces*, Gordon and Breach: New York, 1985.
(54) De Haan JW; Van Den Bogaert HM; Ponjee JJ; Van Den Ven LJM; *Journal of Colloid and Interface Science* **1986**, *110*, 591.
(55) Ming Ma; Zhang Y; Wei Y; Hao-ying S; Hai-qian Z; Ning G; *Colloids and Surfaces A: Physiochemical and Engineering Aspects* **2003**, *212*, 219-226.
(56) Kim DK; Mikhaylova M; Zhang Y; Muhammed M; *Chemistry of Materials* **2003**, *15*, 1617-1627.
(57) Mikhaylova M; Kim DK; Bobrysheva N; Osmolowsky M; Semenov V; Tsakalakos T; Muhammed M; *Langmuir* **2004**, *20*, 2472-2477.
(58) Zhang M; Kohler N; Zhang Y; *Biomaterials* **2002**, *23*, 1553-1561.
(59) Kneuer C; Sameti M; Haltner E; Schiestel T; Shirra H; Schmidt H; Lehr CM; *International Journal of Pharmaceutics* **2000**, *196*, 257-261.
(60) Rezania A; Johnson R; Lefkow A; Healy K; *Langmuir* **1999**, *15*, 6931-6939.
(61) Langer R; Choi IS; *Macromolecules* **2001**, *34*, 5361-5363.
(62) Wieringa RH; Schouten AJ; *Macromolecules* **1995**, *29*, 3032-3034.
(63) Oosterling ML; Willems E; Schouten AJ; *Polymer* **1995**, *36*, 4463-4470.
(64) Gallas JP; Lavalley JC; Burneau A; Barres O; *Langmuir* **1991**, *7*, 1235.
(65) Cosgrove T; Turner M; Thomas DR; *Polymer* **1997**, *38*, 3885-3892.
(66) Mazumder B; In *Silicon and Its Compounds*; Science Publishers Inc: Enfield NH, 2000.
(67) Bruins PF; In *Silicone Technology*; Interscience Publisher: New York, 1970.
(68) Eaborn C; In *Organosilicon Compounds*; Buttersworth Scientific Publication: London, 1962.
(69) Voronkov MG; In *The Siloxane Bond*; Consultants Bureau: New York, 1987.
(70) Chen X; Gardella JA; *Macromolecules* **1994**, *27*, 2206-2210.
(71) Noll W; In *Chemistry and Technology of Silicones*; Academic Press Inc: New York, 1968.
(72) Sauer RO; Scheiber WJ; Brewere SD; *Journal of the American Chemical Society* **1946**, *68*, 962.
(73) Lawrence NJ; Drew MD; Bushell SM; *Journal of the Chemical Soceity, Perkin Transaction 1* **1999**, *23*, 3381.
(74) Cancouet P; Daudet E; Helary G; Moreau M; Sauvet G; *Journal of Polymer Science Part A: Polymer Chemistry* **2000**, *38*, 826-836.
(75) Carraher CE; *Journal of Macromolecules Science Chemistry* **1982**, *A17*, 1293.

(76) Sobolevskii MV; Skorokhodov II; Grinevich KP; In *Oligoorganosiloxanes*; Chimiya: Moscow, 1985.
(77) Dvornic PR; Lenz RW; In *High Temperature Siloxane Elastomers*; Springer Verlag: New York, 1990.
(78) Jovanovic JD; Govedarica MN; Dvornic PR; Popovic IG; In *Polymers Degradation and Stability* **1998**, *61*, 87-93.
(79) Marciniec B; In *Comprehensive Handbook on Hydrosilation*; Pergamon Press: Oxford, 1992.
(80) McGrath MP; Sall ED; *Chemistry Review* **1995**, *95*.
(81) Clarson SJ; Semlyen JA; In *Siloxane Polymers*; PTR Prentic Hall: New Jersey, 1993.
(82) Walsh R; *Accounts of Chemical Research* **1981**, *14*, 246-252.
(83) Chalk AJ; Harrod JF; *Journal of the American Chemical Society* **1965**, *87*, 16-21.
(84) Hazziza-Laskar J; Helary G; Sauvet G; *Journal of Applied Polymer Science* **1995**, *58*, 77-84.
(85) Houser EJ; Keller TM; *Journal of Polymer Science Part A: Polymer Chemistry* **1998**, *36*, 1969-1972.
(86) Chien LC; Cada LG; *Macromolecules* **1994**, *27*, 3721.
(87) Zhu Z; Einset AG; Yang CY; Chen WX; Wnek GE; *Macromolecules* **1994**, *27*, 4076-4079.
(88) Marciniec B; Gulinski J; Kopylova L; Maciejewski H; Grundwald Wyspianska M; Lewandowski M; *Applied Organometallic Chemistry* **1997**, *11*, 843-849.
(89) Yang CY; Wnek GE; *Polymer Preprints* **1989**, *30*, 177.
(90) Fan G; Fall A; Collins W; *227th ACS National Meeting*; The American Chemical Society: Washington DC, 2004.
(91) Gauvin F; Harrod JF; Woo HG; *Advances in Organometallic Chemistry* **1998**, *42*, 363.
(92) Seyferth; In *Silicon-Based Polymer Science. A Comprehensive Resource*; The American Chemical Society: Washington DC, 1990.
(93) Laine RM; Blum YD; Tse D; Glaser R; Zeldin M; Wynne KI; Allock HR; *Inorganic and Organometallic Polymers*; The American Chemical Society: Washington DC, 1998.
(94) Bedard TC; Corey JY; *Journal of Organometallic Chemistry* **1992**, *428*, 315-333.
(95) Lukevics D; Dzintara MJ; *Journal of Organometallic Chemistry* **1985**, *295*, 265.
(96) Barishnikov NN; *Fluorescent Polymers*; Horwood: London, 1994.
(97) Dias FB; Lima LC; Macanita AL; Clarson SJ; Horta A; Pierola IF *Macromolecules* **2000**, *33*, 4772.
(98) Toulokhonova I; Bjerke-Kroll B; West R; *Journal of Organometallic Chemistry* **2003**, *686*, 101-104.
(99) Harris JM; In *Poly(ethylene glycol) chemistry*; Plenum Press: New York, 1992.
(100) Otsuka H; Nagasaki Y; Kataoka K; *Curr Opin Colloid Interface Sci* **2001**,

6, 3-10.
(101) McGrath JE; *Ring Opening Polymerization*; ACS Symposium Series; American Chemical Society: Washington DC, **1985**; Vol. 286.
(102) Chanda M; In *Advanced Polymer Chemistry A Problem Solving Guide*; Marcel Dekker: New York, **2000.**
(103) Yamamoto Y; Nakao W; Atago Y; Koichi I; Yagci Y; *European Polymer Journal* **2003**, 545-550.
(104) Price CC; Vandenberg E; In *Coordination Polymerization*; Plenum: New York, 1984.
(105) Matsushima A; Nishimura H; Ashihara Y; Yakata Y; Inada Y; *Chem Lett* **1980**, 773-776.
(106) Zalipsky S; Lee C; In *Use of funcitonalized poly(ethylene glycol)s for modification of polypeptides,*; Plenum: New York, 1992.
(107) Brissault B; Guis C; Cheradame H; *European Polymer Journal* **2002**, *38*, 219-228.
(108) Jerome C; Martinot L; Jerome R; *Synthetic Materials* **1999**, *105*, 65-71.
(109) Avdeev MV; Balasoiu M; Aksenov VL; Garamus VM; Kohlbrecher J; Bica D; Vekas L; *Journal of Magnetism and Magnetic Materials* **2004**, *270*, 371-379.
(110) Zhang D; Qi L; Ma J; Cheng H; *Chemistry of Materials* **2001**, *13*, 2753-2755.
(111) Bronich T; Keifer P; Shlyakhtenko S; Kabanov A; *Journal of the American Chemical Society* **2004**, *127*, 8236-8237.
(112) Norwig J; Meyer WH; Wegner G; *Chemistry of Materials* **1998**, *10*, 460-463.
(113) Tamaura Y; Takahasi K; Kodera Y; Saito Y; Inada Y; *Biotechnol Lett* **1986**, *8*, 877.
(114) Zhang Y; Kohler N; Zhang MQ; In *Materials Research Society Symposium Proceedings,*; MRS: San Francisco CA, 2002.
(115) Zhang Y; Kohler N; Zhang MQ; *Biomaterials* **2002**, 1553.
(116) Zhang Y; Zhang J; *Journal of Colloid and Interface Science* **2005**, 352-357.
(117) Ibrahim A; Couvreur P; Roland M; Speiser P; *Journal of Pharmacy and Pharmacology* **1983**, *35*, 59.
(118) Meuller RH; Maassen S; Weyhers H; Specht F; Lucks JS; *International Journal of Pharmaceutics* **1996**, *138*, 85.
(119) Weissleder R; Stark DD; Engelstad BL; Bacon BR; Compton CC; White DL; Jacobs P; Lewis J; *American Journal of Reontgenology* **1989**, *152*, 167.
(120) Connolly J; St Pierre TG; Rutnakornpituk M; Riffle JS; *Journal of Physics D: Applied Physics* **2004**, *37*, 2475-2482.
(121) Rutnakornpituk M; Baranauskas VV; Riffle JS; Connolly J; St Pierre TG; Dailey JP; *European Cells and Materials* **2002**, *106*.
(122) Jacobsohn LG; Hawley ME; Cooke DW; HUndley MF; Thompson JD; Schulze RK; Nastasi M; *Journal of Applied Physics* **2004**, *96*, 4444.
(123) Cobalt HCP, *card no 05-0727* **1996**.

(124) Dinenga DP; Bawendi MG; *Angew. Chem. Int. Ed.* **1999**, *38*, 1788.
(125) Cobalt FCC; *card 15-0806* **1996**.
(126) Papirer E; Horny P; Balard H; Anthore R; Petipas C; Martinet A; *Journal of Colloid and Interface Science* **1983**, *94*, 207-219.
(127) Choi IS; Langer R; *Macromolecules* **2001**, *34*, 5361.
(128) Porte-Durrieu MC; Labrugere C; Villars F; Lefebvre F; Dutoya S; Guette A; Bordenave L; Baquey C; *Journal of Biomedical Materials Research* **1999**, *46*, 368.
(129) Behrens S; Matoussevitch N; Modrow H; Palina H; Jan M; *Zeitschrift fuer Physikalische Chemie* **2006**, *220*, 3-40.
(130) De Julian Fernandez C; Mattei G; Maurizio C; Cattaruzza E; Padovani S; Battaglin G; Gonella F; D'Acapito F; Mazzoldi P; *Journal of Magnetism and Magnetic Materials* **2005**, *290*, 187-190.
(131) Herczynska L; Lestel L; Boileau S; Chojnowski J; Polowinski S; *European Polymer Journal* **1999**, *35*, 1115-1122.
(132) Weber WP; Cai G; *Macromolecules* **2001**, *34*, 4355-4360.
(133) Brunelle DJ; In *Ring-opening Polymerization: Mechanisms, Catalysis, Structure, Utility*; Hanser Publishers: Munich, Vienna, New York, Barcelona, 1993.
(134) Cantor SW; Grubb WT; Osthoff RC; *Journal of the American Chemical Society* **1954**, *76*.
(135) Chojnowski J; In *Siloxane Polymers*; PTR Prentice Hall: Englewood Cliffs, NJ, 1993.
(136) Spinu M; McGrath JE; *Journal of Polymer Science Part A: Polymer Chemistry* **1991**, *29*, 657-670.
(137) Graczyk T; Lasocki Z; *Bull Acad Polonaise Sci Ser Sci Chim* **1979**, *27*, 181-185.
(138) Gray GW; Hawthorne WD; Lacey D; White MS; Semlyen JA; *Liq Cryst* **1989**, *6*.
(139) Richard H; Mauzac M; Sigaud G; Achard M; Hardouin F; *Liq Cryst* **1991**, *9*, 679.
(140) Keller TM; *Chemistry of Materials* **1994**, *6*, 302-305.
(141) Sumner MJ; Weyers RY; Rosario AC; Riffle JS; Sorathia U; *Polymer* **2004**, *45*, 5199-5206.
(142) Pileni MP; *Journal of Physical Chemistry* **1993**, *97*, 9661.
(143) Smith TW; 4,252,674 Xerox Corporation: United States Patent; **1981**.
(144) Hirao A; Kitamura K; Takenaka K; Nakahama S; *Macromolecules* **1993**, *26*, 4995.
(145) Makino T; Hogen-Esch TE; *Macromolecules* **1999**, *32*, 5712-5714.
(146) Lu AH; Li WC; Matoussevitch N; Spliethoff B; Boenneman HH; Scheuth F; *Chemical Communications* **2005**, *1*, 98-100.
(147) Baranauskas VV, Ph.D. Dissertation; Virginia Polytechnic Institute and State University, **2005**.
(148) Tannenbaum R; *Inorganica Chimica Acta* **1994**, *227*, 223-240.
(149) Cammas S; Nagasaki Y; Kataoka K *Bioconjugate Chemistry* **1995**, *6*, 226-230.

(150) Bruice PY; *Organic Chemistry* New York, 2005.
(151) Hutchins RO; Taffer IM; *Journal of Organic Chemistry* **1982**, *48*, 1360-1362.
(152) Corey EJ; Nicolaou KC; Shibasaki M; Machida Y; Shiner CS; *Tetrahedron Letters* **1975**, 3183.
(153) Parker AJ; *Journal of Chemistry Reviews* **1969**, *69*, 1.
(154) Reich HJ; Peake SL; *Journal of the American Chemical Society* **1978**, *100*, 4888.